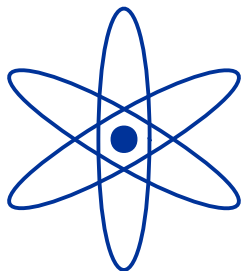# Rare K and B Decays in the MSSM

THORSTEN EWERTH

Lehrstuhl für Theoretische Physik T31
Physik Department, TU München
James-Franck-Straße
85748 Garching
Germany

TECHNISCHE
UNIVERSITÄT
MÜNCHEN

Physik-Department
Technische Universität München
Institut für Theoretische Physik
Lehrstuhl Univ.-Prof. Dr. Andrzej J. Buras

Rare *K* and *B* Decays in the MSSM

Thorsten Ewerth

Contents

Introduction

On the quest for the ultimate theory describing the fundamental interactions of elementary particles a major milestone was the completion of a renormalizable gauge field theory in four space-time dimensions – the Standard Model (SM) of elementary particle physics – which not only incorporates the strong interactions of quarks, but also unifies the electromagnetic and weak interactions of quarks and leptons [1–17]. It has been tested experimentally to a high level of accuracy, and the only missing ingredient intimately connected with the electroweak breaking mechanism that has not yet been directly observed is the Higgs boson.

However, in spite of the tremendous success the common belief is that the SM is not the final answer but rather the low-energy limit of a so-called grand unified theory (GUT) in which the strong and electroweak interactions are described by a single gauge group. This assumption is highly motivated because the extrapolated running gauge couplings of the SM meet approximately at a very high scale of about 10^{15} GeV [18]. The smallest possible GUT, which can be spontaneously broken down to the SM gauge group via the Higgs mechanism, is based on the $SU(5)$ gauge group [18, 19], which in turn can be naturally embedded into the $SO(10)$ gauge group having the nice feature that all fermions belonging to one generation of the SM are unified within a single irreducible representation [20, 21]. Furthermore, this irreducible representation contains the long lost right-handed neutrino being a gauge singlet below the grand unification scale, or in other words, this field does not participate in the strong, weak and electromagnetic interactions. This right-handed neutrino can naturally aquire a large Majorana mass and hence escape from direct experimental detection, while allowing for a tiny Majorana mass for the left-handed neutrinos via a rather attractive scenario known as the see-saw mechanism [22, 23]. And indeed, from experiments we know that left-handed neutrinos do have non-vanishing masses [24, 25].

Nevertheless, how promising these ideas soever may be, the increasing precision in measuring the strong and electroweak coupling constants at low energies has shown that they fail to meet in one point by more than seven standard deviations [26], and hence unification without the introduction of new degrees of freedom in the SM does not take place. Another issue grabbing theorists attention is the so-called hierarchy problem which becomes apparent once the SM is embedded into a GUT. Albeit such a large unification scale is necessary for the stability of the proton, it is difficult to understand the smallness of the electroweak scale with respect to the former. And, even more important, is the fact that the weak scale, which settles the mass scale of the W and Z bosons, is not stable against quantum corrections. It can only be arranged by extremely fine-tuning the parameters of the theory. The reason for this circumstance is the elementary Higgs boson. Being a scalar particle nothing protects its mass from receiving large, quadratically divergent, quantum corrections, which therefore is naturally of the order of the largest involved mass scale of about 10^{15} GeV.

A possible solution is provided by the softly broken minimal supersymmetric extension

of the SM, the so-called Minimal Supersymmetric Standard Model (MSSM)[1], in which the couplings of the Higgs bosons are fixed by supersymmetry, and hence no quadratically divergent quantum corrections occur [31–33]. In this sense supersymmetry solves the hierarchy problem in that it allows for a small and stable weak scale without fine-tuning when embedding the MSSM into $SU(5)$ or $SO(10)$. However, supersymmetry still lacks the explanation why the weak scale is so much smaller than the grand unification scale. Besides this taming of quadratic divergences the gauge couplings unify at a scale of about 10^{16} GeV within the framework of the MSSM [26,34,35] which can be taken as a strong hint for a supersymmetric GUT. Remarkably, the unification scale gets enhanced by an order of magnitude and hence supersymmetry stabilizes the proton. A further shortcoming of the SM is the inability to turn on gravity, which we cannot anymore neglect when going beyond the Planck scale of about 10^{19} GeV, since up to now no renormalizable quantum field theory of gravity has been found. And from the fact that the low-energy limit of a superstring theory, a promising candidate for a unification of all interactions including gravity, is supersymmetric, the belief on a supersymmetric extension of the SM among theorists is all the more strengthened.

So nice and appealing these theoretical arguments are, up to now neither a single sparticle has been observed, nor is there any conclusive indirect experimental evidence pointing towards supersymmetry. This is due to the limited energy reach in present experiments of direct searches, and the relatively large uncertainties, or even only existing lower/upper bounds, from which the indirect searches still suffer. But in the light of continually pursued investigations with increasing energy reach and improving precision from the experimental side, future experiments will hopefully signal the first evidence for supersymmetry. In this respect it is of most importance to improve the theoretical uncertainties of physical quantities in the framework of both the SM and the MSSM in order to keep with the increasing experimental precision and to reveal possible supersymmetric deviations from the former. Of special interest are furthermore observables for which only lower/upper bounds exist, because the rich structure of the MSSM combined with other experimental constraints often allows for order of magnitude enhancements sometimes even saturating these bounds, and therefore lying just around the corner of present experiments.

In this thesis we will attack both above mentioned approaches, the latter for the rare exclusive decays $K^+ \to \pi^+ \nu \bar{\nu}$ and $K_L \to \pi^0 \nu \bar{\nu}$ belonging to the theoretically cleanest processes in the field of meson decays, and the former for the semileptonic $\bar{B} \to X_s l^+ l^-$ decay, where we restrict ourselves to the inclusive decay mode since it is amenable to a cleaner theoretical description. Within the SM both decays, as all other weak decays, are governed by the Cabbibo-Kobayashi-Maskawa (CKM) matrix, the only source of flavor and CP violation [36,37]. Furthermore, there is no tree-level contribution to these decays and it is this fact which makes contributions from virtual superpartners of SM particles so important, especially in the light of the additional sources of flavor and CP violation residing in the soft-breaking terms of the MSSM. In what follows we will argue why both decay modes are of special interest to us.

Let us start with the $K^+ \to \pi^+ \nu \bar{\nu}$ and $K_L \to \pi^0 \nu \bar{\nu}$ decays. As already mentioned they belong to the theoretically cleanest processes, and in fact, their branching ratios can be

---

[1]Other solutions are given by the assumptions that the Higgs boson is not an elementary particle but rather a condensate of strongly interacting fermions, so-called technicolor theories [27], or by models of large extra dimensions, in which the four-dimensional space-time description breaks down beyond the weak scale [28,29]. Also, there exists a fairly new approach of so-called Little Higgs models [30].

computed to an exceptionally high degree of precision that is not matched by any other decay of mesons [38–42]. The reason for this is that the hadronic matrix elements for these decays can be extracted from the well measured branching ratio of the non-rare decay $K^+ \to \pi^0 e^+ \nu_e$ due to isospin symmetry. As emphasized in [43], the clean theoretical character of these decays remains valid in essentially all extensions of the SM. In this context an important virtue of these decays is the possibility of parameterizing the new physics contributions to their branching ratios, in a model-independent manner by just two parameters [44], the magnitude of the short distance function X and its complex phase, $X = |X|e^{i\theta_X}$.

The most recent predictions for the relevant branching ratios within the SM read [43]

$$\mathcal{B}(K^+ \to \pi^+ \nu\bar{\nu})_{\text{SM}} = (7.8 \pm 1.2) \cdot 10^{-11}$$

$$\mathcal{B}(K_L \to \pi^0 \nu\bar{\nu})_{\text{SM}} = (3.0 \pm 0.6) \cdot 10^{-11} \tag{1}$$

in the ballpark of other estimates [45–49]. As discussed in [43] a NNLO calculation of the charm contribution to $K^+ \to \pi^+ \nu\bar{\nu}$ and further progress on the determination of the CKM parameters coming in the next few years dominantly from BaBar, Belle, Tevatron and later from LHC and BTeV, should eventually allow predictions for $\mathcal{B}(K^+ \to \pi^+ \nu\bar{\nu})$ and $\mathcal{B}(K_L \to \pi^0 \nu\bar{\nu})$ with uncertainties of at most $\pm 5\%$.

On the experimental side the two events observed by the AGS E787 collaboration at Brookhaven [50–53] and the additional event observed by AGS E949 [54] imply

$$\mathcal{B}(K^+ \to \pi^+ \nu\bar{\nu}) = (14.7^{+13.0}_{-8.9}) \cdot 10^{-11} \tag{2}$$

While the central value in (2) is about a factor of two higher than the SM value, the large experimental error precludes any claims for signals of new physics in the $K^+ \to \pi^+ \nu\bar{\nu}$ data. Further progress is expected in principle from AGS E949, from the efforts at Fermilab around the CKM experiment [55], the corresponding efforts at CERN around the NA48 collaboration [56] and at JPARC in Japan [57].

On the other hand the present experimental upper bound on $\mathcal{B}(K_L \to \pi^0 \nu\bar{\nu})$ from KTeV [58] reads

$$\mathcal{B}(K_L \to \pi^0 \nu\bar{\nu}) < 5.9 \times 10^{-7} \tag{3}$$

This is about four orders of magnitude above the SM expectation but a $K_L \to \pi^0 \nu\bar{\nu}$ experiment at KEK, E391a [59], which recently took data, should in its first stage improve this bound by three orders of magnitude. While this is insufficient to reach the SM level, a few events could be observed if $\mathcal{B}(K_L \to \pi^0 \nu\bar{\nu})$ turned out to be by one order of magnitude larger due to new physics contributions. Further progress on this decay is expected from KOPIO at Brookhaven [60,61], and from the second stage of the E391 experiment at JPARC [57].

In this context let us recall that a model-independent upper bound on $\mathcal{B}(K_L \to \pi^0 \nu\bar{\nu})$ following from isospin symmetry reads [62]

$$\mathcal{B}(K_L \to \pi^0 \nu\bar{\nu}) < 4.4 \cdot \mathcal{B}(K^+ \to \pi^+ \nu\bar{\nu}) \tag{4}$$

With the data in (2), which imply [54]

$$\mathcal{B}(K^+ \to \pi^+ \nu\bar{\nu}) < 3.8 \cdot 10^{-10} \quad (90\% \text{ C.L.}) \tag{5}$$

one finds then

$$\mathcal{B}(K_L \to \pi^0 \nu \bar{\nu}) < 1.7 \cdot 10^{-9} \quad (90\% \, \text{C.L.}) \tag{6}$$

still two orders of magnitude below the upper bound from the KTeV experiment.

In the present work we will analyze the $K^+ \to \pi^+ \nu \bar{\nu}$ and $K_L \to \pi^0 \nu \bar{\nu}$ decays within the MSSM, taking into account all sources of flavor violation in the squark sector and the, in our opinion, most important existing experimental and theoretical constraints. Also, we will refrain from using the mass-insertion approximation [63] in our numerical analysis, but instead work in the mass eigenstates basis for all sparticles using the exact formula for the short distance function X. Our approach generalizes previous analyses [44,64,65], where the mass-insertion approximation was applied, and only a limited number of MSSM parameters, assumed to be the most important, were used in numerical scans. The questions we will address here are whether the

- phase θ_X can be as large as found in [48,49][2],

- $\mathcal{B}(K^+ \to \pi^+ \nu \bar{\nu})$ can be significantly enhanced over the SM expectation so that it is at least as high as its central experimental value given in (2),

- $\mathcal{B}(K_L \to \pi^0 \nu \bar{\nu})$ can be enhanced by an order of magnitude over the SM expectation with the ratio of both branching ratios of $K_L \to \pi^0 \nu \bar{\nu}$ and $K^+ \to \pi^+ \nu \bar{\nu}$ reaching the bound given in (4).

Answering these questions is a non-trivial numerical task, due to the large number of free parameters and experimental constraints which have to be considered. Here we will demonstrate an efficient method of a random scan over the MSSM parameter space, based on an adaptation of the Monte Carlo integration algorithm VEGAS [66–68]. Such a method is designed to automatically concentrate most of the randomly generated points in the MSSM parameter ranges giving the largest deviations from the SM results, thus allowing for analyzing very large parameter spaces, with 20 or more dimensions, in a reasonable time and without very extensive computer CPU usage.

The second topic of this thesis are higher order corrections to the inclusive decay $\bar{B} \to X_s l^+ l^-$ in the framework of the MSSM. The major theoretical uncertainties arise here from the non-perturbative nature of intermediate $c\bar{c}$ states of the decay chain $\bar{B} \to X_s J/\psi \to X_s l^+ l^-$ and analogous higher resonances. These decay channels interfere with the simple flavor changing decay mechanism $\bar{B} \to X_s l^+ l^-$ and the dilepton invariant mass distribution can be only roughly estimated when the invariant mass of the lepton pair $s = q^2 = (p_{l^-} + p_{l^+})^2$ is not significantly away from $M_{J/\psi}^2$ resulting in uncertainties larger than $\pm 20\%$ [69]. For this reason the charmonium decays are vetoed explicitly in the experimental analysis [70–73] by cuts on the invariant dilepton mass around the masses of the J/ψ and ψ' resonances.

A rather precise determination of the dilepton invariant mass distribution seems to be possible once the values of s are restricted to be below or above these resonances, and indeed, at the moment the low-s region, accessible to $l = e$ and μ, is theoretically best understood.

---

[2]Recently it has been pointed out in [48,49] that the anomalies seen in the $B \to \pi K$ data may imply $|X| = 2.17 \pm 0.12$ and $\theta_X = -(86 \pm 12)^\circ$, to be compared with $|X| = 1.53 \pm 0.04$ and $\theta_X = 0^\circ$ in the SM. In this scenario the prediction for $\mathcal{B}(K^+ \to \pi^+ \nu \bar{\nu})$ is in agreement with the SM, while those for $\mathcal{B}(K_L \to \pi^0 \nu \bar{\nu})$ is enhanced by a factor of about 10.

Here the calculation can be performed using perturbative methods whereas non-perturbative corrections can be systematically taken into account within the framework of Heavy Quark Effective Theory (HQET). Furthermore, the effects related to the tails of $c\bar{c}$ resonances in the low-s region were estimated model-independently by employing an expansion in inverse powers of the charm quark mass in [74]. Because of the smallness of the non-perturbative corrections in the low-s region, the $\bar{B} \to X_s l^+ l^-$ decay rate is precisely predictable up to about 10% uncertainty.

On the experimental side a measurement of the $\bar{B} \to X_s l^+ l^-$ branching ratio with $l = e, \mu$ has been reported by the Belle collaboration for the first time [70], and subsequently a similar value was announced by the BaBar collaboration [72]. A very recent experimental result of Belle valid for the low-s region reads [71]

$$\mathcal{B}(\bar{B} \to X_s l^+ l^-)_{\text{exp}} = (1.493 \pm 0.504^{+0.382}_{-0.283}) \cdot 10^{-6} \tag{7}$$

which is in agreement with the BaBar result quoted in [73], and both having comparable uncertainties. Clearly, in view of the improving experimental situation of the ongoing B-physics dedicated experiments, such as the BaBar and Belle experiments, the experimental uncertainties will decrease.

The calculations of the perturbative contribution [75–77] up to the complete next-to-leading order (NLO) in QCD [78, 79] in the SM had not reached this precision. In a series of recent papers the calculation was extended to the next-to-next-to-leading order (NNLO) in QCD being almost complete up to the missing two-loop matrix element contributions of the four quark operators $\mathcal{O}_{3...6}$ which are expected to be small[3]. These calculations comprise corrections to the Wilson coefficients [82], the anomalous dimensions of the operators under consideration [83–86][4], and virtual and real corrections to the their low-energy matrix elements [87–92]. Within the SM the inclusion of NNLO QCD corrections reduces the branching ratios of $\bar{B} \to X_s e^+ e^-$ and $\bar{B} \to X_s \mu^+ \mu^-$ by typically 12% and 20%, respectively [93]. Furthermore uncertainties due to the dependence on the renormalization scale of the top quark mass, $\mu_t \sim O(m_t)$, become reduced from about $\pm 16\%$ to 3% [82], and the inclusion of the NNLO matrix element corrections decrease the low-energy scale dependence $\mu_b \sim O(m_b)$ from $\pm 13\%$ to a value about $\pm 6.5\%$ [87–89]. Electroweak corrections were found to be a few percent [86] removing the scale ambiguity of the electromagnetic coupling α_{em} when going beyond leading order (LO).

The most recent SM predictions for the branching ratio of $\bar{B} \to X_s l^+ l^-$ with $l = e, \mu$ in the low-s region read [92]

$$\mathcal{B}(\bar{B} \to X_s l^+ l^-)_{\text{SM}} = (1.63 \pm 0.20) \cdot 10^{-6} \tag{8}$$

where a normalization on the semileptonic decay $\bar{B} \to X_c l \nu_l$ was used in order to cancel the factor $(m_b^{\text{pole}})^5$, the origin of large uncertainties, and [86]

$$\mathcal{B}(\bar{B} \to X_s l^+ l^-)_{\text{SM}} = (1.57 \pm 0.16) \cdot 10^{-6} \tag{9}$$

which additionally includes dominant higher order electroweak effects and reduces the uncertainty due to the charm quark mass present in the decay rate $\Gamma(\bar{B} \to X_c l \nu_l)$ owing to

---

[3]The analogous corrections to $\bar{B} \to X_s \gamma$ are 1% [80, 81].

[4]The three-loop self-mixing of the four-quark operators $\mathcal{O}_{1...6}$ and their mixing into $\mathcal{O}_9$ is not published yet [85], however the relevant result for $\bar{B} \to X_s l^+ l^-$ can be found in [86].

a normalization on the charmless semileptonic decay $\bar{B} \to X_u l \nu_l$ in combination with the decay $\bar{B} \to X_c l \nu_l$.

Apart from the branching ratio and the dilepton invariant mass distribution, the differential forward-backward asymmetry of the leptons represents the another interesting observable in the decay $\bar{B} \to X_s l^+ l^-$. The leading contribution to the forward-backward asymmetry arises in the SM at the NLO and thus the inclusion of NNLO corrections drastically reduces the renormalization scale dependence in predictions of this observable. In particular it is very sensitive to new physics effects and further, s_0, the position at which the forward-backward asymmetry vanishes provides an important test of the SM [94, 95]. Within the SM the inclusion of NNLO corrections in the evaluation of s_0 leads to a shift of 10% to higher values accompanied by a reduction of the uncertainty due to renormalization scale dependencies in the prediction from typically 15% to 5% [96–98]. Within the SM the zero of the forward-backward asymmetry has been calculated in [86] and [92] at the NNLO yielding $s_0 = (3.76 \pm 0.33)\,\mathrm{GeV}^2$ and $s_0 = (3.90 \pm 0.25)\,\mathrm{GeV}^2$, respectively. Higher order electroweak corrections are found to shift s_0 by +2% [86].

Besides testing the SM, once the experimental accuracy improves, the inclusive decay $\bar{B} \to X_s l^+ l^-$ will also allow to constrain models involving new physics scenarios beyond the SM. The reliability of such constraints depend crucially on theoretical uncertainties due to higher order corrections in the prediction of observables as demonstrated by the SM analysis in the case of the importance of NNLO QCD corrections. In this work we will calculate QCD corrections to the matching conditions for the Wilson coefficients of operators mediating the transition $b \to s l^+ l^-$ in the context of the MSSM. To ensure the completeness of the calculated QCD corrections we assume that the down-squark mass-squared matrix decomposes into 2×2 matrices for each generation, that the gluino is heavy and decouples from the theory, and furthermore concentrate on the region $\tan \beta \leq 10$. Taking into account the results of [99–101], the known results for the Wilson coefficients of the magnetic penguins, the NNLO corrections to the matrix elements of the relevant operators from [87–89, 92] and their three loop anomalous dimensions calculated recently in [83–86], the only missing ingredients of a complete NNLO analysis of $\bar{B} \to X_s l^+ l^-$ in the considered scenario of the MSSM are the QCD corrections to the Wilson coefficients of the four-quark operators $\mathcal{O}_{1\ldots6}$ and the semileptonic operator $\mathcal{O}_9$. These missing ingredients are calculated here for the first time. Our main objectives are as follows,

- the calculation of Wilson coefficients, the dilepton invariant mass distribution and the forward-backward asymmetry of $\bar{B} \to X_s l^+ l^-$ at $O(\alpha_s)$,

- the investigation of the renormalization scale dependence and of the impact of the NNLO corrections on the observables in question,

- the comparison of the NNLO results of the SM with those of the MSSM and of the size of MSSM corrections with the theoretical uncertainties in the SM.

The remainder of this thesis is organized as follows. In chap. 1 we briefly summarize the properties of Weyl spinors being the fundamental building blocks of fermionic matter fields. The concept of gauge field theories is reviewed focusing on perturbative aspects. The discussion includes the construction of the classical Lagrangian, the quantization and renormalization as well as the background field formulation of such a theory. These ideas are then applied to the SM which gives our current description of the phenomena of elementary

particles. Subsequently, in chap. 2 we review the MSSM, a phenomenologically viable super-symmetric extention of the SM with minimal particle content consistent with observed SM particles and which does not violate SM conservation laws, i.e. baryon and lepton number conservation. The elegant superfield formalism is used to construct Lagrangians invariant under global supersymmetry transformations, and the results enables us to promote the SM to is minimalist supersymmetric extension. A special scenario of the MSSM with a heavy decoupled gluino, which finds it application in chap. 4, is also introduced. In chap. 3 we present formulae for the branching ratios $\mathcal{B}(K^+ \to \pi^+ \nu \bar{\nu})$ and $\mathcal{B}(K_L \to \pi^0 \nu \bar{\nu})$ in terms of the function X in a particularly suitable form for our numerical analysis. We discuss the numerical method we use to cope with the huge space of MSSM parameters under consideration, and afterwards, taking several experimental and theoretical constraints into account, we explore the possible departures of the function X and the branching ratios $\mathcal{B}(K^+ \to \pi^+ \nu \bar{\nu})$ and $\mathcal{B}(K_L \to \pi^0 \nu \bar{\nu})$ from their SM predictions. Chap. 4 is devoted to the calculation of the two-loop QCD corrections to the matching conditions of the $b \to s l^+ l^-$ transition in the context of the MSSM with a heavy decoupled gluino. We review the low-energy effective Lagrangian relevant for this scenario and present our analytical findings for the two-loop Wilson coefficients. As an application, we study the phenomenological implications for the dilepton invariant mass distribution and the forward-backward asymmetry of the leptons in the decay $\bar{B} \to X_s l^+ l^-$ including all NNLO corrections paying special attention to the reduction of renormalization scale uncertainties. Finally, we conclude and give a short outlook in chap. 5. Some technical details, and the analytical formulae for the Wilson coefficients are presented in the appendices. In app. A we list all contributions entering the function X relevant for the $K \to \pi \nu \bar{\nu}$ decays in the general MSSM. The complete set of non-physical operators relevant for the off-shell $b \to s l^+ l^-$ matching can be found in app. B, and app. C summarizes the analytical matching conditions for the considered scenario of the MSSM.

Part I

Strong and Electroweak Interactions

Chapter 1

The Standard Model

In this chapter we briefly summarize the properties of Weyl spinors being the fundamental building blocks of fermionic matter fields. Subsequently, the concept of gauge field theories is reviewed [102–105] focusing on perturbative aspects. The discussion includes the construction of the classical Lagrangian, the quantization and renormalization as well as the background field formulation of such a theory. Some of these ideas are then applied to the SM which gives our current description of the phenomena of elementary particles. Its Lagrangian is introduced in terms of two-component Weyl spinors but, as is standard, we pass to four-component Dirac spinors after electroweak symmetry breaking. This approach is somewhat unconventional but allows for a smooth transitions to its minimal supersymmetric extension discussed in chap. 2.

1.1 Spinor Representations

Two-component Weyl spinors transform under the lowest dimensional non-trivial representation of the Lorentz group, namely the matrices of the group $SL(2, \mathbb{C})$. Here, we have to distinguish between two different inequivalent representations[1],

$$\psi'_L(x') = \exp\left\{\frac{1}{2}\,\omega_{\mu\nu}\,\sigma^{\mu\nu}\right\}\psi_L(x) = M\psi_L(x)$$

$$\psi'_R(x') = \exp\left\{\frac{1}{2}\,\omega_{\mu\nu}\,\bar{\sigma}^{\mu\nu}\right\}\psi_R(x) = (M^\dagger)^{-1}\psi_R(x) \qquad (1.1)$$

where $\sigma^{\mu\nu} = \frac{1}{4}(\sigma^\mu\bar{\sigma}^\nu - \sigma^\nu\bar{\sigma}^\mu)$ and $\bar{\sigma}^{\mu\nu} = \frac{1}{4}(\bar{\sigma}^\mu\sigma^\nu - \bar{\sigma}^\nu\sigma^\mu)$ are the Lorentz group generators in terms of the generalized Pauli matrices $\sigma^\mu = (\mathbb{1}, \vec{\sigma})$ and $\bar{\sigma}^\mu = (\mathbb{1}, -\vec{\sigma})$, and $\omega_{\mu\nu} = -\omega_{\nu\mu}$ collects the rotation and boost parameters of a general Lorentz transformation. The spinors ψ_L and ψ_R are called left- and right-handed Weyl spinors, respectively, and their components are considered as Grassmann numbers, i.e. they are anticommuting numbers.

From (1.1) it follows that $i\sigma^2\psi_R^*$ and $-i\sigma^2\psi_L^*$ transform under the matrices $(M^T)^{-1}$ and M^*, respectively, which in turn are equivalent to M and $(M^\dagger)^{-1}$, respectively. This observation allows us to introduce dotted and undotted spinor indices,

$$\psi_L = (\psi_\alpha), \qquad \psi_R = (\bar{\psi}^{\dot\alpha}), \qquad \psi_L^* = (\bar{\psi}_{\dot\alpha}), \qquad \psi_R^* = (\psi^\alpha) \qquad (1.2)$$

---

[1]We adopt the convention in which the space-time metric $g_{\mu\nu}$ has signature $(+, -, -, -)$.

The transformation properties of these spinors under $SL(2,\mathbb{C})$ are as follows,

$$\psi'_\beta = M_\beta{}^\alpha \psi_\alpha, \qquad\qquad \bar{\psi}'_{\dot\beta} = [M^*]_{\dot\beta}{}^{\dot\alpha} \bar{\psi}_{\dot\alpha} = \bar{\psi}_{\dot\alpha}[M^\dagger]^{\dot\alpha}{}_{\dot\beta}$$

$$\bar{\psi}'^{\dot\beta} = [(M^\dagger)^{-1}]^{\dot\beta}{}_{\dot\alpha}\bar{\psi}^{\dot\alpha}, \qquad\qquad \psi'^\beta = [(M^T)^{-1}]^\beta{}_\alpha \psi^\alpha = \psi^\alpha[M^{-1}]_\alpha{}^\beta \qquad (1.3)$$

Obviously, the spinor indices can be raised and lowered by use of the antisymmetric tensors

$$(\epsilon_{\alpha\beta}) = -(\epsilon^{\alpha\beta}) = (\epsilon_{\dot\alpha\dot\beta}) = -(\epsilon^{\dot\alpha\dot\beta}) = i\sigma^2 \qquad (1.4)$$

according to

$$\psi_\alpha = \epsilon_{\alpha\beta}\psi^\beta, \qquad \psi^\alpha = \epsilon^{\alpha\beta}\psi_\beta, \qquad \bar{\psi}_{\dot\alpha} = \epsilon_{\dot\alpha\dot\beta}\bar{\psi}^{\dot\beta}, \qquad \bar{\psi}^{\dot\alpha} = \epsilon^{\dot\alpha\dot\beta}\bar{\psi}_{\dot\beta} \qquad (1.5)$$

Since the matrices M of $SL(2,\mathbb{C})$ are unimodular ($\det M = 1$), the ϵ-tensors are invariant under $SL(2,\mathbb{C})$ transformations.

The equation of motion of a free spin $\frac{1}{2}$ particle with mass m in terms of two-component Weyl spinors ψ_L and χ_R read

$$i\bar{\sigma}^\mu\partial_\mu\psi_L = m\chi_R, \qquad\qquad i\sigma^\mu\partial_\mu\chi_R = m\psi_L \qquad (1.6)$$

and thus we conclude that the generalized Pauli matrices carry one dotted and one undotted spinor index, $\sigma^\mu = (\sigma^\mu{}_{\alpha\dot\beta})$ and $\bar{\sigma}^\mu = (\bar{\sigma}^{\mu\dot\alpha\beta})$.

Both spinors ψ_L and χ_R can be combined to form a four-component Dirac spinor $\Psi_D = (\psi_L, \chi_R)^T$ satisfying the Dirac equation $(i\gamma^\mu\partial_\mu - m)\Psi_D = 0$ with the γ-matrices in the chiral representation given by

$$\gamma^\mu = \begin{pmatrix} 0 & \sigma^\mu \\ \bar{\sigma}^\mu & 0 \end{pmatrix}, \qquad\qquad \gamma_5 = \gamma^5 = i\gamma^0\gamma^1\gamma^2\gamma^3 = \begin{pmatrix} -\mathbb{1} & 0 \\ 0 & \mathbb{1} \end{pmatrix} \qquad (1.7)$$

The charge conjugated Dirac spinor is defined by $\Psi_D^c = C\bar{\Psi}_D^T$, where C is the charge conjugation matrix,

$$C = i\gamma^2\gamma^0 = \begin{pmatrix} i\sigma^2 & 0 \\ 0 & -i\sigma^2 \end{pmatrix} \qquad (1.8)$$

and $\bar{\Psi}_D = \Psi_D^\dagger\gamma^0$. Hence, $\Psi_D^c = (\chi_L, \psi_R)^T$ with $\chi_L = i\sigma^2\chi_R^*$ and $\psi_R = -i\sigma^2\psi_L^*$.

A Majorana spinor can be obtained from the Dirac spinor by imposing the constraint $\chi_R = \psi_R$, so that $\Psi_M = (\psi_L, \psi_R)^T$. Thus follows $\Psi_M^c = \Psi_M$, i.e. a Majorana fermion is its own antiparticle[2].

In sec. 1.3 the SM Lagrangian will be introduced in terms of two-component Weyl spinors. Hence it will be useful to set up a dictionary to translate bilinears in terms of four-component spinors into bilinears in terms of two-component spinors and vice versa. Defining the abbreviations

$$\chi\psi = \chi^\alpha\psi_\alpha, \qquad \chi\sigma^\mu\bar{\psi} = \chi^\alpha\sigma^\mu{}_{\alpha\dot\beta}\bar{\psi}^{\dot\beta}, \qquad \chi\sigma^{\mu\nu}\psi = \chi^\alpha\sigma^{\mu\nu}{}_\alpha{}^\beta\psi_\beta$$

$$\bar{\chi}\bar{\psi} = \bar{\chi}_{\dot\alpha}\bar{\psi}^{\dot\alpha}, \qquad \bar{\chi}\bar{\sigma}^\mu\psi = \bar{\chi}_{\dot\alpha}\bar{\sigma}^{\mu\dot\alpha\beta}\psi_\beta, \qquad \bar{\chi}\bar{\sigma}^{\mu\nu}\bar{\psi} = \bar{\chi}_{\dot\alpha}\bar{\sigma}^{\mu\nu\dot\alpha}{}_{\dot\beta}\bar{\psi}^{\dot\beta} \qquad (1.9)$$

---

[2]From now on we will drop the subscripts D and M on Dirac or Majorana spinors, respectively. It will become clear from the text what is meant.

and considering two four-component Dirac spinors $\Psi_i = (\psi_{Li}, \chi_{Ri})^T$, $i = 1, 2$, we obtain

$$\bar\Psi_1 \Psi_2 = \chi_1 \psi_2 + \bar\chi_2 \bar\psi_1, \qquad\qquad \bar\Psi_1 \gamma^\mu \Psi_2 = \bar\psi_1 \bar\sigma^\mu \psi_2 - \bar\chi_2 \bar\sigma^\mu \chi_1$$

$$\bar\Psi_1 \gamma_5 \Psi_2 = -\chi_1 \psi_2 + \bar\chi_2 \bar\psi_1, \qquad\qquad \bar\Psi_1 \gamma^\mu \gamma_5 \Psi_2 = -\bar\psi_1 \bar\sigma^\mu \psi_2 - \bar\chi_2 \bar\sigma^\mu \chi_1 \qquad (1.10)$$

for bilinears behaving like scalars, pseudoscalars, vectors and axialvectors under Lorentz transformations, respectively.

1.2 Foundations of Gauge Field Theories

Quantum field theories are characterized by a Lagrangian density with the interactions described by products of fields at the same space-time point. In elementary particle physics we observe two kinds of fields, namely matter fields and the forces acting between them. It is the concept of gauge field theories that seem to describe the interaction of both types of fields correctly.

Classical Lagrangian for Gauge Field Theories

Gauge field theories are defined as theories which are locally invariant under particular symmetry transformations. In the following discussion we will for simplicity consider only one Dirac spinor Ψ transforming in the fundamental representation of the non-abelian gauge group $SU(N)$. A general element of this group can be written as $U(\theta) = \exp\{i\theta^a T^a\}$ where in the case at hand the T^a are the generators in the fundamental representation and the θ^a space-time dependent functions. The structure constants belonging to this group will be denoted by f^{abc} and the coupling constant by g.

The most general renormalizable classical Lagrangian invariant under the non-abelian symmetry transformations

$$\Psi' = U(\theta)\Psi$$

$$V_\mu^{a'} T^a = U(\theta) V_\mu^a T^a U(\theta)^\dagger + \frac{i}{g} \left[\partial_\mu U(\theta)\right] U(\theta)^\dagger \qquad (1.11)$$

of the fermion field Ψ and the real gauge fields V_μ^a is given by[3]

$$\mathcal{L}_{\text{classical}} = -\frac{1}{4} V_{\mu\nu}^a V^{a\mu\nu} + \bar\Psi(i\slashed{D} - m)\Psi \qquad (1.12)$$

Here, m is the mass of the fermion field,

$$D_\mu = \partial_\mu + ig V_\mu^a T^a \qquad (1.13)$$

the covariant derivative coupling the fermion fields to the gauge bosons, and

$$V_{\mu\nu}^a = \partial_\mu V_\nu^a - \partial_\nu V_\mu^a - g f^{abc} V_\mu^b V_\nu^c \qquad (1.14)$$

the field strength tensor transforming under the adjoint representation of $SU(N)$. In abelian gauge theories the self-interactions of the gauge bosons contained in the gauge kinetic term given in (1.12) are absent due to the vanishing structure constants.

---

[3]A possible term proportional to $\epsilon_{\mu\nu\alpha\beta} V^{a\mu\nu} V^{a\alpha\beta}$ can be written as a total derivative and does not contribute in perturbation theory. Therefore it is not taken into account here.

Quantization of Gauge Field Theories

We will quantizise the classical Lagrangian given in the previous section using the path integral formalism. The generating functional for Green functions is given by

$$Z[J_\Psi, J_{\bar\Psi}, J_V] = \int \mathcal{D}V \, \mathcal{D}\bar\Psi \, \mathcal{D}\Psi \exp\left\{ i \int d^4x \left(\mathcal{L}_{\text{classical}} + J_\Psi \Psi - \bar\Psi J_{\bar\Psi} + J_V^{a\mu} V_\mu^a \right) \right\}$$
(1.15)

where J_Ψ, $J_{\bar\Psi}$ and J_V are external sources. However, this generating functional is mathematically inconsistent due to the gauge invariance of the classical Lagrangian. The emerging singularity results from the integration over configurations of the gauge fields V_μ^a which are related by gauge invariance by one another.

This problem has been solved by Faddeev and Popov by introducing a gauge fixing condition in the generating functional to avoid this overcounting. Their finding reads [106]

$$Z[J_\Psi, J_{\bar\Psi}, J_u, J_{\bar u}, J_V] = \int \mathcal{D}V \, \mathcal{D}\bar\Psi \, \mathcal{D}\Psi$$

$$\times \exp\left\{ i \int d^4x \left(\mathcal{L}_{\text{eff}} + J_\Psi \Psi - \bar\Psi J_{\bar\Psi} + J_{\bar u}^a u^a - \bar u^a J_u^a + J_V^{a\mu} V_\mu^a \right) \right\}$$
(1.16)

where the "effective" Lagrangian consists of the classical, a gauge fixing and the Faddeev-Popov Lagrangian,

$$\mathcal{L}_{\text{eff}} = \mathcal{L}_{\text{classical}} + \mathcal{L}_{\text{GF}} + \mathcal{L}_{\text{FP}}$$
(1.17)

Writing $F^a = \partial^\mu V_\mu^a$, the gauge fixing term is given by

$$\mathcal{L}_{\text{GF}} = -\frac{1}{2\xi} F^a F^a$$
(1.18)

with ξ being the gauge parameter, and the Faddeev-Popov Lagrangian reads

$$\mathcal{L}_{\text{FP}} = g \int d^4y \, \bar u^a(x) \frac{\delta F^a(x)}{\delta \theta^b(y)} \bar u^b(y) = -\bar u^a \partial^\mu \left(\partial_\mu \delta^{ac} + g f^{acd} V_\mu^d \right) u^c$$
(1.19)

which involves interactions of unphysical ghost fields. These fields, however, are essential in order to obtain a unitary S-matrix, and indeed they have already been introduced by Feynman to solve exactly this problem [107]. In the case of an abelian gauge theory, where all structure constants are equal to zero, the ghost fields decouple from the theory.

The generating functional for Green functions given in (1.16) is now well-defined and serves as the starting point for perturbative calculations. But, as is evident, this functional is no longer invariant under the $SU(N)$ gauge group and thus the Ward identities [108, 109] following from the classical Lagrangian are no longer valid in the quantizised theory. Fortunately, the gauge transformations can be extended by including transformations of the ghost fields to the so-called BRST transformations [110–112][4]. They give rise to generalized Ward identities known as Slavnov-Taylor identities [9, 11, 115, 116] which summarize all relationships between the Green functions resulting from local gauge invariance.

---

[4]The BRST symmetry can be formulated in a more symmetric form by linearizing the gauge fixing Lagrangian, $\mathcal{L}_{\text{GF}} = B^a F^a + \xi/2 \, B^a B^a$, where the auxiliary scalar field B^a is the so-called Nakanishi-Lautrup field [113, 114]. Eliminating this field by its purely algebraic equation of motion one recovers (1.18).

Renormalization of Gauge Field Theories

It is well known that the quantizised theory presented in the previous section suffers from divergencies arising in the calculation of Green functions when going beyond the tree-level approximation in perturbation theory. In renormalizable theories it is possible to redefine all involved parameters and fields order by order in perturbation theory to absorb these infinities systematically[5]. Calculating physical quantities within this redefined theory produces meaningful results which can be compared with experiments.

Practically this means that we replace the so-called bare quantities present in the original Lagrangian through renormalized ones,

$$g^{\text{bare}} = Z_g g, \qquad m^{\text{bare}} = Z_m m, \qquad \xi^{\text{bare}} = Z_V \xi$$

$$V_\mu^{a,\text{bare}} = \sqrt{Z_V} V_\mu^a, \quad \Psi^{\text{bare}} = \sqrt{Z_\Psi}\Psi, \quad u^{a,\text{bare}} = \sqrt{Z_u} u^a, \quad \bar{u}^{a,\text{bare}} = \sqrt{Z_u}\bar{u}^a \quad (1.20)$$

with some quantities having equal renormalization constants which is a consequence of Slavnov-Taylor identities. The resulting Lagrangian will then be split into a sum of one that resembles the bare Lagrangian, except that the bare parameters are now replaced by the renormalized ones, and a counterterm Lagrangian which individual terms will be treated as interactions,

$$\mathcal{L}_{\text{eff}}^{\text{bare}} = \mathcal{L}_{\text{eff}}^{\text{renormalized}} + \mathcal{L}_{\text{CT}} \tag{1.21}$$

The standard method to isolate the infinities within gauge theories in perturbation theory is dimensional regularization. Here, four dimensional space-time is analytically continued to $D = 4 - 2\epsilon$, dimensions and the singularities, which occur in integrals over loop momenta, emerge as simple poles in the parameter ϵ. As the unrenormalized Lagrangian is now defined in D dimensions the unrenormalized coupling constant becomes a dimensionfull parameter. By keeping the renormalized coupling constant dimensionless the t'Hooft mass scale μ appears,

$$g^{\text{bare}} = Z_g g \mu^\epsilon \tag{1.22}$$

In perturbation theory the renormalization constants can be expanded in powers of the coupling constant,

$$Z = 1 + \sum_{k=1}^\infty \left(\frac{\alpha}{4\pi}\right)^k \delta Z^{(k)} = 1 + \sum_{k=1}^\infty \sum_{l=0}^k \left(\frac{\alpha}{4\pi}\right)^k \frac{1}{\epsilon^l}\, \delta Z^{(k,l)} \tag{1.23}$$

where $\alpha = g/(4\pi)$. So far we only required the renormalization constants to absorb the infinities resulting in loop calculations, but also finite terms can be absorbed which defines different renormalization schemes. A particular useful renormalization scheme, especially for QCD corrections, is the $\overline{\text{MS}}$ scheme [117] which is obtained by replacing the t'Hooft mass scale, $\mu \to \mu\, e^{\gamma_E}/\sqrt{4\pi}$, where γ_E is Euler's constants, and afterward absorbing only infinities in the counterterms. In this way all renormalization constants are uniquely defined.

The dependence of the coupling constant g and the mass m on the t'Hooft mass scale μ is governed by the renormalization group equations [102–105, 118–120]. These equations

---

[5]Even in the case when everything is finite it is necessary to redefine parameters and fields order by order in perturbation theory in order to stay within a given renormalization prescription.

are derived from the definitions (1.20) using the fact that bare quantities are μ-independent. One finds

$$\mu\frac{dg}{d\mu} = -\epsilon g + \beta(g), \qquad\qquad \mu\frac{dm}{d\mu} = -\gamma_m(g)m \qquad\qquad (1.24)$$

where the β function and the anomalous dimension γ_m of the mass are given by

$$\beta(g) = -gZ_g^{-1}\,\mu\frac{dZ_g}{d\mu}, \qquad\qquad \gamma_m(g) = Z_m^{-1}\,\mu\frac{dZ_m}{d\mu} \qquad\qquad (1.25)$$

In so-called mass independent renormalization schemes, to which class the $\overline{\text{MS}}$ scheme belongs, the coefficients $\delta Z^{(k,l)}$ given in (1.23) are constants and hence the only μ-dependence of the renormalization constants resides in the coupling constant[6]. In such schemes, the perturbative expansion of β and γ_m reads

$$\beta(g) = 2g^3\frac{d}{dg^2}\sum_{k=1}^{\infty}\left(\frac{\alpha}{4\pi}\right)^k \delta Z_g^{(k,1)}$$

$$\gamma_m(g) = -2g^2\frac{d}{dg^2}\sum_{k=1}^{\infty}\left(\frac{\alpha}{4\pi}\right)^k \delta Z_m^{(k,1)} \qquad\qquad (1.26)$$

An efficient method to calculate the β function will be introduced in the next subsection.

Background Field Formalism

As already mentioned the generating functional given in (1.16) is not gauge-invariant but only invariant under BRST transformations. As a consequence, its associated Green functions do not directly reflect the underlying gauge invariance, but rather obey complicated Slavnov-Taylor identities resulting from BRST invariance. In addition, the Green functions depend on the particular gauge fixing chosen, and only physical quantities are gauge independent.

To avoid the explicit breaking the gauge symmetry the background field formalism was introduced [121, 122]. By decomposing the usual fields present in the classical Lagrangian given in (1.15) into quantum and background fields,

$$\Psi \to \Psi + \hat{\Psi}, \qquad\qquad V_\mu^a \to V_\mu^a + \hat{V}_\mu^a \qquad\qquad (1.27)$$

one can impose the gauge fixing necessary for quantization while maintaining the gauge invariance with respect to the background gauge field,

$$F^a = \hat{D}_\mu^{ab}V^{b\mu} = \left(\partial_\mu\delta^{ab} + gf^{abc}\hat{V}_\mu^c\right)V^{b\mu} \qquad\qquad (1.28)$$

Consequently, the Faddeev-Popov Lagrangian is also modified,

$$\mathcal{L}_{\text{FP}} = -\bar{u}^a\hat{D}_\mu^{ab}\left(\partial^\mu\delta^{bc} + gf^{bcd}[V^{d\mu} + \hat{V}^{d\mu}]\right)u^c \qquad\qquad (1.29)$$

---

[6]Strictly speaking this statement depends on the Lagrangian under consideration. For example, it is true within the SM, but the $\overline{\text{MS}}$ renormalized MSSM defines no mass independent renormalization scheme.

Since the fermion field does not enter the gauge fixing Lagrangian, the Feynman rules for background and quantum fermions are the same, and hence there is no need to distinguish them. The equivalence of the S-matrix in the background field formalism and the conventional one has been proven in [123].

As a result of the gauge transformations with respect to the background gauge field the derived Green functions fulfill Ward identities following from the classical Lagrangian. This is especially important for applications dealing with off-shell Green functions. Also, some calculations become greatly simplified in the background formalism. For example, due to the Ward identities, the renormalization constant linking the bare and renormalized background gauge field is given by the inverse of that of the coupling constant, $Z_{\hat{V}} = Z_g^{-2}$, which allows to calculate the β function from the two-point Green functions with background gauge fields on the external legs[7].

1.3 Lagrangian of the SM

The Lagrangian of the SM is based on the local $SU(3)_C \otimes SU(2)_L \otimes U(1)_Y$ symmetry, where the first factor describes the strong interactions of the fundamental particles, and the last two factors unify the electromagnetic and weak interactions. The spectrum of particles includes three generations of quarks and leptons, gauge bosons and one Higgs doublet.

Classical Lagrangian of the SM

The fermions incorporated in the SM together with their quantum number assignments are displayed in table 1.1. All of them are expressed in terms of left-handed Weyl spinors in the weak weak eigenstates basis indicated by the attached prime. More precisely, we define lepton and quark $SU(2)_L$ doublets to have lower spinor index while lepton and quark $SU(2)_L$ singlets, denoted by a superscript c, have upper spinor index. The corresponding right-handed singlets can be obtained by complex conjugation, $f_I'^{c*} = \bar{f}_I'^c$ with $f = e, u, d$. The index $I = 1, 2, 3$ labels generations, and upper indices $i, j, \ldots$, when present, will label components of $SU(2)_L$-doublets. The electric charge Q_{em} listed in the last column defines the weak hypercharge Y through $Q_{\text{em}} = \tau^3 + Y$, where τ^3 is the third component of the weak isospin.

For each factor of the SM gauge group we have as many gauge bosons as generators: for $SU(3)_C$ a gluon octet denoted by G_μ^a, for $SU(2)_L$ a weak isospin gauge boson triplet denoted by W_μ^a, and for the abelian factor $U(1)_Y$ a weak hypercharge gauge boson denoted by B_μ.

The classical Lagrangian of the SM invariant under local $SU(3)_C \otimes SU(2)_L \otimes U(1)_Y$ gauge transformations consists of several parts,

$$\mathcal{L}_{\text{SM}} = \mathcal{L}_{\text{gauge}} + \mathcal{L}_{\text{matter}} + \mathcal{L}_{\text{Yukawa}} + \mathcal{L}_{\text{Higgs}} \tag{1.30}$$

which will be discussed in some detail in what follows.

The Lagrangian containing the kinetic and self-interaction terms for all gauge bosons

---

[7]In fact, we have used this formalism to calculate the renormalization constants of QCD in the $\overline{\text{MS}}$ scheme up to two-loops, which are necessary for the calculation presented in chap. 4. Our findings agree with [84].

Matter and gauge fields		$SU(3)_C$	$SU(2)_L$	$U(1)_Y$	Q_{em}
Leptons	$l'_I = \begin{pmatrix} \nu'_I \\ e'_I \end{pmatrix}$	**1**	**2**	$-\frac{1}{2}$	$\begin{pmatrix} 0 \\ -1 \end{pmatrix}$
	e'^c_I	**1**	**1**	1	1
Quarks	$q'_I = \begin{pmatrix} u'_I \\ d'_I \end{pmatrix}$	**3**	**2**	$\frac{1}{6}$	$\begin{pmatrix} \frac{2}{3} \\ -\frac{1}{3} \end{pmatrix}$
	u'^c_I	$\bar{\mathbf{3}}$	**1**	$-\frac{2}{3}$	$-\frac{2}{3}$
	d'^c_I	$\bar{\mathbf{3}}$	**1**	$\frac{1}{3}$	$\frac{1}{3}$
Higgs boson	$\phi = \begin{pmatrix} \phi^+ \\ \phi^0 \end{pmatrix}$	**1**	**2**	$\frac{1}{2}$	$\begin{pmatrix} 1 \\ 0 \end{pmatrix}$
Gauge bosons	G^a_μ	**3**	**1**	0	0
	W^a_μ	**1**	**3**	0	$(0, \pm 1)$
	B_μ	**1**	**1**	0	0

Table 1.1: Particle spectrum of the SM.

expressed in terms of the field strength tensors

$$G^a_{\mu\nu} = \partial_\mu G^a_\nu - \partial_\nu G^a_\mu - g_s f_{abc} G^b_\mu G^c_\nu$$
$$W^a_{\mu\nu} = \partial_\mu W^a_\nu - \partial_\nu W^a_\mu - g_2 \epsilon_{abc} W^b_\mu W^c_\nu$$
$$B_{\mu\nu} = \partial_\mu B_\nu - \partial_\nu B_\mu \tag{1.31}$$

is given by

$$\mathcal{L}_{\mathrm{gauge}} = -\frac{1}{4} G^a_{\mu\nu} G^{a\mu\nu} - \frac{1}{4} W^a_{\mu\nu} W^{a\mu\nu} - \frac{1}{4} B_{\mu\nu} B^{\mu\nu} \tag{1.32}$$

Here, f_{abc} and ϵ_{abc} are the structure constants of $SU(3)_C$ and $SU(2)_L$, respectively. Furthermore, the gauge couplings corresponding to the three factors of the SM gauge group have been denoted by g_s, g_2 and g_1, respectively.

Kinetic terms for fermions and their couplings to gauge bosons are contained in

$$\mathcal{L}_{\mathrm{matter}} = i l'^\dagger_I \bar{\sigma}^\mu \left(\partial_\mu + i g_2 W^a_\mu \tau^a + i g_1 B_\mu Y \right) l'_I$$
$$+ i \bar{e}'^c_I \bar{\sigma}^\mu \left(\partial_\mu + i g_1 B_\mu Y \right) e'^c_I$$
$$+ i q'^\dagger_I \bar{\sigma}^\mu \left(\partial_\mu + i g_s G^a_\mu T^a + i g_2 W^a_\mu \tau^a + i g_1 B_\mu Y \right) q'_I$$

$$+ i\bar{u}_I'^c \bar{\sigma}^\mu \left(\partial_\mu + ig_s G_\mu^a \bar{T}^a + ig_1 B_\mu Y \right) u_I'^c$$

$$+ i\bar{d}_I'^c \bar{\sigma}^\mu \left(\partial_\mu + ig_s G_\mu^a \bar{T}^a + ig_1 B_\mu Y \right) d_I'^c \tag{1.33}$$

with T^a and τ^a being the generators of $SU(3)_C$ and $SU(2)_L$ in the **3** and **2** representations, respectively, $\bar{T}^a = -(T^a)^T$ the generator of $SU(3)_C$ in the $\bar{\mathbf{3}}$ representation, and Y the generator of $U(1)_Y$.

Mass terms for fermions are forbidden by gauge invariance, and therefore the Higgs field given in table 1.1 is introduced. Breaking the electroweak gauge symmetry of the SM down to electromagnetism with a non-vanishing vacuum expectation value (VEV) for the Higgs field, the fermions will aquire their masses. The couplings of the latter to the Higgs doublet are described by[8]

$$\mathcal{L}_{\text{Yukawa}} = -Y_E^{JI}(l_I'^T \phi^*)e_J'^c - Y_U^{JI}(q_I'^T \tilde{\phi})u_J'^c - Y_D^{JI}(q_I'^T \phi^*)d_J'^c + \text{h.c.} \tag{1.34}$$

where we defined $\tilde{\phi} = i\sigma^2 \phi^*$. The $U(1)_Y$ quantum number assignment of the Higgs doublet follows from the requirement that $\mathcal{L}_{\text{Yukawa}}$ is gauge invariant. In order to pass from the weak to the mass eigenstates basis we diagonalize the Yukawa couplings by the following redefinition of fermion fields with unitary matrices,

$$l_I'^1 = [S^{N\dagger}]_{IJ} l_J^1$$

$$l_I'^2 = [S^{E_L\dagger}]_{IJ} l_J^2, \qquad\qquad\qquad e_I'^{c*} = [S^{E_R\dagger}]_{IJ} e_J^{c*}$$

$$q_I'^1 = [S^{U_L\dagger}]_{IJ} q_J^1, \qquad\qquad\qquad u_I'^{c*} = [S^{U_R\dagger}]_{IJ} u_J^{c*}$$

$$q_I'^2 = [S^{D_L\dagger}]_{IJ} q_J^2, \qquad\qquad\qquad d_I'^{c*} = [S^{D_R\dagger}]_{IJ} d_J^{c*} \tag{1.35}$$

Since there are no mass terms for neutrinos in (1.34), we are free to choose $S^N = S^{E_L}$. The consequence of the operation (1.35) is the appearance of the CKM mixing matrix

$$K = S^{U_L\dagger} S^{D_L} \tag{1.36}$$

in the charged weak current interactions of quarks, which is the only source of flavor and CP violation in the SM [36, 37].

The gauge-kinetic term for the weak isospin Higgs doublet, its interactions with the gauge bosons and its self-interactions are contained in

$$\mathcal{L}_{\text{Higgs}} = \phi^\dagger \left(\overleftarrow{\partial}_\mu -ig_2 W_\mu^a \tau^a - ig_1 B_\mu Y \right) \left(\partial^\mu + igW^{a\mu}\tau^a + ig_1 B^\mu Y \right) \phi - V(\phi) \tag{1.37}$$

where

$$V(\phi) = -\mu^2 \phi^\dagger \phi + \lambda(\phi^\dagger \phi)^2 \tag{1.38}$$

is the potential for the Higgs doublet. In order for this potential to be bounded from below $\lambda > 0$ has to hold. Furthermore, the parameter μ^2 has to be real.

The potential for the Higgs doublet has for $\mu^2 < 0$ an absolute minimum at $\phi = 0$, but for $\mu^2 > 0$ it has an absolute minimum at $\phi^\dagger \phi = \mu^2/(2\lambda)$ which is clearly invariant under

---

[8]Note that for Grassmann numbers complex conjugation is defined by $(\psi\chi\cdots\xi)^* = \xi^*\cdots\chi^*\psi^*$, i.e. complex conjugation is equivalent to hermitian conjugation.

$SU(2)_L \otimes U(1)_Y$ transformations. In the latter case a VEV for the neutral component of the Higgs doublet,

$$\phi = \begin{pmatrix} G^+ \\ \frac{1}{\sqrt{2}}(v + h^0 + iG^0) \end{pmatrix} \tag{1.39}$$

where $v = \sqrt{\mu^2/\lambda}$, breaks electroweak symmetry down to electromagnetism. Here, h^0 is the physical Higgs field, and G^0 as well as G^+ are the unphysical Goldstone bosons corresponding to the broken generators of $SU(2)_L \otimes U(1)_Y$.

Particle Mass Spectrum

The physical gauge boson fields are obtained via[9]

$$W_\mu^\pm = \frac{1}{\sqrt{2}}(W_\mu^1 \mp iW_\mu^2), \qquad \begin{pmatrix} A_\mu \\ Z_\mu \end{pmatrix} = \begin{pmatrix} c_W & s_W \\ -s_W & c_W \end{pmatrix} \begin{pmatrix} B_\mu \\ W_\mu^3 \end{pmatrix} \tag{1.40}$$

where

$$s_W = \sin\theta_W = \frac{g_1}{\sqrt{g_1^2 + g_2^2}}, \qquad c_W = \cos\theta_W = \sqrt{1 - s_W} \tag{1.41}$$

and θ_W is the weak mixing angle. The masses of the Z and W bosons resulting from (1.37) read

$$M_Z^2 = \frac{1}{4}(g_1^2 + g_2^2)v^2, \qquad M_W^2 = \frac{1}{4}g^2v^2 \tag{1.42}$$

from which follows the tree-level relation $M_W = c_W M_Z$. The photon and gluons remain of course massless. The electromagnetic coupling is given by

$$e = g_1 c_W = g_2 s_W \tag{1.43}$$

Furthermore, the relations given in (1.42) fix the value of the parameter v.

The physical leptons and quarks are described by the Dirac spinors

$$\nu_I = \begin{pmatrix} l_I^1 \\ 0 \end{pmatrix}, \qquad e_I = \begin{pmatrix} l_I^2 \\ \bar{e}_I^c \end{pmatrix}, \qquad u_I = \begin{pmatrix} q_I^1 \\ \bar{u}_I^c \end{pmatrix}, \qquad d_I = \begin{pmatrix} q_I^2 \\ \bar{d}_I^c \end{pmatrix} \tag{1.44}$$

The neutrinos remain massless, $M_\nu = 0$, and the electron-type lepton, up-type and down-type quark masses read

$$M_E = \frac{v}{\sqrt{2}}S^{E_R}Y_E S^{E_L\dagger} = \mathrm{diag}(m_{e_1}, m_{e_2}, m_{e_3})$$

$$M_U = \frac{v}{\sqrt{2}}S^{U_R}Y_U S^{U_L\dagger} = \mathrm{diag}(m_{u_1}, m_{u_2}, m_{u_3})$$

$$M_D = \frac{v}{\sqrt{2}}S^{D_R}Y_D S^{D_L\dagger} = \mathrm{diag}(m_{d_1}, m_{d_2}, m_{d_3}) \tag{1.45}$$

The last physical particle is the Higgs boson h^0 with mass $M_{h^0}^2 = 2\lambda v^2$.

---

[9]The electric charge assignments can be easily seen by observing that $W_\mu^\pm$ and W_μ^a are eigenstates of the charge operator $[\tau^3]_{ab} = -i\epsilon^{3ab}$ in the adjoint representation with eigenvalues ± 1 and 0, respectively.

Quantization of the SM

In order to quantizise the classical SM Lagrangian given in (1.30) one has to add a gauge fixing term and the Faddeev-Popov Lagrangian. We choose a gauge fixing term in the so-called R_ξ gauge,

$$\mathcal{L}_{\mathrm{GF}} = -\frac{1}{2\xi_A}F_A F_A - \frac{1}{2\xi_Z}F_Z F_Z - \frac{1}{\xi_W}F_W^+ F_W^- - \frac{1}{2\xi_G}F_G^a F_G^a \tag{1.46}$$

where

$$F_A = \partial^\mu A_\mu, \qquad\qquad F_Z = \partial^\mu Z_\mu - M_Z \xi_Z G^0$$

$$F_W^\pm = \partial^\mu W_\mu^\pm \mp i M_W \xi_W G^\pm, \qquad\qquad F_G^a = \partial^\mu G_\mu^a \tag{1.47}$$

This ensures that all mixed gauge boson and Goldstone boson propagators present in (1.30) cancel. The loop calculations presented in later chapters will be performed in a general R_ξ gauge in which also the non-physical Goldstone bosons G^0 and G^+ with masses $M_{G^0}^2 = \xi_Z M_Z^2$ and $M_{G^+}^2 = \sqrt{\xi_W} M_W^2$, respectively, are present[10]. Since physical observables are independent of the gauge parameters, this serves as a non-trivial check of our calculations.

The next step is the introduction of the Faddeev-Popov Lagrangian. For the calculations presented in later chapters we only need the interactions of ghost fields with gluons,

$$\mathcal{L}_{\mathrm{FP}}^{\mathrm{QCD}} = -\bar{u}_G^a \partial^\mu \left(\partial_\mu \delta^{ac} + g_s f^{acd} G_\mu^d \right) u_G^c \tag{1.48}$$

The Faddeev-Popov Lagrangian relevant for the quantization of the electroweak sector of the SM is irrelevant for our purposes and thus we will not display it here (cf. [105]).

1.4 Background Field Formalism

In the background field formulation of the SM we split the fermions, the gauge bosons and the Higgs doublet contained in the classical Lagrangian in the (1.30) in quantum and background fields. In order to avoid tree-level mixing between gauge bosons and Goldstone bosons, and also between the photon and the Z boson, we choose as gauge fixing condition [124]

$$\mathcal{L}_{\mathrm{GF}} = -\frac{1}{2\xi_G}\hat{D}_\mu^{ab}\, G^{b\mu}$$

$$- \frac{1}{2\xi}\left[\partial_\mu B^\mu + i g_1 \xi(\hat{\phi}^\dagger Y \phi)^2\right]^2 - \frac{1}{2\xi}\left[\hat{D}_\mu^{ab}\, W^{b\mu} + i g_2 \xi(\hat{\phi}^\dagger \tau^a \phi)(\hat{\phi}^\dagger \tau^a \phi)\right]^2 \tag{1.49}$$

The second term within the square brackets expresses the R_ξ gauge condition. The interactions contained in this gauge fixing Lagrangian relevant for our purposes are given by[11]

---

[10]The physical gauge, in which the Goldstone bosons decouple from the theory, is obtained by sending the gauge parameters to infinity.

[11]Note that only the background Higgs doublet will aquire a non-vanishing VEV when breaking the electroweak symmetry down to electromagnetism.

$$\mathcal{L}_{\text{GF}} \supset \frac{1}{2\xi_G} G_\mu^a \partial^\mu \partial^\nu G_\nu^a + \frac{1}{2\xi} Z_\mu \partial^\mu \partial^\nu Z_\nu + \frac{1}{2\xi} A_\mu \partial^\mu \partial^\nu A_\nu + \frac{1}{\xi} W_\mu^+ \partial^\mu \partial^\nu W_\nu^-$$

$$- \frac{1}{2} \xi M_Z^2 G^0 G^0 - \xi M_W^2 G^+ G^- + M_Z Z_\mu \partial^\mu G^0$$

$$- M_W \left[i W_\mu^+ \partial^\mu G^- + \text{h.c.} \right] - g_s \frac{1}{\xi_G} f^{abc} (\partial^\mu G_\mu^a) G_\nu^b \hat{G}^{c\nu}$$

$$- e \left[\frac{i}{\xi} (\partial^\nu W_\nu^-) W_\mu^+ + M_W W_\mu^+ G^- + \text{h.c.} \right] \left(\hat{A}^\mu + \frac{c_W}{s_W} \hat{Z}^\mu \right) \tag{1.50}$$

Thus follows that in the background field formulation of the SM there is no $W^\pm G^\mp \hat{A}$ coupling.

The Faddeev-Popov Lagrangian involving the the interactions of ghost fields with quantum and background gluons reads

$$\mathcal{L}_{\text{FP}}^{\text{QCD}} = -\bar{u}_G^a \hat{D}_\mu^{ab} \left(\partial^\mu \delta^{bc} + g_s f^{bcd} [G^{d\mu} + \hat{G}^{d\mu}] \right) u_G^c \tag{1.51}$$

The one following from the electroweak part of the gauge fixing condition is irrelevant for our purposes and thus we will not display it here (cf. [124]).

Chapter 2

The Minimal Supersymmetric Extension of the Standard Model

In this chapter we present the MSSM, a phenomenologically viable supersymmetric extention of the SM with minimal particle content consistent with observed SM particles and which does not violate SM conservation laws [31–33, 125–127]. To construct supersymmetric Lagrangians we will use the elegant superfield formalism [128, 129]. Again we express the Lagrangian in terms of two-component Weyl spinors, since they are contained in chiral and gauge superfields which are the fundamental building blocks of supersymmetric models. We will break supersymmetry explicitly by adding additional soft supersymmetry-breaking terms and study the physical particle spectrum after electroweak symmetry breaking in terms of four-component spinors. A scenario with a heavy decoupled gluino, which finds it application in chap. 4, is also introduced.

2.1   Supersymmetric Lagrangians

Supersymmetry is a symmetry that turns a bosonic state into a fermionic state, and vice versa. Therefore the generators of the supersymmetry transformation must transform in the spinor representation of the Lorentz group. These new fermionic generators form together with the four momentum P_μ and the generators of the Lorentz transformations $M_{\mu\nu}$ a graded Lie algebra which features in addition to commutators also anticommutators in their defining relations.

The simplest supersymmetry algebra involves only one Weyl spinor generator Q_α, and is composed out of the Poincaré algebra supplemented with the following commutators and anticommutators,

$$[Q_\alpha, P_\mu] = [\bar{Q}_{\dot\alpha}, P_\mu] = 0$$

$$[Q_\alpha, M^{\mu\nu}] = i\sigma^{\mu\nu}{}_\alpha{}^\beta Q_\beta, \qquad\qquad [\bar{Q}^{\dot\alpha}, M^{\mu\nu}] = i\bar\sigma^{\mu\nu\dot\alpha}{}_{\dot\beta}\bar{Q}^{\dot\beta}$$

$$\{Q_\alpha, Q_\beta\} = \{\bar{Q}_{\dot\alpha}, \bar{Q}_{\dot\beta}\} = 0, \qquad\qquad \{Q_\alpha, \bar{Q}_{\dot\beta}\} = 2\sigma^\mu{}_{\alpha\dot\beta}P_\mu \qquad\qquad (2.1)$$

The irreducible representations of a supersymmetric field theory can be conveniently obtained working in real superspace which elements are composed out of four bosonic and four

fermionic coordinates, $\{x_\mu, \theta_\alpha, \bar{\theta}_{\dot\alpha}\}$, where x_μ is the coordinate in four-dimensional Minkowski space and θ_α a two-component Weyl spinor. The generators acting on so-called superfields in real superspace and fulfilling (2.1) are found to be [129][1]

$$P_\mu = i\partial_\mu, \qquad Q_\alpha = -i\partial_\alpha + (\sigma^\mu\bar{\theta})_\alpha\partial_\mu, \qquad \bar{Q}_{\dot\alpha} = i\bar{\partial}_{\dot\alpha} - (\theta\bar{\sigma}^\mu)_{\dot\alpha}\partial_\mu \qquad (2.2)$$

where $\partial_\alpha = \partial/\partial\theta^\alpha$ and $\bar{\partial}_{\dot\alpha} = \partial/\partial\bar{\theta}^{\dot\alpha}$. For our purposes it is sufficient to consider only superfields transforming as Lorentz scalars, which in full generality can be written as

$$\mathcal{F}(x,\theta,\bar{\theta}) = f(x) + \theta\phi(x) + \bar{\theta}\bar{\chi}(x) + (\theta\theta)M(x) + (\bar{\theta}\bar{\theta})N(x)$$

$$+ (\theta\sigma^\mu\bar{\theta})V_\mu(x) + (\theta\theta)\bar{\theta}\bar{\lambda}(x) + (\bar{\theta}\bar{\theta})\theta\eta(x) + \frac{1}{2}(\theta\theta)(\bar{\theta}\bar{\theta})D(x) \qquad (2.3)$$

The so-called component fields f, M, N, D are complex scalars fields, ϕ, η and $\bar{\chi}$, $\bar{\lambda}$ left-handed and right-handed Weyl spinors fields, respectively, and V_μ is a complex vector field. This superfield is however reducible. To find irreducible superfields we define covariant derivatives,

$$D_\alpha = \partial_\alpha - i(\sigma^\mu\bar{\theta})_\alpha\partial_\mu, \qquad \bar{D}_{\dot\alpha} = -\bar{\partial}_{\dot\alpha} + i(\theta\bar{\sigma}^\mu)_{\dot\alpha}\partial_\mu \qquad (2.4)$$

which anticommute with the generators Q_α and $\bar{Q}_{\dot\alpha}$. Hence we can impose further covariant conditions, i.e. invariant under supersymmetry transformations, on the general superfield resulting chiral superfields, $\bar{D}_{\dot\alpha}\mathcal{F} = 0$, antichiral superfields, $D_\alpha\mathcal{F} = 0$, and vector superfields, $\mathcal{F} = \mathcal{F}^\dagger$. It turns out that these superfields are irreducible.

Chiral Superfields

Let us consider from the very beginning a non-abelian supersymmetric gauge theory. The coupling constant of the non-abelian gauge group, here again assumed to be $SU(N)$, will be denoted by g, the generators by T^a with the index a running over the dimension of the adjoint representation, and the structure constants by f^{abc}.

An important consequence of the theorems of [130, 131] is the fact that the generators T^a have to commute with the supersymmetry generators,

$$[T^a, Q_\alpha] = [T^a, \bar{Q}_{\dot\alpha}] = 0 \qquad (2.5)$$

Therefore all members of chiral and vector superfields have to have to reside in the same representation of the gauge group.

Chiral superfields are characterized by the condition $\bar{D}_{\dot\alpha}\Phi = 0$, where in our case $\Phi = (\Phi_1, \ldots, \Phi_N)^T$ is in the fundamental representation. For simplicity we will again consider only one chiral superfield. From the defining condition it follows that the most general form of this chiral superfield is given by

$$\Phi(y,\theta) = \phi(y) + \sqrt{2}\,\theta\psi(y) + (\theta\theta)F(y) \qquad (2.6)$$

where $y^\mu = x^\mu - i(\theta\sigma^\mu\bar{\theta})$. Re-expressing this in terms of x^μ results in

$$\Phi(x,\theta,\bar{\theta}) = \phi(x) + \sqrt{2}\,\theta\psi(x) + (\theta\theta)F(x)$$

$$- i(\theta\sigma^\mu\bar{\theta})\,\partial_\mu\phi(x) + \frac{i}{\sqrt{2}}(\theta\theta)\,\partial_\mu\psi(x)\sigma^\mu\bar{\theta} - \frac{1}{4}(\theta\theta)(\bar{\theta}\bar{\theta})\,\partial_\mu\partial^\mu\phi(x) \qquad (2.7)$$

---

[1]The irreducible representations can be found considering only the sub-algebra of (2.1) consisting out of the generators P_μ and Q_α.

Thus the chiral superfield contains a complex scalar field $\phi(x)$, a left-handed Weyl spinor field $\psi(x)$ and a complex scalar field $F(x)$. Antichiral superfields characterized by the condition $D_\alpha \Phi^\dagger$ are simply obtained by hermitian conjugation of the above given chiral superfield as the notation suggests.

Acting with a infinitesimal supersymmetric transformation $i\epsilon Q + i\bar{\epsilon}\bar{Q}$, where ϵ is a constant Weyl spinor parameter, on a chiral superfield, we find the supersymmetry transformations of the component fields,

$$\delta_S \phi = \sqrt{2}\epsilon\psi$$

$$\delta_S \psi_\alpha = \sqrt{2}\left[\epsilon_\alpha F - i(\sigma^\mu\bar{\epsilon})_\alpha \partial_\mu \phi\right]$$

$$\delta_S F = i\sqrt{2}\partial_\mu(\psi\sigma^\mu\bar{\epsilon}) \tag{2.8}$$

Hence we find that fermions transform into bosons, and vice versa.

Vector Superfields

Vector superfields are characterized by the condition $V = V^\dagger$. In our case this vector field is matrix-valued, $V = V^a T^a$, and its most general form in terms of component fields is given by

$$V(x,\theta,\bar{\theta}) = C(x) + \left\{i\theta\chi(x) + \frac{i}{2}(\theta\theta)M(x) + \text{h.c}\right\} + (\theta\sigma^\mu\bar{\theta})V_\mu$$

$$+ \left\{i(\theta\theta)\bar{\theta}\left[\bar{\lambda}(x) - \frac{i}{2}\bar{\sigma}^\mu\partial_\mu\phi(x)\right] + \text{h.c}\right\} + \frac{1}{2}(\theta\theta)(\bar{\theta}\bar{\theta})\left[D(x) - \frac{1}{2}\partial_\mu\partial^\mu C(x)\right] \tag{2.9}$$

where the last two terms are chosen such that the component fields $\lambda(x)$ and $D(x)$ will be invariant under abelian supersymmetric gauge transformations. Applying a infinitesimal supersymmetric transformation gives obviously lengthier expressions for the transformations of the component fields than for the chiral superfield. We will only quote the important result

$$\delta_S D = \partial_\mu\left(\epsilon\sigma^\mu\bar{\lambda} + \lambda\sigma^\mu\bar{\epsilon}\right) \tag{2.10}$$

Non-abelian supersymmetric gauge transformations for vector superfields are defined through

$$e^{2gV} \rightarrow e^{2gV'} = e^{-2ig\Lambda^\dagger}e^{2gV}e^{2ig\Lambda} \tag{2.11}$$

where $\Lambda = \Lambda^a T^a$ with Λ^a being chiral superfields. Expanding this in orders of the coupling constant g results in

$$V'^a = V^a + i(\Lambda^a - \Lambda^{a\dagger}) - gf^{abc}V^b(\Lambda^c - \Lambda^{c\dagger} - i\Lambda^b\Lambda^{c\dagger}) + \ldots \tag{2.12}$$

This expansion shows that we can adjust the chiral superfield Λ^a to obtain the vector superfield in the so-called Wess-Zumino gauge,

$$V(x,\theta,\bar{\theta}) = (\theta\sigma^\mu\bar{\theta})V_\mu(x) + i(\theta\theta)\bar{\theta}\bar{\lambda}(x) - i(\bar{\theta}\bar{\theta})\theta\lambda(x) + \frac{1}{2}(\theta\theta)(\bar{\theta}\bar{\theta})D(x) \tag{2.13}$$

This vector superfield contains a real vector field $V_\mu^a(x)$, a left-handed Weyl spinor field $\lambda^a(x)$ and a real scalar field $D^a(x)$. However, the vector superfield in the Wess-Zumino gauge is not invariant under supersymmetry transformations in the sense, that the M and the χ components are reintroduced.

Performing a supersymmetric gauge transformation on this vector superfield with the component fields of Λ^a fulfilling $\psi^a = F^a = 0$ and ϕ^a being real and infinitesimally small we obtain

$$V_\mu'^a = V_\mu^a + 2\partial_\mu\phi^a - 2gf_{abc}V_\mu^b\phi^c$$

$$\lambda_\alpha'^a = \lambda_\alpha^a - 2gf_{abc}\lambda_\alpha^b\phi^c$$

$$D'^a = D^a - 2gf_{abc}D^b\phi^c \tag{2.14}$$

Therefore, the vector component field transforms under a usual non-abelian gauge transformation, and the field strength tensor

$$F_{\mu\nu}^a = \partial_\mu V_\nu^a - \partial_\nu V_\mu^a - gf_{abc}V_\mu^b V_\nu^c \tag{2.15}$$

under the adjoint representation.

The supersymmetric field strength tensor of the non-abelian vector superfield V is defined through

$$W_\alpha = -\frac{1}{8g}(\bar{D}\bar{D})e^{-2gV}D_\alpha e^{2gV} = -\frac{1}{4}(\bar{D}\bar{D})D_\alpha V - \frac{1}{4}g(\bar{D}\bar{D})[D_\alpha V, V] \tag{2.16}$$

The last equality is only valid if V is in the Wess-Zumino gauge which we will assume from now on. It is important to note that under a supersymmetric gauge transformation

$$W_\alpha \rightarrow W_\alpha' = e^{-2ig\Lambda}W_\alpha e^{2ig\Lambda} \tag{2.17}$$

which is also valid for general vector superfields V. In terms of component fields $W_\alpha = W_\alpha^a T^a$ can be written as

$$W_\alpha^a(y, \theta, \bar{\theta}) = i\lambda_\alpha^a(y) - \theta_\alpha D^a(y) + i(\sigma^{\mu\nu}\theta)_\alpha F_{\mu\nu}^a(y) + (\theta\theta)(\sigma^\mu D_\mu^{ac}\bar{\lambda}^c(y))_\alpha \tag{2.18}$$

with the gauge-covariant derivative $D_\mu^{ac} = \partial_\mu\delta^{ac} - gf^{abc}V_\mu^b$.

Constructing Supersymmetric Lagrangians

First of all we have to define a gauge transformation for the chiral superfields,

$$\Phi \rightarrow \Phi' = e^{-2ig\Lambda}\Phi \tag{2.19}$$

where Λ is the matrix-valued chiral superfield which was already introduced in (2.11). Indeed, since Φ' should be a chiral superfield the Λ^a have to also to be chiral superfields.

To construct supersymmetric Lagrangians one only has to take the term of a superfield or products thereof which contains the component field of highest mass dimension[2]. The

---

[2]We note that chiral and vector superfields have mass dimension 1 and 0, respectively, while those of θ is $-\frac{1}{2}$. Therefore both the scalar field ϕ and the gauge boson V_μ^a have mass dimension 1, the fermion fields ψ and λ have mass dimension $\frac{3}{2}$, and the auxiliary fields F and D^a have mass dimension 2.

component fields with this property are called the highest components and are identified with the F_i and D^a components in the case of a single chiral or vector superfield. The resulting Lagrangian density then transforms into a total derivative under a supersymmetry transformation, see e.g. (2.8) and (2.10), which leaves the corresponding action invariant.

A gauge-invariant supersymmetric Lagrangian for chiral superfields can now be written down,

$$\mathcal{L}_{\text{chiral}} = \Phi^\dagger e^{2gV} \Phi \big|_{\theta\theta\bar\theta\bar\theta} = (D_\mu \phi_i)^* (D^\mu \phi_i) + i\bar\psi_i \bar\sigma^\mu D_\mu \psi_i$$
$$+ F_i^* F_i + \left[i\sqrt{2} g(\phi_i^* T_{ij}^a \psi_j)\lambda^a + \text{h.c.} \right] + g(\phi_i^* T_{ij}^a \phi_j)D^a \qquad (2.20)$$

with the covariant derivatives given by

$$D_\mu \phi_i = \partial_\mu \phi_i + ig V_\mu^a T_{ij}^a \phi_j, \qquad\qquad D_\mu \psi_i = \partial_\mu \psi_i + ig V_\mu^a T_{ij}^a \psi_j \qquad (2.21)$$

A gauge-invariant supersymmetric Lagrangian for vector superfields reads

$$\mathcal{L}_{\text{vector}} = \frac{1}{2}\text{Tr}[W^\alpha W_\alpha]\Big|_{\theta\theta, y\to x} + \text{h.c.} = -\frac{1}{4} F_{\mu\nu}^a F^{a\mu\nu} + i\bar\lambda^a \bar\sigma^\mu D_\mu \lambda^a + \frac{1}{2} D^a D^a \qquad (2.22)$$

The last term we have to specify is the so-called superpotential. Requiring renormalizability of the theory its most general form reads

$$W(\Phi) = \frac{1}{2} m_{ij} \Phi_i \Phi_j + \frac{1}{6} y_{ijk} \Phi_i \Phi_j \Phi_k$$
$$= W(\phi) + W_i \left[\sqrt{2}\theta\psi_i + (\theta\theta)F_i \right] - \frac{1}{2} W_{ij}(\theta\theta)\psi_i \psi_j \qquad (2.23)$$

where we defined

$$W_i = \frac{\partial W(\phi)}{\partial \phi_i}, \qquad\qquad W_{ij} = \frac{\partial^2 W(\phi_K)}{\partial \phi_i \partial \phi_j} \qquad (2.24)$$

The mass parameters m_{ij} and the Yukawawa couplings y_{ijk} appearing in the superpotential are totally symmetric under the interchange of their indices. Further constraints on these parameters follow from gauge-invariance. The Lagrangian build up from the superpotential in terms of component fields reads

$$\mathcal{L}_{\text{pot}} = W(\Phi)\big|_{\theta\theta, y\to x} + \text{h.c.} = -\frac{1}{2} W_{ij}\psi_i \psi_j + W_i F_i + \text{h.c.} \qquad (2.25)$$

To summarize, the most general renormalizable supersymmetric and gauge-invariant Lagrangian for non-abelian gauge groups is given by

$$\mathcal{L}_{\text{susy}} = -\frac{1}{4} F_{\mu\nu}^a F^{a\mu\nu} + i\bar\lambda^a \bar\sigma^\mu D_\mu \lambda^a + (D_\mu \phi_i)^* (D^\mu \phi_i) + i\bar\psi_i \bar\sigma^\mu D_\mu \psi_i$$
$$- \left[\frac{1}{2} \frac{\partial^2 W}{\partial \phi_i \partial \phi_j} \psi_i \psi_j - \left(\frac{\partial W}{\partial \phi_i} \right) F_i + \text{h.c.} \right] + F_i^* F_i$$
$$+ \left[i\sqrt{2} g(\phi_i^* T_{ij}^a \psi_j)\lambda^a + \text{h.c.} \right] + g(\phi_i^* T_{ij}^a \phi_j)D^a + \frac{1}{2} D^a D^a \qquad (2.26)$$

The auxiliary fields, which appear naturally in the superfield formalism, guarantee that we have a supersymmetric algebra which closes off-shell. We can eliminate them to obtain the on-shell Lagrangian by their purely algebraic equations of motion,

$$F_i = - \left(\frac{\partial W}{\partial \phi_i} \right)^* , \qquad\qquad D^a = -g(\phi_i^* T_{ij}^a \phi_j) \qquad (2.27)$$

The complete scalar potential of this theory is given by

$$V_{\text{scalar}} = F_i^* F_i + \frac{1}{2} D^a D^a = \left(\frac{\partial W}{\partial \phi_i} \right)^* \left(\frac{\partial W}{\partial \phi_i} \right) + \frac{1}{2} g^2 (\phi_i^* T_{ij}^a \phi_j)^2 \geq 0 \qquad (2.28)$$

and hence is always positive semi-definit. The two terms appearing in this scalar potential are called F- and D-terms.

An important consequence of the supersymmetric Lagrangian given in (2.26) is that the component fields belonging to a chiral or vector superfield are degenerate in mass. Therefore supersymmetry cannot be exact in nature and thus has to be broken either spontaneously or explicitly. Breaking supersymmetric spontaneously is of course from a theoretical point of view more appealing. To this end we first recall that supersymmetry is spontaneously broken if, and only if, the scalar potential given in (2.28) is unequal to zero. Thus non-vanishing F- and D-terms signal spontaneous supersymmetry-breaking. However, in models which do lead to non-vanishing F- or D-terms [132,133] problems arise from so-called "mass sum rules" which hold in any theory with spontaneously broken supersymmetry [134]. Nature requires a large mass difference between particles and their superpartners in order to make them invisible in present experiments, and the "mass sum rules" valid within a spontaneously broken supersymmetric SM cannot be arranged to fulfill this boundary condition. Furthermore, we have a massless Goldstone fermion in the particle spectrum after spontaneously breaking the global supersymmetry.

To summarize, breaking global supersymmetry spontaneously runs into phenomenological difficulties. The only way out is an explicit breaking of global supersymmetry. This explicit breaking should however solve the naturalness problem, i.e. stabilize the Higgs boson mass and thus the weak scale without fine-tuning[3]. Such terms which break supersymmetry explicitely and generate no quadratic divergences are called "soft-breaking" terms.

Returning to our $SU(N)$ supersymmetric gauge theory with one chiral superfield Φ, the most general renormalizable soft supersymmetric-breaking Lagrangian can be written as [126,136]

$$\mathcal{L}_{\text{soft}} = \frac{1}{2} \left(M_\lambda \lambda^a \lambda^a + \text{h.c.} \right) - m_{ij}^2 \phi_i \phi_j^*$$

$$- \left[\frac{1}{2} b_{ij} \phi_i \phi_j + \frac{1}{6} a_{ijk} \phi_i \phi_j \phi_k + \frac{1}{2} c_{ijk} \phi_i^* \phi_j \phi_k + \text{h.c.} \right] \qquad (2.29)$$

---

[3]Fermion masses behave natural in the sense that they do not receive large quantum corrections if their tree-level masses are small, owing to an approximate chiral symmetry which gets restored in the limit where the fermion masses are set to zero. For scalar masses this is however completely different. They behave unnatural, since even in the case when its tree-level mass is set to zero nothing protects this mass from receiving large, quadratically divergent, quantum corrections. In supersymmetric theories, however, cancellation of quadratic divergences occurs as a consequence of the non-renormalization theorem [135].

which consists of gaugino and scalar mass terms and trilinear scalar interactions[4]. Further constraints on the soft parameters come from gauge-invariance. We have not included soft mass terms for chiral superfield fermions because these could always be removed by a redefinition of the superpotential parameters and the parameters m_{ij}^2 and c_{ijk}.

2.2 Lagrangian of the MSSM

Our starting point for the construction of the MSSM Lagrangian is (2.26) taking into account (2.27). But let us first give a precise definition of the MSSM [137]:

- Minimal particle content consistent with observed SM particles and supersymmetry.

- $SU(3)_C \otimes SU(2)_L \otimes U(1)_Y$ gauge invariance.

- Most general soft (dim < 4) supersymmetric breaking terms.

For every field of the SM one has to postulate a superpartner with exactly the same quantum numbers but with different spin. More specifically, the quarks and leptons are promoted to chiral superfields adding scalar quarks and leptons to the spectrum. The scalar superpartners of leptons and quarks are called sleptons and squarks, respectively. For distinction these scalar partners are dressed with a tilde. The superscript c denotes here charge conjugated scalars being singlets under $SU(2)_L$.

The gauge bosons are promoted to vector superfields by adding the corresponding gauginos to the spectrum. Each SM gauge boson has to get a spin $\frac{1}{2}$ supersymmetric partner: gluinos λ_G^a belonging to the gluons G_μ^a, winos λ_W^a belonging to the W_μ^a bosons, and the bino λ_B belonging to the B-boson.

Finally, the Higgs boson is also promoted to a chiral superfield with a higgsino as superpartner. However, in the MSSM we need at least two weak isospin Higgs doublets,

$$h_1 = \begin{pmatrix} h_1^1 \\ h_1^2 \end{pmatrix}, \qquad\qquad h_2 = \begin{pmatrix} h_2^1 \\ h_2^2 \end{pmatrix} \tag{2.30}$$

with $U(1)_Y$ quantum numbers $-\frac{1}{2}$ and $\frac{1}{2}$, respectively. This is because the superpotential must not contain complex conjugated scalar fields, as can be seen from (2.23), and therefore we need Yukawa couplings of type II in order to give all SM fermions masses. Furthermore the two Higgs doublets must have opposite weak hypercharge. Only in this case cancellation of the triangle anomalies with higgsinos, the spin $\frac{1}{2}$ superpartners of the Higgs bosons, in the loops occurs. Again, higgsinos will be dressed with a tilde.

Having the full particle content of the MSSM by hand, we can write down the most general renormalizable superpotential respecting $SU(3)_C \otimes SU(2)_L \otimes U(1)_Y$ gauge invariance,

$$W_{\text{MSSM}} = -\mu\epsilon_{ij}h_1^i h_2^j + Y_E^{JI}\epsilon_{ij}h_1^i \tilde{l}_I^{\prime j}\tilde{e}_J^{\prime c} - Y_U^{JI}\epsilon_{ij}h_2^i \tilde{q}_I^{\prime j}\tilde{u}_J^{\prime c} + Y_D^{JI}\epsilon_{ij}h_1^i \tilde{q}_I^{\prime j}\tilde{d}_J^{\prime c} \tag{2.31}$$

Here, we tacitly imposed a multiplicatively defined quantum number called R-parity, defined as

$$P_R = (-1)^{3(B-L)+2s} \tag{2.32}$$

---

[4]Higher powers of ϕ are forbidden since they generate quadratic divergences at the two-loop level [136].

where s is the spin, B the baryon and L the lepton number of the MSSM particle. The terms which are allowed by gauge invariance but forbidden by R-parity conservation would either violate baryon or lepton number conservation, and thus can easily lead to unacceptable physical consequences, e.g. the proton could become unstable. Thus our superpotential is the most general version respecting SM conservation laws. An immediate consequence of this additional symmetry is the fact that the lightest supersymmetric particle is necessarily stable.

To obtain the supersymmetric Lagrangian of the MSSM we only have to plug this superpotential into the Lagrangian given in (2.26). It is interesting to observe that this Lagrangian has one parameter less than the SM. The coupling λ defined in (1.38) is expressed in terms of gauge couplings as can be seen in (2.33) due to supersymmetry invariance. However, supersymmetry-breaking will introduce lots of new parameters.

Besides the problem that all particles and their corresponding superpartners have equal masses, we have another problem related with electroweak symmetry-breaking. The minimum of the scalar Higgs potential

$$V_{\text{Higgs}} = |\mu|^2(h_1^\dagger h_1 + h_2^\dagger h_2) + \frac{1}{2}g_2^2|h_2^i h_1^{i*}|^2 + \frac{1}{8}(g_1^2 + g_2^2)(h_2^\dagger h_2 - h_1^\dagger h_1)^2 \qquad (2.33)$$

sits necessarily at $\langle h^1 \rangle = \langle h^2 \rangle = 0$ corresponding to a vacuum with unbroken electroweak symmetry. This is obvious since the scalar potential of a supersymmetric Lagrangian is always positive semi-definit. Therefore our MSSM Lagrangian specified so far cannot accommodate a vacuum with spontaneously broken electroweak symmetry and thus breaking supersymmetry is necessarily related with electroweak symmetry-breaking.

Specializing to the case of the MSSM with R-parity conservation we can write down the most general soft-breaking Lagrangian[5]

$$\mathcal{L}_{\text{soft}} = \frac{1}{2}\left\{M_3\lambda_G^a\lambda_G^a + M_2\lambda_W^a\lambda_W^a + M_1\lambda_B\lambda_B + \text{h.c.}\right\} - m_{h_1}^2 h_1^\dagger h_1 - m_{h_2}^2 h_2^\dagger h_2$$

$$- [M_{\tilde{L}}^2]_{IJ}\tilde{l}_I^{\prime\dagger}\tilde{l}_J^\prime - [M_{\tilde{E}}^2]_{JI}\tilde{e}_I^{\prime c*}\tilde{e}_J^{\prime c} - [M_{\tilde{Q}}^2]_{IJ}\tilde{q}_I^{\prime\dagger}\tilde{q}_J^\prime - [M_{\tilde{U}}^2]_{JI}\tilde{u}_I^{\prime c*}\tilde{u}_J^{\prime c} - [M_{\tilde{D}}^2]_{JI}\tilde{d}_I^{\prime c*}\tilde{d}_J^{\prime c}$$

$$+ \left\{b\epsilon_{ij}h_1^i h_2^j - [A_E^{\prime*}]_{IJ}\epsilon_{ij}h_1^i\tilde{l}_I^{\prime j}\tilde{e}_J^{\prime c} + [A_U^{\prime*}]_{IJ}\epsilon_{ij}h_2^i\tilde{q}_I^{\prime j}\tilde{u}_J^{\prime c} - [A_D^{\prime*}]_{IJ}\epsilon_{ij}h_1^i\tilde{q}_I^{\prime j}\tilde{d}_J^{\prime c} + \text{h.c.}\right\} \quad (2.34)$$

Due to $SU(2)_L$ gauge invariance both components of the slepton and the squark doublets must have the same mass matrices $M_{\tilde{L}}^2$ and $M_{\tilde{Q}}^2$, respectively.

Adding this soft breaking Lagrangian to the supersymmetric part we get the total Lagrangian of the MSSM with softly broken supersymmetry, SM gauge group and R-parity invariance, $\mathcal{L}_{\text{MSSM}} = \mathcal{L}_{\text{susy}} + \mathcal{L}_{\text{soft}}$. This Lagrangian defines a theory with an huge parameter space but not all of them are physical. In order to eliminate unnecessary degrees of freedom we redefine fields and parameters such, that the parameter b is real and positive, and furthermore, the Yukawa couplings are diagonal. The latter can be achieved if we change to the so-called super-CKM basis of fields, in which we redefine the leptons and quarks according to (1.35) and perform the same redefinitions for sleptons and squarks. Having done all redefinitions we still have 105 new parameters in addition to the ones of the SM. However,

---

[5]Here, we follow the standard approach and neglect the c_{ijk}-terms, which is consistent with renormalization. Once setting them equal to zero they are not generated through renormalization group running to all orders in perturbation theory [137].

not all of these parameters are arbitrary but quite a number of them are experimentally constraint. The inclusion of the soft-breaking Lagrangian shows that the sparticles can now easily be heavy and therefore out of reach of present experiments. Furthermore, the Higgs potential is changed and electroweak symmetry-breaking can be arranged.

2.3 Electroweak Symmetry-Breaking

The minimum of the Higgs potential (2.33) including terms from (2.34) with pure Higgs field content should break electroweak symmetry down to electromagnetism. To have an unbroken $U(1)_{\text{em}}$ at the minimum of the potential only the neutral components of the Higgs doublets have to get vacuum expectation values. Performing a $SU(2)_L$ gauge transformation we can take $h_1^2 = 0$ at the minimum without loss of generality. Then the minimization condition

$$\left.\frac{\partial V_{\text{Higgs}}}{\partial h_1^2}\right|_{h_1^2=0} \overset{!}{=} 0 \tag{2.35}$$

requires that also $h_2^1 = 0$ at the minimum. So we are left with the simpler potential

$$V_{\text{Higgs}} = M_{h_1}^2|h_1^1|^2 + M_{h_2}^2|h_2^2|^2 - \left[bh_1^1 h_2^2 + \text{h.c.}\right] + \frac{1}{8}(g_1^2 + g_2^2)(|h_2^2|^2 - |h_1^1|^2)^2 \tag{2.36}$$

where $M_{h_i}^2 = m_{h_i}^2 + |\mu|^2$ for $i = 1, 2$. Since b is real and positive $h_1^1 h_2^2$ also has to be real and positive in order to have a minimum which spontaneously breaks electroweak symmetry. Thus $\langle h_1^1 \rangle$ and $\langle h_2^2 \rangle$ must have opposite phases. By a $U(1)_Y$ gauge transformation we can make them both real and positive without loss of generality,

$$\langle h_1^1 \rangle = \frac{v_1}{\sqrt{2}} = \frac{v}{\sqrt{2}}\cos\beta, \qquad\qquad \langle h_2^2 \rangle = \frac{v_2}{\sqrt{2}} = \frac{v}{\sqrt{2}}\sin\beta \tag{2.37}$$

Hence we have no spontaneously broken CP symmetry in the Higgs sector.

Expanding the Higgs fields around their vacuum expectation values,

$$h_1 = \begin{pmatrix} \frac{1}{\sqrt{2}}(v_1 + \sigma_1^0 + i\varphi_1^0) \\ \varphi_1^- \end{pmatrix}, \qquad h_2 = \begin{pmatrix} \varphi_2^+ \\ \frac{1}{\sqrt{2}}(v_2 + \sigma_2^0 + i\varphi_2^0) \end{pmatrix} \tag{2.38}$$

we see that the Higgs potential contains terms linear in fields,

$$V_{\text{Higgs}} \supset t_1\sigma_1^0 + t_2\sigma_2^0, \tag{2.39}$$

where

$$t_{1,2} = v_{1,2}\left[M_{h_{1,2}}^2 - b\frac{v_{2,1}}{v_{1,2}} + \frac{1}{8}(g_1^2 + g_2^2)(v_{1,2}^2 - v_{2,1}^2)\right] \tag{2.40}$$

are the tree-level tadpoles. At the correct minimum of the Higgs potential these tadpoles vanish. This follows from the minimization conditions for the neutral Higgs fields

$$\frac{\partial V_{\text{Higgs}}}{\partial h_1^1} = \frac{\partial V_{\text{Higgs}}}{\partial h_2^2} \overset{!}{=} 0, \tag{2.41}$$

taken at $h_1^1 = v_1/\sqrt{2}$ and $h_2^2 = v_2/\sqrt{2}$.

In addition to the vanishing of the tadpoles we have two further constraints on the parameters of the Higgs potential. For arbitrarily large values of h_1^1 and h_2^2 the Higgs potential must be bounded from below. This is always satisfied for $|h_1^1| \neq |h_2^2|$ since the $|h_1^1|^4$ and $|h_2^2|^4$ terms have positive coefficients. But for $|h_1^1| = |h_2^2|$ the last term in the potential (2.36) vanishes. Thus

$$M_{h_1}^2 + M_{h_2}^2 > 2b \tag{2.42}$$

must hold to guarantee the bound in that case. A minimum of the potential (2.36) exists only if the Hessian

$$V''_{\text{Higgs}}\big|_{h_1^1 = h_2^2 = 0} = \begin{pmatrix} M_{h_1}^2 & -b \\ -b & M_{h_2}^2 \end{pmatrix} \tag{2.43}$$

has at least one negative eigenvalue. Together with (2.42) this can only be satisfied if the Hessian is indefinite, which gives

$$M_{h_1}^2 M_{h_2}^2 < b^2 \tag{2.44}$$

It is customary to replace the parameters v_1 and v_2 by v and β, as we did in equation (2.37). The parameter v is again fixed by the requirement that it should give the proper W- and Z-boson masses, whereas the parameter β is at first look only constrained to satisfy $0 < \beta < \pi/2$.

A proper minimization of the scalar potential of the MSSM requires to take into account all scalar fields and not truncate to the neutral Higgs bosons. It is possible, and does occur in certain regions of the parameterspace of the MSSM, that there exist minima which do not only break the electroweak symmetry but also $SU(3)_C$ and/or $U(1)_{\text{em}}$ [138–140].

From (2.40) we obtain

$$M_Z^2 = \frac{2}{\cos 2\beta}\left(b \tan\beta - M_{h_1}^2\right) = -\frac{2}{\cos 2\beta}\left(b \cot\beta - M_{h_2}^2\right) \tag{2.45}$$

which give an additional constraint on the supersymmetry-breaking parameters. Note that the parameter b is proportional to the sum $M_{h_1}^2 + M_{h_2}^2$ as can be seen in the first equation given in (2.53). In order to stabilize the weak scale all soft parameters appearing in this equation should be of the same order of magnitude as the weak scale M_Z or at most in the TeV range [141]. Otherwise we have to fine-tune all soft parameters. This in turn implies that supersymmetry breaking should occur at the weak scale and that most likely all supersymmetric particles have masses in that range. Therefore supersymmetric particles should be accessible in future experiments. Of course the parameter μ appearing in the superpotential has also to be of the order of the weak scale, a circumstance which is known as the μ-problem [31].

2.4   Particle Mass Spectrum

The gauge bosons are exactly the same as in the SM. One only has to replace v^2 in the Z and W boson masses given in (1.42) by $v_1^2 + v_2^2$.

Leptons and Quarks

The lepton and quark mass eigenstates are described by four-component Dirac spinors,

$$
\nu_I = \begin{pmatrix} l_I^1 \\ 0 \end{pmatrix}, \qquad e_I = \begin{pmatrix} l_I^2 \\ \bar{e}_I^c \end{pmatrix}, \qquad u_I = \begin{pmatrix} q_I^1 \\ \bar{u}_I^c \end{pmatrix}, \qquad d_I = \begin{pmatrix} q_I^2 \\ \bar{d}_I^c \end{pmatrix} \tag{2.46}
$$

The neutrinos remain massless, $M_\nu = 0$, and the electron-type lepton, up-type and down-type quark masses read

$$
M_E = \frac{v_1}{\sqrt{2}} S^{E_R} Y_E S^{E_L\dagger}, \qquad M_U = \frac{v_2}{\sqrt{2}} S^{U_R} Y_U S^{U_L\dagger}, \qquad M_D = \frac{v_1}{\sqrt{2}} S^{D_R} Y_D S^{D_L\dagger} \tag{2.47}
$$

The only difference compared to (1.45) is that the up-squarks obtain there masses from the vacuum expectation value of the second Higgs doublet.

Higgs Bosons

When the electroweak symmetry is broken, the Higgs interaction eigenstates h_1 and h_2 mix to give charged Higgs mass eigenstates $H^\pm$, $G^\pm$ and neutral Higgs mass eigenstates H^0, h^0, A^0 and G^0. The mass terms of the Higgs bosons are

$$
-\frac{1}{2} \left[(\varphi_1^0, \varphi_2^0) \, M_{\varphi^0}^2 \begin{pmatrix} \varphi_1^0 \\ \varphi_2^0 \end{pmatrix} + (\sigma_1^0, \sigma_2^0) \, M_{\sigma^0}^2 \begin{pmatrix} \sigma_1^0 \\ \sigma_2^0 \end{pmatrix} \right] - (\varphi_1^-, \varphi_2^-) \, M_{\varphi^\pm}^2 \begin{pmatrix} \varphi_1^+ \\ \varphi_2^+ \end{pmatrix} \tag{2.48}
$$

where

$$
M_{\varphi^0}^2 = \begin{pmatrix} b\tan\beta + \frac{t_1}{v_1} & b \\ b & b\cot\beta + \frac{t_2}{v_2} \end{pmatrix}
$$

$$
M_{\sigma^0}^2 = \begin{pmatrix} b\tan\beta + M_Z^2\cos^2\beta + \frac{t_1}{v_1} & -b - M_Z^2\sin\beta\cos\beta \\ -b - M_Z^2\sin\beta\cos\beta & b\cot\beta + M_Z^2\sin^2\beta + \frac{t_2}{v_2} \end{pmatrix}
$$

$$
M_{\varphi^\pm}^2 = \begin{pmatrix} b\tan\beta + M_W^2\sin^2\beta + \frac{t_1}{v_1} & b + M_W^2\sin\beta\cos\beta \\ b + M_W^2\sin\beta\cos\beta & b\cot\beta + M_W^2\cos^2\beta + \frac{t_2}{v_2} \end{pmatrix} \tag{2.49}
$$

After setting the tadpoles equal to zero we diagonalize these mass matrices to obtain CP-odd neutral Higgs mass eigenstates

$$
\begin{pmatrix} A^0 \\ G^0 \end{pmatrix} = \begin{pmatrix} \sin\beta & \cos\beta \\ -\cos\beta & \sin\beta \end{pmatrix} \begin{pmatrix} \varphi_1^0 \\ \varphi_2^0 \end{pmatrix} = X_H^T \begin{pmatrix} \varphi_1^0 \\ \varphi_2^0 \end{pmatrix} \tag{2.50}
$$

and CP-even neutral Higgs mass eigenstates

$$
\begin{pmatrix} H^0 \\ h^0 \end{pmatrix} = \begin{pmatrix} \cos\alpha & \sin\alpha \\ -\sin\alpha & \cos\alpha \end{pmatrix} \begin{pmatrix} \sigma_1^0 \\ \sigma_2^0 \end{pmatrix} = X_R^T \begin{pmatrix} \sigma_1^0 \\ \sigma_2^0 \end{pmatrix} \tag{2.51}
$$

and charged Higgs mass eigenstates

$$
\begin{pmatrix} H^+ \\ G^+ \end{pmatrix} = X_H^T \begin{pmatrix} \varphi_1^+ \\ \varphi_2^+ \end{pmatrix} \tag{2.52}
$$

The eigenvalues are the tree-level masses

$$m_{A^0}^2 = M_{h_1}^2 + M_{h_2}^2 = \frac{2b}{\sin 2\beta}, \qquad m_{G^0}^2 = 0,$$

$$m_{H^0,h^0}^2 = \frac{1}{2}\left[m_{A^0}^2 + M_Z^2 \pm \sqrt{(m_{A^0}^2 + M_Z^2)^2 - 4m_{A^0}^2 M_Z^2 \cos^2 2\beta} \right]$$

$$m_{H^\pm}^2 = m_{A^0}^2 + M_W^2, \qquad m_{G^\pm}^2 = 0 \tag{2.53}$$

Obviously, these tree-level masses fulfill

$$m_{H^\pm} \geq M_W, \qquad\qquad m_{H^0} \geq M_Z, \qquad\qquad m_{h^0} \leq M_Z \tag{2.54}$$

However, these are all tree-level relations and, especially the last relation gets large contributions from loop corrections [142, 143].

The mixing angle α defined in (2.51) fulfills

$$\frac{\sin 2\alpha}{\sin 2\beta} = -\frac{m_{H^0}^2 + m_{h^0}^2}{m_{H^0}^2 - m_{h^0}^2}, \qquad\qquad \frac{\cos 2\alpha}{\cos 2\beta} = -\frac{m_{A^0}^2 - M_Z^2}{m_{H^0}^2 - m_{h^0}^2} \tag{2.55}$$

It is shown in appendix A of [144] that $-\pi/2 \leq \alpha \leq 0$.

Charginos, Neutralinos and Gluinos

The charged higgsinos $\tilde{h}_2^1$ and $\tilde{h}_1^2$, and the winos λ_W^+ and λ_W^-, where $\lambda_W^\pm = \frac{1}{\sqrt{2}}(\lambda_W^1 \mp i\lambda_W^2)$, combine to form two Dirac fermions χ_1^+ and χ_2^+, called charginos. In the basis $(\psi^+)^T = (-i\lambda_W^+, \tilde{h}_2^1)$ and $(\psi^-)^T = (-i\lambda_W^-, \tilde{h}_1^2)$ the chargino mass terms in the MSSM Lagrangian are

$$-(\psi^-)^T \mathcal{M}_{\chi^\pm} \psi^+ + \text{h.c.} \tag{2.56}$$

where the chargino mass matrix is

$$\mathcal{M}_{\chi^\pm} = \begin{pmatrix} M_2 & \sqrt{2}M_W \sin\beta \\ \sqrt{2}M_W \cos\beta & \mu \end{pmatrix} \tag{2.57}$$

This mass matrix can be diagonalized by two unitary 2×2 matrices U and V defined by

$$U^* \mathcal{M}_{\chi^\pm} V^\dagger = \text{diag}(m_{\chi_1^+}, m_{\chi_2^+}) \tag{2.58}$$

The chargino mass eigenstates are given by

$$\chi_i^+ = \begin{pmatrix} \kappa_i^+ \\ \bar{\kappa}_i^- \end{pmatrix}, \quad \text{where} \quad \kappa_i^+ = V_{ij}\psi_j^+, \quad \kappa_i^- = U_{ij}\psi_j^- \tag{2.59}$$

The neutral higgsinos $\tilde{h}_1^1$ and $\tilde{h}_2^2$, the wino λ_W^3 and the bino λ_B mix to form four Majorana fermions χ_i^0, $i = 1, \ldots, 4$, called neutralinos. In the basis $(\psi^0)^T = (-i\lambda_B, -i\lambda_W^3, \tilde{h}_1^1, \tilde{h}_2^2)$ the neutralino mass terms in the MSSM Lagrangian are

$$-\frac{1}{2}(\psi^0)^T \mathcal{M}_{\chi^0} \psi^0 + \text{h.c.} \tag{2.60}$$

where the neutralino mass matrix is

$$\mathcal{M}_{\chi^0} = \begin{pmatrix} M_1 & 0 & -M_Z s_W \cos\beta & M_Z s_W \sin\beta \\ 0 & M_2 & M_Z c_W \cos\beta & -M_Z c_W \sin\beta \\ -M_Z s_W \cos\beta & M_Z c_W \cos\beta & 0 & -\mu \\ M_Z s_W \sin\beta & -M_Z c_W \sin\beta & -\mu & 0 \end{pmatrix} \tag{2.61}$$

This mass matrix can be diagonalized by a unitary 4×4 matrix N such that

$$N^* \mathcal{M}_{\chi^0} N^\dagger = \text{diag}(m_{\chi_1^0}, \ldots, m_{\chi_4^0}) \tag{2.62}$$

The neutralino mass eigenstates are given by

$$\chi_i^0 = \begin{pmatrix} \kappa_i^0 \\ \bar{\kappa}_i^0 \end{pmatrix}, \quad \text{where} \quad \kappa_i^0 = N_{ij} \psi_j^0 \tag{2.63}$$

The gluinos mass eigenstates form Majorana spinors

$$\tilde{g}^a = \begin{pmatrix} -i\lambda_G^a \\ i\bar{\lambda}_G^a \end{pmatrix} \tag{2.64}$$

with masses $M_{\tilde{g}} = M_3$.

Sleptons and Squarks

In the super-CKM basis of fields we define

$$\tilde{N} = \tilde{l}^1, \qquad \tilde{E} = \begin{pmatrix} \tilde{l}^2 \\ \tilde{e}^{c*} \end{pmatrix}, \qquad \tilde{U} = \begin{pmatrix} \tilde{q}^1 \\ \tilde{u}^{c*} \end{pmatrix}, \qquad \tilde{D} = \begin{pmatrix} \tilde{q}^2 \\ \tilde{d}^{c*} \end{pmatrix} \tag{2.65}$$

where $\tilde{l}^{1,2}$, $\tilde{e}^{c*}$, $\tilde{q}^{1,2}$, $\tilde{u}^{c*}$ and $\tilde{d}^{c*}$ are three-component objects in flavor space. Then the slepton and squark mass terms in the MSSM Lagrangian read

$$-\tilde{N}^\dagger \mathcal{M}_N^2 \tilde{N} - \tilde{E}^\dagger \mathcal{M}_E^2 \tilde{E} - \tilde{U}^\dagger \mathcal{M}_U^2 \tilde{U} - \tilde{D}^\dagger \mathcal{M}_D^2 \tilde{D} \tag{2.66}$$

Adopting the notation of [137] the mass matrices are[6]

$$\mathcal{M}_N^2 = [M_E^2]_{LL} + \frac{1}{2} M_Z^2 \, c_{2\beta} \mathbb{1}$$

$$\mathcal{M}_E^2 = \begin{pmatrix} [M_E^2]_{LL} + M_E^2 + \frac{1}{2}(M_Z^2 - 2M_W^2)\, c_{2\beta} \mathbb{1} & [M_E^2]_{LR} - M_E \mu \, t_\beta \\ [M_E^2]_{LR}^\dagger - M_E \mu^* \, t_\beta & [M_E^2]_{RR} + M_E^2 - M_Z^2 s_W^2 \, c_{2\beta} \mathbb{1} \end{pmatrix}$$

$$\mathcal{M}_U^2 = \begin{pmatrix} [M_U^2]_{LL} + M_U^2 + \frac{1}{6}(4M_W^2 - M_Z^2)\, c_{2\beta} \mathbb{1} & [M_U^2]_{LR} - M_U \mu \, ct_\beta \\ [M_U^2]_{LR}^\dagger - M_U \mu^* \, ct_\beta & [M_U^2]_{RR} + M_U^2 + \frac{2}{3} M_Z^2 s_W^2 \, c_{2\beta} \mathbb{1} \end{pmatrix}$$

$$\mathcal{M}_D^2 = \begin{pmatrix} [M_D^2]_{LL} + M_D^2 - \frac{1}{6}(M_Z^2 + 2M_W^2)\, c_{2\beta} \mathbb{1} & [M_D^2]_{LR} - M_D \mu \, t_\beta \\ [M_D^2]_{LR}^\dagger - M_D \mu^* \, t_\beta & [M_D^2]_{RR} + M_D^2 - \frac{1}{3} M_Z^2 s_W^2 \, c_{2\beta} \mathbb{1} \end{pmatrix} \tag{2.67}$$

---

[6]Here we defined $c_\varphi = \cos\varphi$, $t_\varphi = \tan\varphi$ and $ct_\varphi = \cot\varphi$.

where

$$[M_E^2]_{LL} = S^{E_L} M_{\tilde{L}}^2 S^{E_L\dagger}, \quad [M_E^2]_{RR} = S^{E_R} M_{\tilde{E}}^2 S^{E_R\dagger}, \quad [M_E^2]_{LR} = \frac{v_1}{\sqrt{2}} S^{E_L} A_E' S^{E_R\dagger}$$

$$[M_U^2]_{LL} = S^{U_L} M_{\tilde{Q}}^2 S^{U_L\dagger}, \quad [M_U^2]_{RR} = S^{U_R} M_{\tilde{U}}^2 S^{U_R\dagger}, \quad [M_U^2]_{LR} = \frac{v_2}{\sqrt{2}} S^{U_L} A_U' S^{U_R\dagger}$$

$$[M_D^2]_{LL} = S^{D_L} M_{\tilde{Q}}^2 S^{D_L\dagger}, \quad [M_D^2]_{RR} = S^{D_R} M_{\tilde{D}}^2 S^{D_R\dagger}, \quad [M_D^2]_{LR} = \frac{v_1}{\sqrt{2}} S^{D_L} A_D' S^{D_R\dagger} \quad (2.68)$$

Following standard conventions we rewrite the LR-terms without loss of generality as

$$[M_X^2]_{LR} = M_X S^{X_R} A_X S^{X_R\dagger}, \qquad X = E, U, D \quad (2.69)$$

where we introduced $A_X = (Y_X^\dagger)^{-1} A_X'$.

It is important to note that in the super-CKM basis we have

$$[M_D^2]_{LL} = K^\dagger [M_U^2]_{LL} K \quad (2.70)$$

due to $SU(2)$ gauge invariance.

The sneutrino mass matrix can be diagonalized by one 3×3 unitary matrix Γ^N, and the selectron, up- and down-type squark mass matrices by three 6×6 unitary matrices Γ^E, Γ^U and Γ^D, respectively, according to

$$\Gamma^N \mathcal{M}_N^2 \Gamma^{N\dagger} = \text{diag}(m_{\tilde{\nu}_1}, \ldots, m_{\tilde{\nu}_3}), \qquad \Gamma^E \mathcal{M}_E^2 \Gamma^{E\dagger} = \text{diag}(m_{\tilde{e}_1}, \ldots, m_{\tilde{e}_6})$$

$$\Gamma^U \mathcal{M}_U^2 \Gamma^{U\dagger} = \text{diag}(m_{\tilde{u}_1}, \ldots, m_{\tilde{u}_6}), \qquad \Gamma^D \mathcal{M}_D^2 \Gamma^{D\dagger} = \text{diag}(m_{\tilde{d}_1}, \ldots, m_{\tilde{d}_6}) \quad (2.71)$$

The mass eigenstates for sneutrinos, selectrons, up-type and down-type squarks read

$$\tilde{\nu} = \Gamma^N \tilde{N}, \quad \tilde{e} = \Gamma^E \tilde{E}, \quad \tilde{u} = \Gamma^U \tilde{U}, \quad \tilde{d} = \Gamma^D \tilde{D} \quad (2.72)$$

It is convenient to split the 6×6 matrices into 6×3 sub-blocks

$$\Gamma_{6\times6}^X = \left(\Gamma_{6\times3}^{X_L}, \Gamma_{6\times3}^{X_R}\right), \quad X = E, U, D \quad (2.73)$$

Therefore we have

$$\tilde{l}_I^2 = [\Gamma^{E_L\dagger}]_{Ia} \tilde{e}_a, \qquad \tilde{q}_I^1 = [\Gamma^{U_L\dagger}]_{Ia} \tilde{u}_a, \qquad \tilde{q}_I^2 = [\Gamma^{D_L\dagger}]_{Ia} \tilde{d}_a$$

$$\tilde{e}_I^{c*} = [\Gamma^{E_R\dagger}]_{Ia} \tilde{e}_a, \qquad \tilde{u}_I^{c*} = [\Gamma^{U_R\dagger}]_{Ia} \tilde{u}_a, \qquad \tilde{d}_I^{c*} = [\Gamma^{D_R\dagger}]_{Ia} \tilde{d}_a \quad (2.74)$$

where the index I runs from 1 to 3 and the index a from 1 to 6.

A particularly useful basis, especially in the context of the $K^+ \to \pi^+ \nu\bar{\nu}$ and $K_L \to \pi^0 \nu\bar{\nu}$ decays discussed in the next chapter, is the one defined in [44], which we will call BRS basis from now on. It is obtained starting from the super-CKM basis with the redefinition

$$\tilde{q}_{I,\text{BRS}}^1 = K_{IK}^\dagger \tilde{q}_I^1 \quad (2.75)$$

while all other fields remain unchanged. In this basis the matrix $\mathcal{M}_U^2$ is modified such that $SU(2)$ gauge invariance for the LL mixing matrices in $\mathcal{M}_U^2$ and $\mathcal{M}_D^2$ is automatically preserved,

$$[M_D^2]_{LL,\text{BRS}} = [M_U]_{LL,\text{BRS}}^2 \quad (2.76)$$

to be compared with (2.70).

Also, with respect to the numerical discussion of these decay channels it is useful to define so-called mass-insertions through [137]

$$[\delta_X]^{IJ}_{AB} = \frac{[M_U^2]^{IJ}_{AB}}{\sqrt{[M_U^2]^{II}_{AA}[M_U^2]^{JJ}_{BB}}}, \qquad A, B \in \{L, R\} \tag{2.77}$$

which depend obviously from the basis of the slepton and squark fields chosen in flavor space.

2.5   The MSSM with a Heavy and Decoupled Gluino

In chap. 4 we will calculate QCD corrections to the matching conditions for the Wilson coefficients of operators mediating the transition $b \to sl^+l^-$ in the context of the MSSM. This corrections include virtual gluons and gluinos, and the latter necessitates the introduction of additional four-quark operators. Such a calculation at the NNLO is however beyond the scope of the present work since it not only includes the calculation of the two-loop matching conditions but also the three-loop mixing of the new operators. We will instead assume that the gluino is much heavier than all other particles present in the theory, and therefore can be decoupled to ensure the completeness of the calculated QCD corrections.

This leads us to an "effective MSSM" with decoupled gluino at the scale $\mu_{\tilde{g}} \sim O(M_{\tilde{g}})$ [100]. Taking furthermore the down-squark mass-squared matrix to be flavor diagonal so that there are no neutralino contributions to flavor-changing $b \to s$ transitions[7], and neglecting all the $1/M_{\tilde{g}}$ effects, the only modified couplings relevant for the NNLO corrections to $\bar{B} \to X_s l^+ l^-$ come from the "chargino – up-squark – down-quark" vertex[8],

$$X_i^{U_L} = -g_2 \left[a_g V_{i1}^* \Gamma^{U_L} - a_Y V_{i2}^* \Gamma^{U_R} \frac{M_U}{\sqrt{2}M_W \sin\beta} \right] K$$

$$X_i^{U_R} = g_2 a_Y U_{i2} \Gamma^{U_L} K \frac{M_D}{\sqrt{2}M_W \cos\beta} \tag{2.78}$$

where

$$a_g = 1 - \frac{\alpha_s(\mu_{\tilde{g}})}{4\pi}\left[\frac{7}{3} + 4\ln\left(\frac{\mu_{\tilde{g}}}{M_{\tilde{g}}}\right)\right], \qquad a_Y = 1 + \frac{\alpha_s(\mu_{\tilde{g}})}{4\pi}\left[1 + 4\ln\left(\frac{\mu_{\tilde{g}}}{M_{\tilde{g}}}\right)\right] \tag{2.79}$$

These couplings as well as the up-squark masses $m_{\tilde{u}_a}$ and mixing matrices Γ^{U_L} and Γ^{U_R} of the "effective MSSM" are determined in the matching with the full MSSM at the scale $\mu_{\tilde{g}}$. All of them are understood to be $\overline{\text{MS}}$ renormalized quantities in dimensional regularization and can be determined from the one-loop corrected mass-squared matrix [146, 147].

This approach limits the validity of the results with respect to the parameter space of the general MSSM, nevertheless it is interesting to compute the QCD corrections to the decay $\bar{B} \to X_s l^+ l^-$ within this special scenario, and to investigate their phenomenological consequences. Indeed, similar analysis of the inclusive $\bar{B} \to X_s \gamma$ decay [99, 100] have shown that QCD corrections can be of the magnitude of the current experimental uncertainties.

---

[7]This assumption corresponds to "Scenario B" described in detail in [145].
[8]These couplings are defined in the super-CKM basis.

Part II

Rare K and B Decays

Chapter 3

$K \to \pi \nu \bar{\nu}$ in the General MSSM

Here, we present formulae for the branching ratios $\mathcal{B}(K^+ \to \pi^+ \nu \bar{\nu})$ and $\mathcal{B}(K_L \to \pi^0 \nu \bar{\nu})$ in terms of the function X in a particularly suitable form for our numerical analysis. We discuss the numerical method we use to cope with the huge space of MSSM parameters under consideration, and afterwards, taking several experimental and theoretical constraints into account, we explore the possible departures of the function X and the branching ratios $\mathcal{B}(K^+ \to \pi^+ \nu \bar{\nu})$ and $\mathcal{B}(K_L \to \pi^0 \nu \bar{\nu})$ from their SM predictions.

3.1 Effective Hamiltonian

The effective Hamiltonian relevant for the $K^+ \to \pi^+ \nu \bar{\nu}$ and $K_L \to \pi^0 \nu \bar{\nu}$ decays in the general MSSM can be written as follows[1],

$$\mathcal{H}_{\text{eff}} = \frac{4 G_F}{\sqrt{2}} \frac{\alpha_{\text{em}}}{2\pi \, \text{s}_W^2} \left[\mathcal{H}_{\text{eff}}^{(c)} + \mathcal{H}_{\text{eff}}^{(t)} \right] \tag{3.1}$$

where the internal charm part

$$\mathcal{H}_{\text{eff}}^{(c)} = \sum_{l=e,\mu,\tau} K_{cs}^* K_{cd} X_{\text{NL}}^l (\bar{s} P_L d)(\bar{\nu}_l P_L \nu_l) \tag{3.2}$$

is fully dominated by the SM contributions and

$$\mathcal{H}_{\text{eff}}^{(t)} = \sum_{l=e,\mu,\tau} K_{ts}^* K_{td} \left[X_L (\bar{s} P_L d)(\bar{\nu}_l P_L \nu_l) + X_R (\bar{s} P_R d)(\bar{\nu}_l P_L \nu_l) \right] \tag{3.3}$$

with X_L receiving both the SM and supersymmetric contributions and X_R only the latter ones that also include charged Higgs boson exchanges. In the SM X_L is real and given for $\overline{m}_t(m_t) = (168.1 \pm 4.1)\,\text{GeV}$ by [43]

$$X_L^{SM} = 1.53 \pm 0.04 \tag{3.4}$$

---

[1]A detailed discussion of the "charm" and "top sector" within the SM including $O(\alpha_s)$ corrections can be found for example in [148]. Also note that in writing (3.1) we made use of the fact that in the general MSSM there exists no right-handed neutrino. Furthermore, we ignored possible lepton flavor number violating interactions, and hence the neutrino current is diagonal.

The dependence of the the functions $X_{L,R}$ on the charged lepton masses resulting from the box diagrams is negligible for the top contribution. In the charm sector this is the case only for the electron and the muon but not for the τ-lepton.

This parameterization of $\mathcal{H}_{\text{eff}}^{(t)}$ is very useful for phenomenological applications within the SM, but one should remember that in the general MSSM scenario considered here not all contributions to $\mathcal{H}_{\text{eff}}^{(t)}$ are proportional to $K_{ts}^* K_{td}$. This means that parameterizing $\mathcal{H}_{\text{eff}}^{(t)}$ as given in (3.3), necessarily puts some CKM dependence into X_L and X_R.

Now, as the strong interactions are not sensitive to the chirality of the quarks, the hadronic matrix elements of $(\bar{s} P_L d)$ and $(\bar{s} P_R d)$ are equal to each other, and consequently the function X playing the central role in our analysis is simply given by

$$X = X_L + X_R = |X| e^{i\theta_X} \tag{3.5}$$

The explicit expressions for X_L and X_R are collected in app. A. As one can see there, chargino and part of the neutralino contributions to X_R are strongly suppressed by small Yukawa couplings of the down quarks. As we will see, the remaining neutralino contribution proportional to the $U(1)$ gauge coupling is typically also much smaller than the dominant terms in X_L, so that $|X_R| \ll |X_L|$ also in the general MSSM (except may be for some non-interesting points where X_L is small due to cancellations) and can be neglected for all practical purposes.

3.2   Branching Ratios

The branching ratios for the $K^+ \to \pi^+ \nu \bar{\nu}$ and $K_L \to \pi^0 \nu \bar{\nu}$ decays resulting from (3.1) can be written as follows [43],

$$\mathcal{B}(K^+ \to \pi^+ \nu \bar{\nu}) = \kappa_+ \left[\left(\frac{\text{Im}(\lambda_t X)}{\lambda^5} \right)^2 + \left(\frac{\text{Re}\lambda_c}{\lambda} P_c(X) + \frac{\text{Re}(\lambda_t X)}{\lambda^5} \right)^2 \right]$$

$$Br(K_L \to \pi^0 \nu \bar{\nu}) = \kappa_L \left(\frac{\text{Im}(\lambda_t X)}{\lambda^5} \right)^2 \tag{3.6}$$

with $\lambda = 0.224$ being one of the Wolfenstein parameters [149], $\lambda_t = K_{ts}^* K_{td}$, $\lambda_c = K_{cs}^* K_{cd}$, κ-factors equal to [43]

$$\kappa_+ = (4.84 \pm 0.06) \cdot 10^{-11}, \qquad \kappa_L = (2.12 \pm 0.03) \cdot 10^{-10} \tag{3.7}$$

and

$$P_c(X) = \frac{1}{\lambda^4} \left[\frac{2}{3} X_{\text{NL}}^e + \frac{1}{3} X_{\text{NL}}^\tau \right] = 0.39 \pm 0.07 \tag{3.8}$$

resulting from the NLO calculations in [40, 41]. The anatomy of the error in $P_c(X)$ has been recently presented in [43].

As discussed in the next section we will use as our input parameters

$$|K_{us}| = \lambda = 0.224, \qquad |K_{cb}| = A\lambda^2 = 0.0415, \qquad R_b = 0.37 \tag{3.9}$$

where

$$R_b = \frac{(1 - \lambda^2/2)}{\lambda} \left| \frac{K_{ub}}{K_{cb}} \right| \tag{3.10}$$

We recall that A is a Wolfenstein parameter [149] with $A = 0.83 \pm 0.02$ and R_b is one of the sides of the unitarity triangle.

While the parameters in (3.9) contain uncertainties, the latter are sufficiently small so that they can be neglected in comparison with huge uncertainties in the values of supersymmetric parameters. The choice of these three parameters is dictated by the fact that they are extracted from tree-level decays and consequently their values are not subject to new physics uncertainties.

As the fourth variable we will take the angle γ in the unitarity triangle that is equal to the CKM phase δ_{CKM} in the standard parameterization of this matrix. The angle γ can be in principle measured without any new physics pollution in tree-level B decay strategies that will be only available at LHC and BTeV [150]. In the general MSSM the value of γ may deviate from the one extracted from the usual analysis of the unitarity triangle that uses SM expressions. For this reason we will allow γ to vary in the full range

$$-180° \leq \gamma \leq 180° \tag{3.11}$$

but as we will see in the next section, only the range $20° \leq \gamma \leq 110°$ is allowed when all constraints are taken into account.

We define next $\overline{X}_{SUSY}$ through

$$\lambda_t X = \lambda_t X_{SM} + \lambda^5 \overline{X}_{SUSY} \tag{3.12}$$

and introduce

$$a = P_c(X) + \frac{|K_{cb}|^2}{\lambda^4} X_{SM} \approx 1.43, \qquad b = R_b \frac{|K_{cb}|^2}{\lambda^4} X_{SM} \approx 0.39 \tag{3.13}$$

that do not depend on supersymmetric parameters. We find then

$$\mathcal{B}(K^+ \to \pi^+ \nu\bar{\nu}) = \kappa_+ \left[(Q_{eff}(\gamma) + \mathrm{Im}\overline{X}_{SUSY})^2 + (P_{eff}(\gamma) - \mathrm{Re}\overline{X}_{SUSY})^2 \right]$$

$$\mathcal{B}(K_L \to \pi^0 \nu\bar{\nu}) = \kappa_L \left(Q_{eff}(\gamma) + \mathrm{Im}\overline{X}_{SUSY} \right)^2 \tag{3.14}$$

where

$$P_{eff}(\gamma) = (1 - \frac{\lambda^2}{2}) \left[a - b\cos\gamma \right], \qquad Q_{eff}(\gamma) = b\sin\gamma \tag{3.15}$$

As $P_{eff}(\gamma)$ and $Q_{eff}(\gamma)$ can be fully determined within the SM, provided γ can be measured through tree-level decays, the formulae given in (3.14) transparently exhibit supersymmetric contributions. With $\gamma \approx 65°$ we have

$$P_{eff}(\gamma) \approx 1.23, \qquad Q_{eff}(\gamma) \approx 0.35 \tag{3.16}$$

Cabbibo-Kobayashi-Maskawa phase	$-180° \leq \gamma \leq 180°$
CP-odd Higgs boson mass	$150 \leq M_{A^0} \leq 400$
$SU(2)$ gaugino mass; we use M_1 GUT-related to M_2	$50 \leq M_2 \leq 800$
Gluino mass	$195 \leq M_{\tilde{g}} \leq 2000$
Supersymmetric Higgs mixing parameter	$-400 \leq \mu \leq 400$
Common flavor diagonal slepton mass parameter ($I = 1, 2, 3$ and $A = L, R$)	$95 \leq M_{sl} \equiv \sqrt{[M_E^2]_{XX}^{II}} \leq 1000$
Common mass parameter for the first two generations of squarks ($X = U, D, I = 1, 2$ and $A = L, R$), as well as $\tilde{b}_R$ ($X = D, I = 3$ and $A = R$)	$240 \leq M_{sq} \equiv \sqrt{[M_X^2]_{AA}^{II}} \leq 1000$
Squark mass parameter for the left-handed stop and sbottom	$50 \leq M_{\tilde{t}_L} \equiv \sqrt{[M_U^2]_{LL}^{33}} \leq 1000$
Squark mass parameter for the right-handed stop	$50 \leq M_{\tilde{t}_R} \equiv \sqrt{[M_U^2]_{RR}^{33}} \leq 1000$
Flavor universal trilinear scalar mixing parameter normalized to the fermion mass ($I = 1, 2, 3$ and $X = E, U, D$)	$-1 \leq A \equiv (M_X)^{-1} [M_X^2]_{LR}^{II} \leq 1$
Mass-insertion $\delta_{LL}^{12} \equiv [\delta_U]_{LL}^{12} = [\delta_D]_{LL}^{12}$	$|\delta_{LL}^{12}| \leq 0.135$
Mass-insertion $\delta_{ULR}^{13} \equiv [\delta_U]_{LR}^{13}$	$|\delta_{ULR}^{13}| \leq 1.65$
Mass-insertion $\delta_{ULR}^{23} \equiv [\delta_U]_{LR}^{23}$	$|\delta_{ULR}^{23}| \leq 1.65$

Table 3.1: Parameters and their ranges used in the "constrained" scan (16 real degrees of freedom). All mass parameters are in GeV. Furthermore, we adopt the notation commonly used in the literature: $\tilde{t}_L = \tilde{q}_3^1$, $\tilde{t}_R = \tilde{u}_3^c$, $\tilde{b}_L = \tilde{q}_3^2$ and $\tilde{b}_R = \tilde{d}_3^c$.

3.3   Numerical Analysis

In the general MSSM, the predictions for the branching ratios considered here and various experimental constraints can depend on almost every MSSM parameter. However, the dependence on the majority of them is weak enough to be safely neglected in principle for the purpose of computing $Br(K^+ \to \pi^+\nu\bar{\nu})$ and $Br(K_L \to \pi^0\nu\bar{\nu})$. Still, the parameters may indirectly enter through the expressions for other observables, which we use to constrain the parameter space. Taking a conservative approach we allow for the independent variation of more free parameters than included in the existing literature.

Independent MSSM Parameters

To start with, we assume that $\mathcal{B}(K^+ \to \pi^+\nu\bar{\nu})$ and $Br(K_L \to \pi^0\nu\bar{\nu})$ may depend significantly on the set of unknown SM and MSSM parameters listed in table 3.1. We took as fixed the other SM parameters, including fermion masses and the CKM parameters given in (3.9),
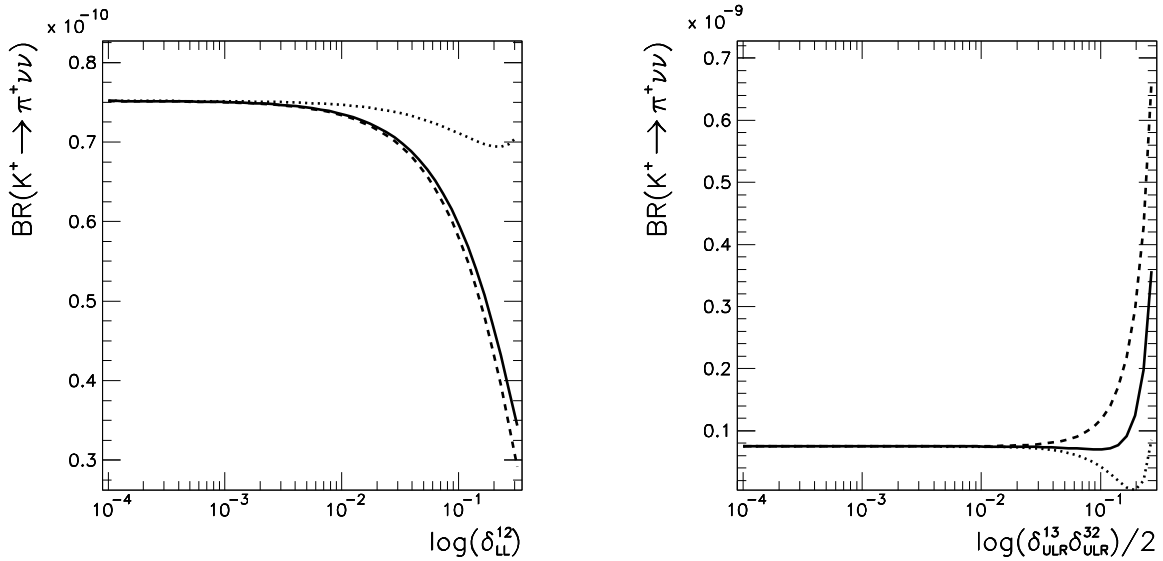
Figure 3.1: Dependence of $Br(K^+ \to \pi^+ \nu\bar{\nu})$ on chosen mass-insertions for $\gamma = 65°$, $\tan\beta = 2$, $M_{sq} = M_{\tilde{t}_L} = M_{\tilde{t}_R} = 500$, $M_{sl} = 300$, $M_2 = 200$, $M_{\tilde{g}} = 3M_2$, $\mu = 100$, $M_{A^0} = 200$ (all masses in GeV). Solid, dashed and dotted lines: δ_{LL}^{12} and $\delta_{ULR}^{13}\delta_{ULR}^{32}$ complex, real and imaginary, respectively.

as their measurements are known to be relatively insensitive to physics beyond the SM. This leaves as our only free SM parameter the CKM angle γ, which to date has not been determined from tree-level decays.

Apart from the flavor diagonal supersymmetric mass parameters, we vary several off-diagonal ones. For a transparent parameterization and easy comparison with the literature, it is useful to use the mass-insertions defined in (2.77), even though our actual computation makes use of exactly diagonalized sfermion, chargino, and neutralino mass matrices. These mass-insertions depend obviously on the basis of the slepton and squark fields chosen in flavor space, and in the context of $K \to \pi\nu\bar{\nu}$ decays particularly useful is the BRS basis defined in [44]. In this basis the gluino and neutralino couplings are flavor conserving, while the CKM elements from the chargino couplings to the left-handed up squarks are eliminated, and in particular from the term in the mass-insertion approximation of the function X that is believed to be dominant [64]. Since the BRS basis ensures that any choice of δ's automatically preserves $SU(2)$ invariance, we also omit the "sector" index on the δ_{LL}.

The decays $K^+ \to \pi^+ \nu\bar{\nu}$ and $K_L \to \pi^0 \nu\bar{\nu}$ are $\Delta S = 1$ processes and correspond to a transition between the first and second quark generations. Thus, they could certainly depend on (12) squark mass-insertions. However, as pointed out in [64], both decays are sensitive also to second-order terms in the mass-insertion expansion, namely, to products of a (13) and (the conjugate of) a (23) mass-insertion. Therefore, we start from varying independently five (12) mass-insertions, δ_{LL}^{12}, δ_{DRR}^{12}, δ_{URR}^{12}, δ_{DLR}^{12} and δ_{ULR}^{12}, plus five more (13) and five (23) mass-insertions (assuming for the moment that all LR mass insertions are hermitian, e.g. $\delta_{DLR}^{13} = \delta_{DLR}^{31*}$). Even assuming that all flavor diagonal quantities from the list above are real (there is no reason to constrain mass-insertions to be real), we have listed

Quantity	Measured value	Experimental error
Lightest neutralino mass	> 46.0 GeV	
Second lightest neutralino mass	> 62.4 GeV	
Lightest chargino mass	> 94.0 GeV	
The two "sbottom" masses	> 89.0 GeV	
The two "stop" masses	> 95.7 GeV	
All other squark masses	> 250.0 GeV	
$\lvert \varepsilon_K \rvert$	$2.280 \cdot 10^{-3}$	$0.013 \cdot 10^{-3}$
ΔM_K	$3.489 \cdot 10^{-15}$ GeV	$0.008 \cdot 10^{-15}$
ΔM_d	$3.31 \cdot 10^{-13}$ GeV	$0.04 \cdot 10^{-13}$
ΔM_s	$> 9.5 \cdot 10^{-12}$ GeV	
$Br(B_s \to X_s \gamma)$	$3.28 \cdot 10^{-4}$	$^{+0.41}_{-0.36} \cdot 10^{-4}$
$(\sin 2\beta)_{\psi K_{\mathrm{S}}}$	0.736	0.049

Table 3.2: Experimental measurements used to constrain the MSSM parameter space. Limits on supersymmetric particles masses published in [151] are used. The quotes on "sbottom" and "stop" indicate that these are only approximate flavor states.

already 40 free real parameters. This is a huge number for any reasonably dense numerical scan. To avoid excessive computation time, we first tested how sensitive to the various mass-insertions the predictions for our branching ratios really are. In fig. 3.1 we plot the dependence of $Br(K^+ \to \pi^+ \nu\bar{\nu})$ on δ_{LL}^{12} and the product $\delta_{ULR}^{13} \delta_{ULR}^{23*}$ for a chosen set of MSSM parameters. The dependence on the other mass-insertions, not shown in the plots, is much weaker and can be neglected in the first approximation.

Fig. 3.1 suggests that it is sufficient in the numerical scan to vary only three independent mass-insertions, δ_{LL}^{12}, δ_{ULR}^{13} and δ_{ULR}^{23}. In fact the dependence on δ_{LL}^{12}, which is tightly constrained from mixing in the neutral kaon system, is almost negligible for realistic values. Thus, the large but already numerically more feasible total number of 16 free parameters appears to be sufficient to explore the possible ranges of $Br(K^+ \to \pi^+ \nu\bar{\nu})$ and $Br(K_L \to \pi^0 \nu\bar{\nu})$ in the framework of the MSSM. However, this is not true when trying to satisfy experimental bounds and selecting allowed values of the MSSM parameters. For example, keeping the product $\delta_{LL}^{13} \delta_{LL}^{23*}$ constant but varying δ_{LL}^{13} independently does not affect $Br(K^+ \to \pi^+ \nu\bar{\nu})$ and $Br(K_L \to \pi^0 \nu\bar{\nu})$ but allows to satisfy bounds coming from ΔM_d, the measured $B_d^0 - \bar{B}_d^0$ mass difference. This motivates keeping, in δ_{LL}^{12}, one more flavor violating parameter even in the "minimal" 16-parameter scan. Later, we will see that our numerical method is powerful enough to study the consequences of further increasing the number of degrees of freedom, which turn out to be unimportant.

Theoretical and Experimental Bounds

The enormous freedom in the MSSM parameter space is reduced by a number of phenomenological constraints the theory must satisfy. From the experimental side we take into account the set of bounds and measurements listed in table 3.2. As can be seen, we do not take into

account the ε'/ε constraint, as its calculation still has very large theoretical uncertainties. Doing this we are aware of the fact that ε'/ε could one day offer a very powerful constraint on the size of MSSM contributions [65, 152].

Due to the large number of unknown parameters and substantial theoretical uncertainties present in many calculations, it is pointless (and certainly very difficult to implement from a practical point of view) to use everywhere higher order QCD corrections and other non-leading effects calculated in the literature[2]. Nevertheless, whenever feasible we try to avoid unnecessary simplifications made in many papers. In particular:

- For low-energy flavor-changing neutral current and CP-violating processes, we do not restrict ourselves to the most commonly used mass-insertion approximation. Instead, we calculate all Wilson coefficients relevant for a given process in the mass eigenstate approach, taking into account the full set of contributions. Further, we compare experimental results with the full one-loop MSSM expressions, not just the dominant (usually gluino) term.

- To complete the bounds coming from the low-energy data, we also compare lower mass bounds for MSSM particles, obtained from accelerator experiments, with the tree-level eigenvalues of the MSSM mass matrices.

For comparing theoretical predictions for the low-energy observables with experiment, we apply the following procedure. For a given set of MSSM parameters, we calculate all appropriate parton-level diagrams. Next, we construct expressions for the considered quantities using the central values of the QCD evolution factors and necessary hadronic matrix elements, obtained by perturbative SM and lattice-QCD computations, respectively. Finally, for every quantity Q we require:

$$|Q^{exp} - Q^{th}| \leq 3\Delta Q^{exp} + q|Q^{th}|, \qquad q = 0.5 \qquad (3.17)$$

with the exception of ΔM_s, for which we require $(1 + q)|Q^{th}| \geq Q^{exp}$.

The first term on the r.h.s. of (3.17) represents the 3σ experimental error. The second term corresponds to the theoretical error. In principle, such an error differs from quantity to quantity and is usually smaller than $q = 50\%$, which we assumed as a generic number in all calculations. However, apart from the theoretical errors coming from uncertainties in the QCD evolution and hadronic matrix elements calculations, one should take into account also problems arising due to the limited numerical scan density. In principle, with a very dense scan, it should be possible to find MSSM parameters fulfilling (3.17) within the "true" theoretical errors of present calculations. Such a dense scan requires, however, a huge amount of computer time - with 16 or more free parameters and rather complicated mass eigenstate formulae, it would take months of CPU time. This does not seem to be necessary and may even be undesirable. Our goal is to find "generic" allowed values for the $K \to \pi\nu\bar{\nu}$ decay rates, i.e. values possible to obtain for fairly wide ranges of MSSM parameters, without strong fine-tuning and resorting to some very particular points of the parameter space where the experimental bounds are satisfied due to precise cancellations of various types of contributions. Thus, in our scan we use wide "theoretical" errors, assuming that this procedure points to the correct ranges of the MSSM parameters, and if necessary

---

[2]Once the experimental uncertainties in the $K \to \pi\nu\bar{\nu}$ decays are improving, it is, however, unavoidable to include higher order QCD corrections and other non-leading effects.

the exact values of such parameters fulfilling the bound in (3.17) with smaller q could always (or at least almost always) be found. This could be achieved e.g. by a denser scan or by more advanced numerical routines, possibly even solving numerically the set of non-linear equations given by all constraints.

The only exception from the procedure described above is the imposition of the constraint from the CP asymmetry $a_{\psi K_{\mathrm{S}}}(t)$. Making the safe assumption that the supersymmetric contributions to the decay amplitude can be neglected, this asymmetry measures the phase of the $B_d^0 - \bar{B}_d^0$ amplitude

$$M_{12} = \langle B_d^0 | H_{eff}(\Delta B = 2) | \bar{B}_d^0 \rangle = |M_{12}| e^{i2(\beta + \theta_d)} \tag{3.18}$$

through

$$a_{\psi K_{\mathrm{S}}}(t) = -a_{\psi K_{\mathrm{S}}} \sin(\Delta M_d t) = \sin 2(\beta + \theta_d) \sin(\Delta M_d t) \tag{3.19}$$

Here $-\beta$ is the phase of K_{td}, while θ_d is the new effective phase coming from the supersymmetric contributions. As in the general MSSM the presence of non-vanishing sfermion mass-insertions implies contributions of several local operators to M_{12}, the phase θ_d suffers from potential uncertainties related to the hadronic matrix elements of these operators. Only if one of these operators dominates over the others in the full amplitude can θ_d be cleanly related to supersymmetric parameters. In other cases its error can be sometimes very large and moreover is hard to estimate – it would require additional scanning over hadronic uncertainties for each given set of MSSM parameters. To avoid such problems, in our analysis we assume conservatively

$$|a_{\psi K_{\mathrm{S}}}^{exp} - \sin 2(\beta + \theta_d)| \leq 2\Delta a_{\psi K_{\mathrm{S}}}^{exp} \tag{3.20}$$

with $\sin 2(\beta + \theta_d)$ calculated in the MSSM for central values of the hadronic parameters and $a_{\psi K_{\mathrm{S}}}^{exp} = 0.736 \pm 0.049$. Expressing everything in degrees we require then

$$|23.7° - (\beta + \theta_d)| \leq 4.2° \tag{3.21}$$

Assuming only experimental and no theoretical errors on the r.h.s. of (3.20), we reject some otherwise valid points from our scan, but we checked that this does not have any significant effect on the results discussed in following sections.

Apart form the experimental bounds, there are also bounds from the requirement that the vacuum is stable, or that the true ground state of the theory does not break color and charge. We apply the corresponding charge and color breaking and unbounded from below MSSM scalar potential bounds [138–140], which give constraints on the soft supersymmetry breaking trilinear couplings, and consequently on the left-right elements of the sfermion mass matrices.

The Adaptive Scan Algorithm

The numerical analysis laid out in the previous subsections requires us to scan an N-dimensional ($N \geq 16$) parameter space sufficiently densely to account for all regions where the quantity X possibly is large. A straightforward approach is to scan over a uniform N-dimensional grid. However, this is both time-consuming and ineffective.

Compared to this brute force approach a random generation of parameters is much more efficient to find possible large deviations of the function X from the SM prediction. But still a random scan with a uniform distribution may miss values where the deviation is largest because in this regions it also tends to vary more strongly. And what we are interested in are actually the maximal allowed regions of the parameter space and the extremal values of the function X that are possible. To find this information, a very time-consuming scan is necessary. It would be desirable to generate points more densely where the function X is large and/or varies quickly - such a procedure would be particularly efficient if, as is expected, our results mainly depend on just a few parameters.

Recently, Brein [66] has suggested using an adaptive Monte-Carlo integration algorithm such as VEGAS [67,68] for a similar purpose. VEGAS performs "importance sampling" via an iterative algorithm. At each iteration, it generates a certain number of points according to a probability distribution determined by the integrand values encountered during the previous iterations. The probability distribution is chosen to be separable and is adjusted after each iteration. The initial distribution is chosen to be uniform. This procedure is designed to minimize the statistical error of the integration by increasing the number of points in those parts of the integration volume where the integrand is found to be large. While we are not interested in computing any integral to any given precision, VEGAS does provide what we desire, if we choose our integration volume as the parameter space (suitably rescaled) and the integrand such that it becomes large for large values of X. We found the following "integrand" useful:

$$f = \begin{cases} 0 & \text{parameter set rejected by constraints} \\ \left| X - X_L^{SM} \right|^n & \text{constraints satisfied} \end{cases} \tag{3.22}$$

where X is the quantity defined in (3.5), X_L^{SM} is its SM central value (3.4) and we varied the power n between 3 and 8. We "integrated" this function numerically with the VEGAS routine, storing all generated Monte Carlo points in a separate file along with the values of various observables for the analysis. The parameter ranges used for the integration are given in table 3.1.

Using the VEGAS algorithm has the great advantage of sampling mostly the important regions of parameter space, where the function X really depends significantly on at least some of the parameters. It also allows us to increase safely the number of the degrees of freedom – adding new variables has only a moderate effect on total computation time as long as the function X, or in general the VEGAS integrand, is weakly dependent on them. In fact, we were able to perform Monte Carlo sampling over huge portions of the MSSM parameter space, probably never tried before, of up to 63 dimensions (parameters), and to judge only afterwards, from the obtained distributions, which of the parameters where important for a given problem.

3.4 Numerical Results

Sensitivity to Scan Parameters

As a first step of our analysis, we plotted the distributions of $|X|$ obtained in the "constrained" scan versus various flavor diagonal and off-diagonal parameters, in order to check
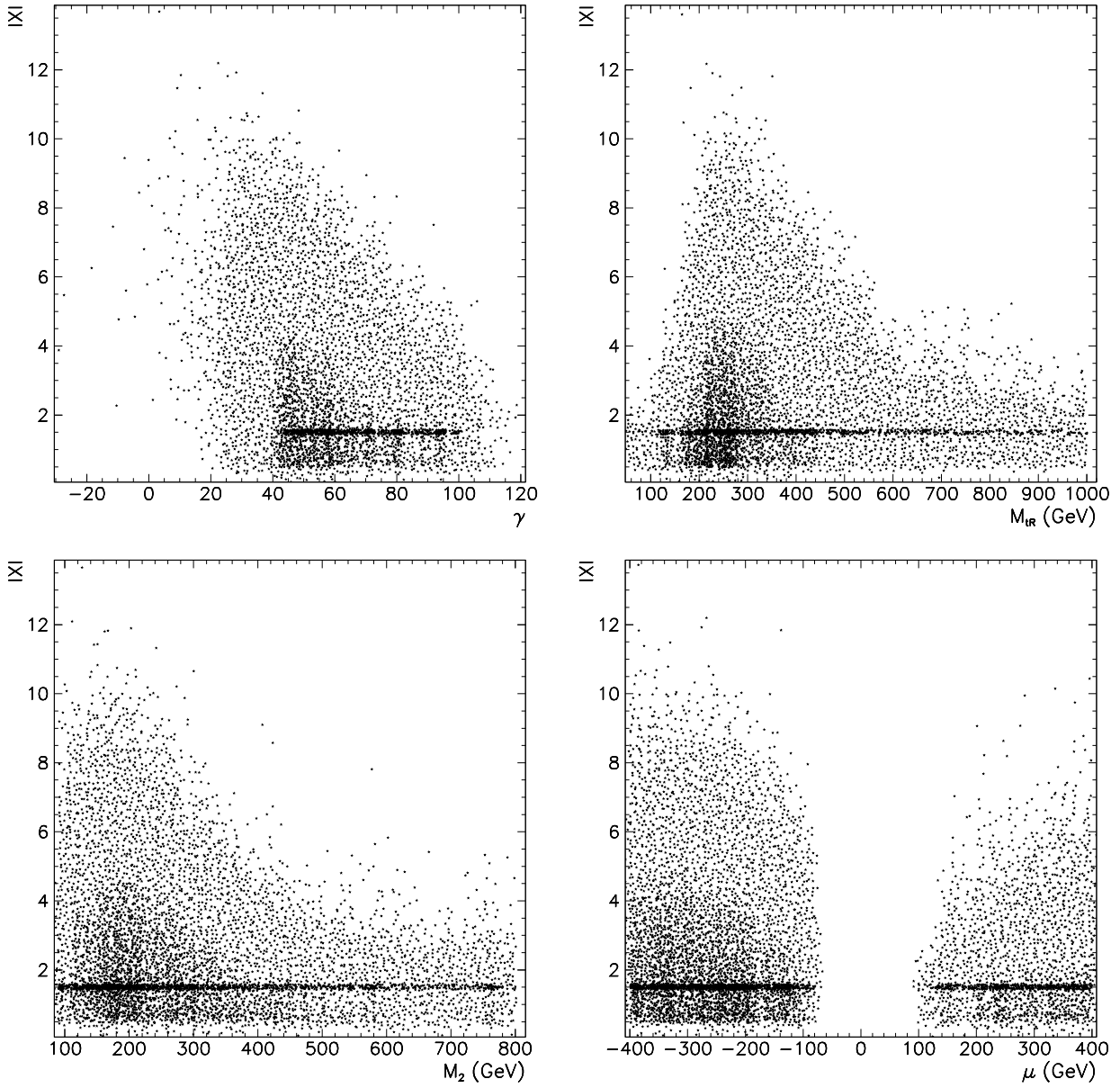
Figure 3.2: Distributions of X versus γ, M_{sq}, $M_{\tilde{t}_L}$, $M_{\tilde{t}_R}$, M_2 and μ for $\tan \beta = 2$ in data set generated during VEGAS integration.
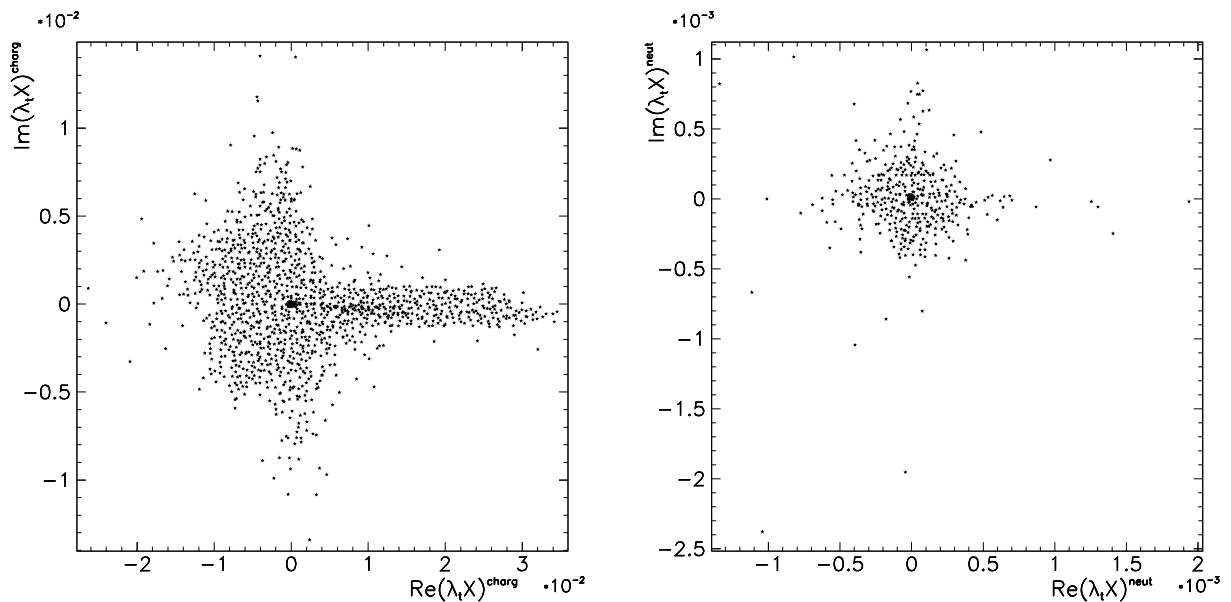
Figure 3.3: Chargino and neutralino contributions to $\lambda_t X$ for $\tan \beta = 2$.

the sensitivity of the considered decay rates to them. The plots obtained support our conjecture that only a modest subset of the MSSM parameters is in the first approximation relevant for our analysis, even after including the complicated set of additional bounds. Most of the obtained distributions for flavor diagonal parameters are flat (dependence on M_{A^0}, M_1, $M_{\tilde{g}}$) or almost flat (dependence on M_{sl}, A). A more pronounced dependence could be observed only in the case of γ and the MSSM parameters plotted in fig. 3.2.

The dependence visible for the other parameters can be explained by looking at fig. 3.3, where we plotted the contributions from the chargino and neutralino sectors to $\lambda_t X$. The chargino diagrams are always strongly dominant, typically one order of magnitude larger than the neutralino contributions. Gluino exchanges (in our case penguin diagrams only) can be always completely neglected, as we checked that they are several orders of magnitude smaller than other contributions. Thus, the size of both decay rates, $Br(K^+ \to \pi^+ \nu \bar{\nu})$ and $Br(K_L \to \pi^0 \nu \bar{\nu})$, is determined by the chargino-up-squark contribution and should depend mostly on the parameters entering the expression for this amplitude, in agreement with the results of [44, 64, 65]. This is not true for the variety of experimental and theoretical bounds we took into account in constraining the MSSM parameter space – they also depend on other parameters (e.g., the hole in the μ distribution comes of course from the bounds on the lightest neutralino and chargino masses). This has some secondary influence on the shape of the plots in fig. 3.2, as the imposed constraints can lead to a correlation between the allowed ranges of some of the parameters directly relevant for the $K \to \pi \nu \bar{\nu}$ decay calculation. For instance, attainable values of $|X|$ grow first with MSSM masses like $M_{\tilde{t}_R}$ or M_2, because experimental constraints for squark mass-insertions are easier to satisfy for heavier sparticles (similarly for distributions with $M_{\tilde{t}_L}$ or M_{sq}, not included in fig. 3.2). Later they go down again because the suppression of MSSM loop diagrams contributing to $K \to \pi \nu \bar{\nu}$ decays for heavy virtual particles dominates above the effect of weakening the impact of the experimental constraints. One should also note that the distribution of γ in fig. 3.2 shows an increased density of points around SM-preferred value $\gamma \approx 70° \pm 30°$ – for
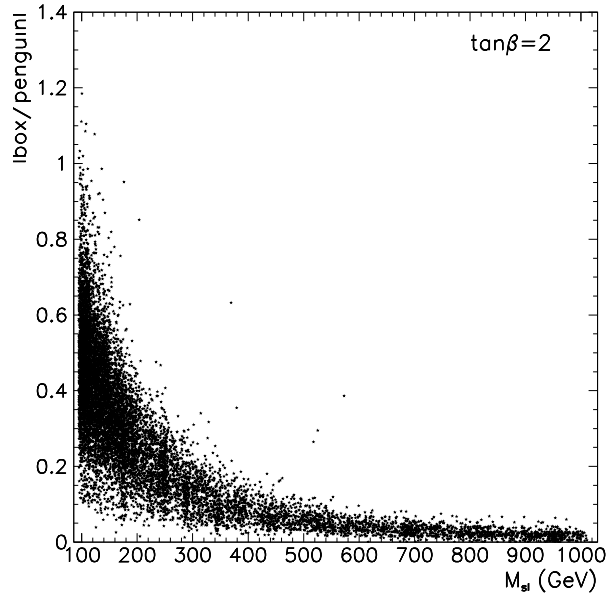
Figure 3.4: Absolute value of the ratio of box to penguin contributions as a function of slepton mass for $\tan\beta = 2$. Only points for which $\mathcal{B}(K^+ \to \pi^+\nu\bar{\nu}) \geq 1.5 \cdot 10^{-10}$ are plotted.

the remaining points, the larger or smaller value of the CKM phase must be compensated by the phases of some mass-insertions.

An interesting observation can be made by comparing the relative size of penguin- and box-type contributions to the $K \to \pi\nu\bar{\nu}$ decay amplitude. A common assumption used in the literature says that box diagrams are parametrically suppressed by $\mathcal{O}(M_W^2/M_{slepton}^2)$ and can be safely neglected when compared with Z penguin contribution. This is certainly not justified for light slepton masses, and not very accurate even for moderate $M_{sl} \sim 300$ GeV. In fig. 3.4 we plot the absolute value of the ratio of box to penguin contribution against the slepton mass, including in the distribution only particularly interesting points for which the $K^+ \to \pi^+\nu\bar{\nu}$ decay rate is large, $\mathcal{B}(K^+ \to \pi^+\nu\bar{\nu}) \geq 1.5 \cdot 10^{-10}$. As can be immediately seen, for slepton masses just above 100 GeV the box and penguin contributions are in a substantial number of cases comparable in amplitude, and even for $M_{sl} = 300$ GeV their ratio can still reach 30%. Thus box diagrams definitely should be taken into account in realistic calculations. Of course, their presence introduces a slepton mass dependence into the considered branching ratios, which would otherwise be negligible.

In our "constrained" scan we varied 3 types of mass-insertions, δ_{LL}^{12}, δ_{ULR}^{13} and $\delta_{ULR}^{23\star}$. We checked that the dependence on δ_{LL}^{12} is actually almost negligible, as expected because it is strongly constrained by bounds coming from ϵ_K and ΔM_K measurements: $\delta_{LL}^{12} \leq 0.05$. In fig. 3.5 we plot the dependence on the moduli of the remaining two ULR mass-insertions. The dependence on them is quite pronounced, in agreement with the conclusions of [64] that the second order ULR terms in the mass-insertion expansion give the dominant contribution to the considered decays. For comparison, we also plot $|X|$ against just the real part of δ_{ULR}^{13}, which exhibits less correlation.
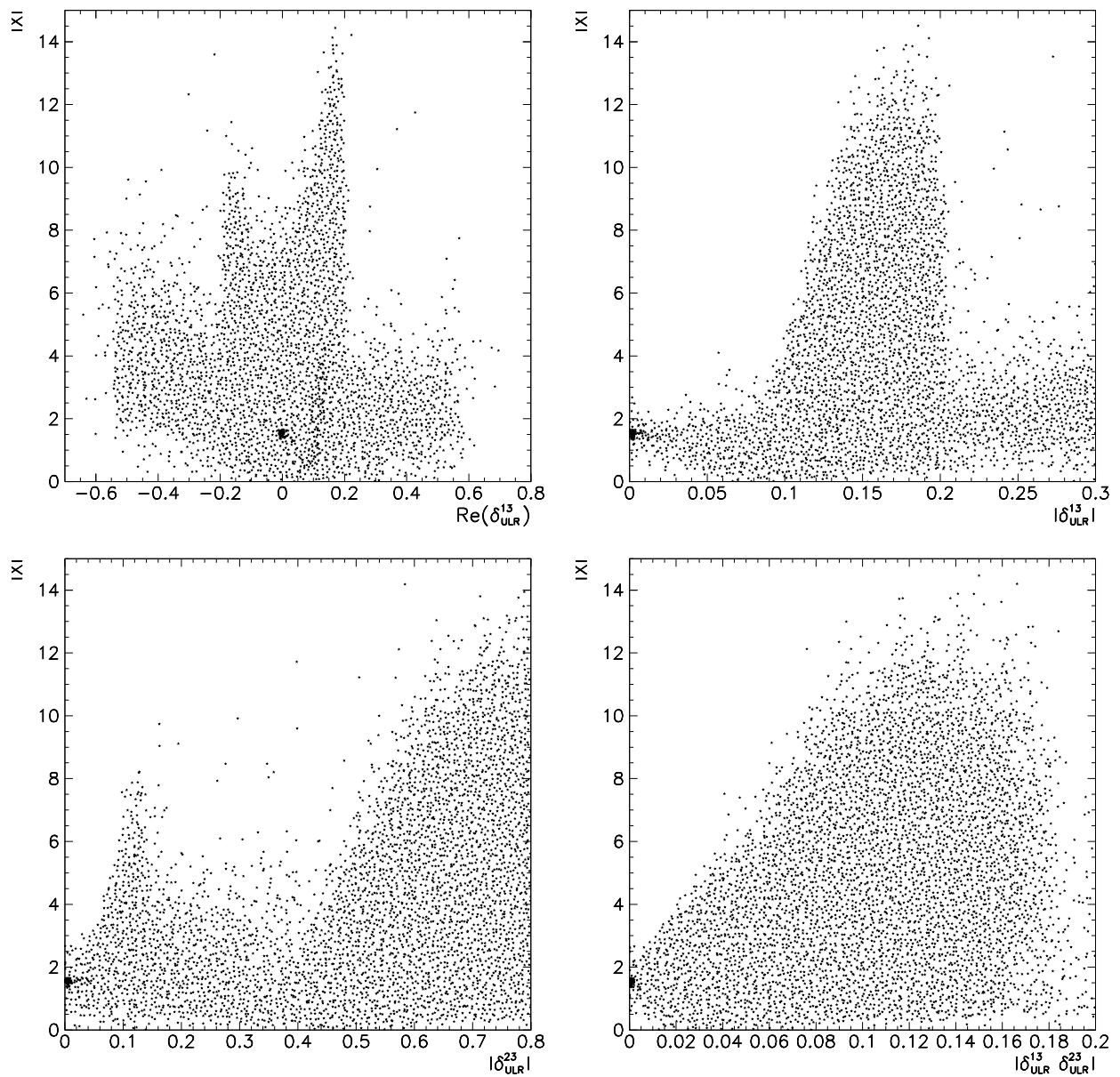
Figure 3.5: Distributions of X versus the real part and the modulus of δ_{ULR} mass-insertions for $\tan\beta = 2$. These plots have been produced using the exact results given in app. A and not the mass-insertion approximation.
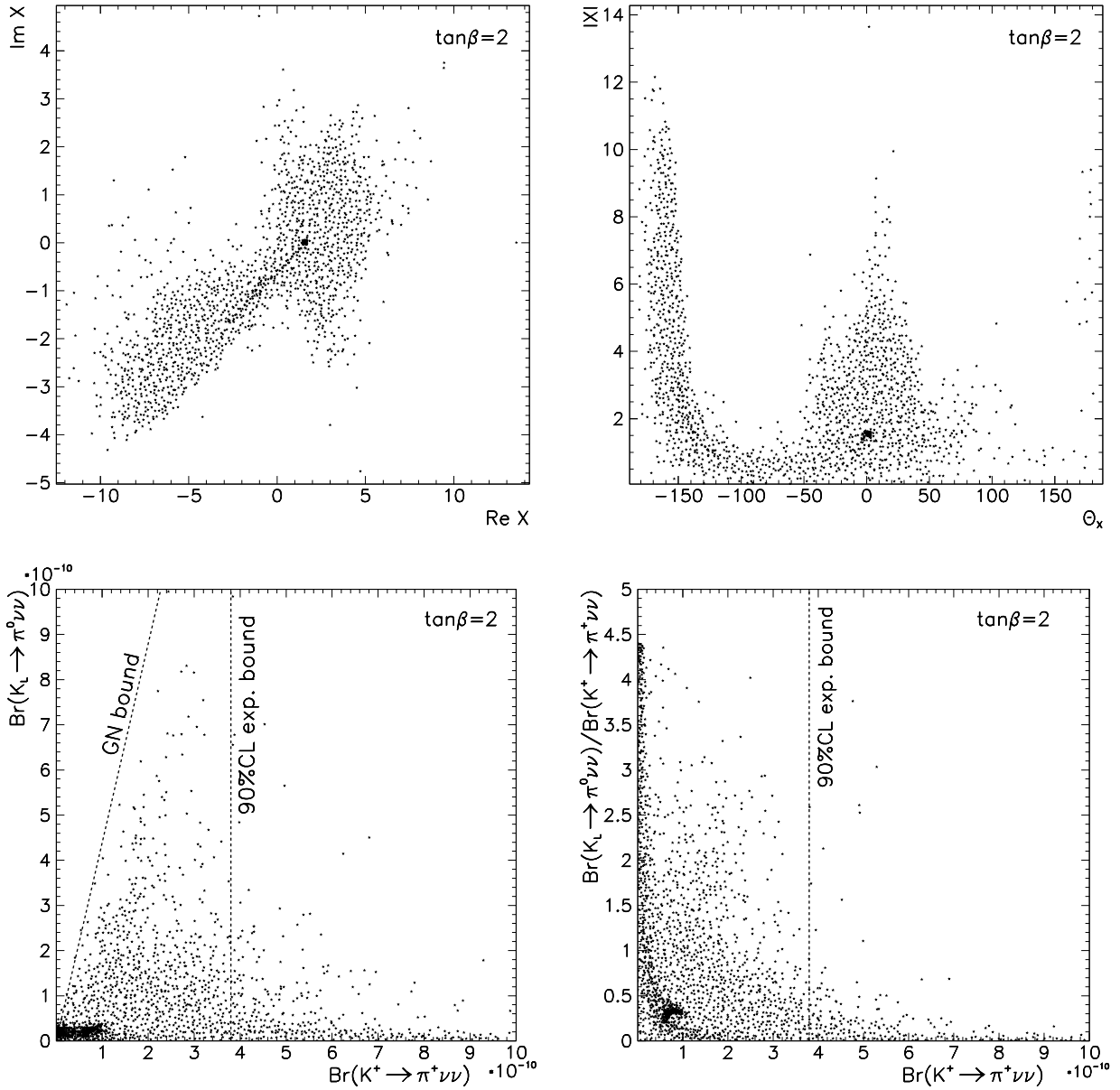
Figure 3.6: Distributions of X and $\mathcal{B}(K^+ \to \pi^+\nu\bar{\nu})$, $Br(K_L \to \pi^+\nu\bar{\nu})$ for $\tan\beta = 2$.
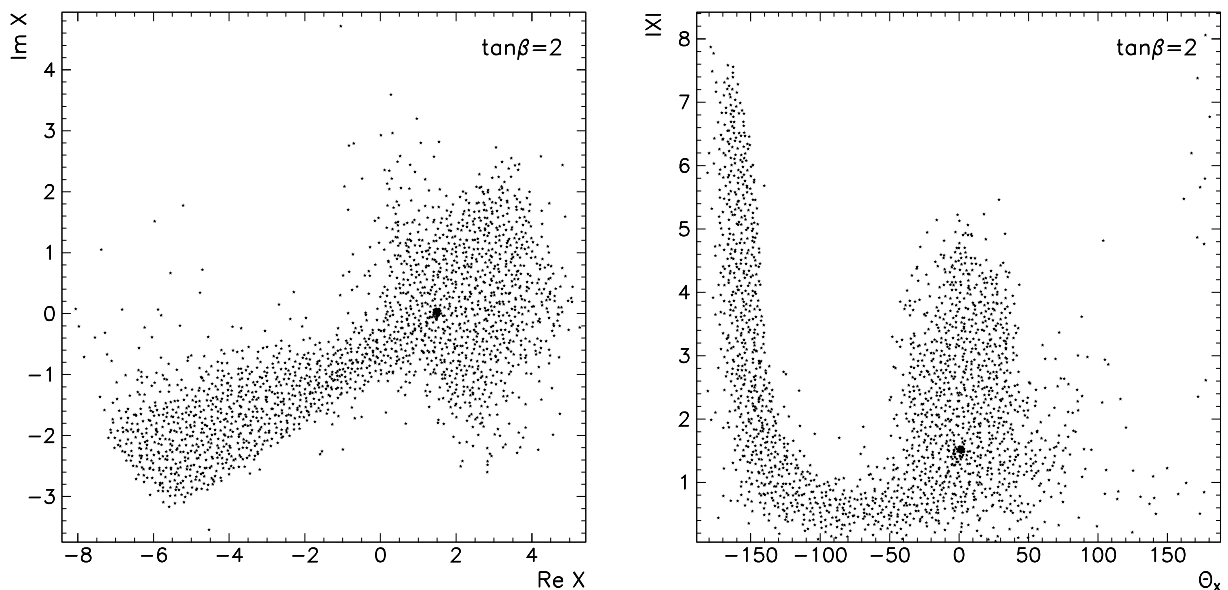
Figure 3.7: Distributions of X for $\tan\beta = 2$ after imposing the constraint $Br(K^+ \rightarrow \pi^+\nu\bar{\nu}) < 3.8 \cdot 10^{-10}$.

Allowed Ranges for X, $Br(K^+ \rightarrow \pi^+\nu\bar{\nu})$ and $Br(K_L \rightarrow \pi^0\nu\bar{\nu})$

The most interesting information from scanning over MSSM parameters are the maximal values of $|X|$, θ_X and the branching ratios $\mathcal{B}(K^+ \rightarrow \pi^+\nu\bar{\nu})$, $Br(K_L \rightarrow \pi^+\nu\bar{\nu})$ which can be obtained taking into account the bounds given by other processes. In fig. 3.6 we plot the distributions of those quantities for $\tan\beta = 2$.

As can be seen from fig. 3.6, the allowed values for $\mathcal{B}(K^+ \rightarrow \pi^+\nu\bar{\nu})$ and $Br(K_L \rightarrow \pi^+\nu\bar{\nu})$ can be significantly enhanced compared to the SM prediction, even by an order of magnitude. Such large values are higher than the 90%CL experimental bound [54], $Br(K^+ \rightarrow \pi^+\nu\bar{\nu}) < 3.8 \cdot 10^{-10}$, therefore this decay can already be used to constrain the MSSM parameter space. One should note that the obtained values for the branching ratios do not violate the Grossman-Nir (GN) [62] bound $Br(K_L \rightarrow \pi^0\nu\bar{\nu})/Br(K^+ \rightarrow \pi^+\nu\bar{\nu}) \leq 4.4$, which can be regarded as a simple cross-check of the correctness of our numerical codes.

In fig. 3.7 we plot the allowed range of X after imposing the cut [54] $Br(K^+ \rightarrow \pi^+\nu\bar{\nu}) < 3.8 \cdot 10^{-10}$. Even with this constraint, $|X|$ could be several times bigger than the SM value (3.4). Also, its phase can still vary almost freely, however is preferred to be in a broad range $-160° \leq \theta_X \leq 70°$. Such a freedom leads to a possible enhancement of the ratio $\mathcal{B}(K_L \rightarrow \pi^0\nu\bar{\nu})/\mathcal{B}(K^+ \rightarrow \pi^+\nu\bar{\nu})$ even for large values of $\mathcal{B}(K^+ \rightarrow \pi^+\nu\bar{\nu})$, as can be observed in fig. 3.6.

The plots of X in figs. 3.6 and 3.7 display a conspicuous correlation between the phase and modulus. This can be understood from the allowed region in the complex plane for the chargino contribution to $\lambda_t X$ shown in fig. 3.3. The experimental constraints we apply constrain its imaginary part to be relatively small, especially when the real part becomes large. Taken together with the fact that $\mathrm{Re}\lambda_t < 0$ (any γ) and that γ is sufficiently constrained (cf. fig. 3.2) to always imply $\mathrm{Im}\lambda_t > 0$, this explains the shape of the allowed region in the complex X plane.
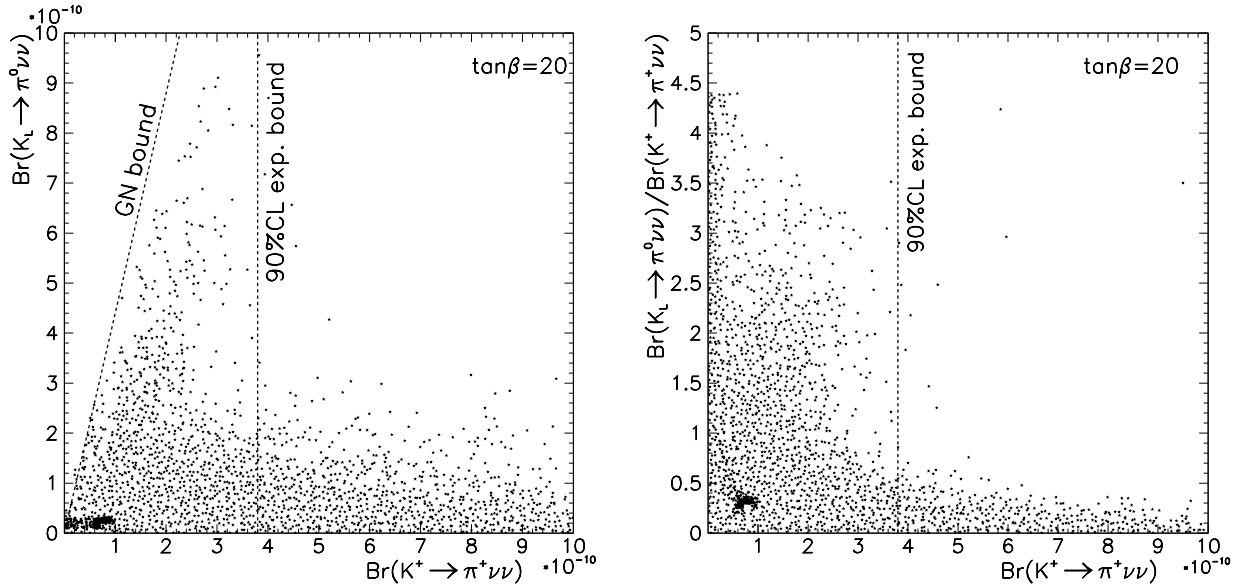
Figure 3.8: Distributions of $Br(K^+ \to \pi^+ \nu \bar{\nu})$ and $\mathcal{B}(K_L \to \pi^0 \nu \bar{\nu})$ for $\tan \beta = 20$.

Finally, in fig. 3.8 we plot the distributions of $Br(K^+ \to \pi^+ \nu \bar{\nu})$ and $\mathcal{B}(K_L \to \pi^0 \nu \bar{\nu})$ for higher value of $\tan \beta = 20$. Results are qualitatively similar to those obtained for $\tan \beta = 2$, however for larger $\tan \beta$ (particularly $\tan \beta \geq 10$) it is easier to generate parameters sets giving high branching ratios (or their ratio).

Extended Scan over MSSM Parameters

The "adaptive scan" method [66] described in an earlier subsection allows for efficient exploration of really huge multi-dimensional parameter spaces, especially when the dependence of the analyzed results on most of those parameters is not very strong. Therefore, we tried to check how our results change if we get rid of virtually all assumptions usually used to relate MSSM parameters and treat them all as free independent quantities. We varied randomly the following quantities:

- the angle γ (real)

- CP-odd Higgs mass M_{A^0} (real)

- $U(1)$ gaugino mass M_1 (complex)

- $SU(2)$ gaugino mass M_2 (complex)

- gluino mass $M_{\tilde{g}}$ (real)

- μ parameter (complex)

- diagonal LL mixing slepton mass matrix $[M_E^2]_{LL}$, common for all generations (real)

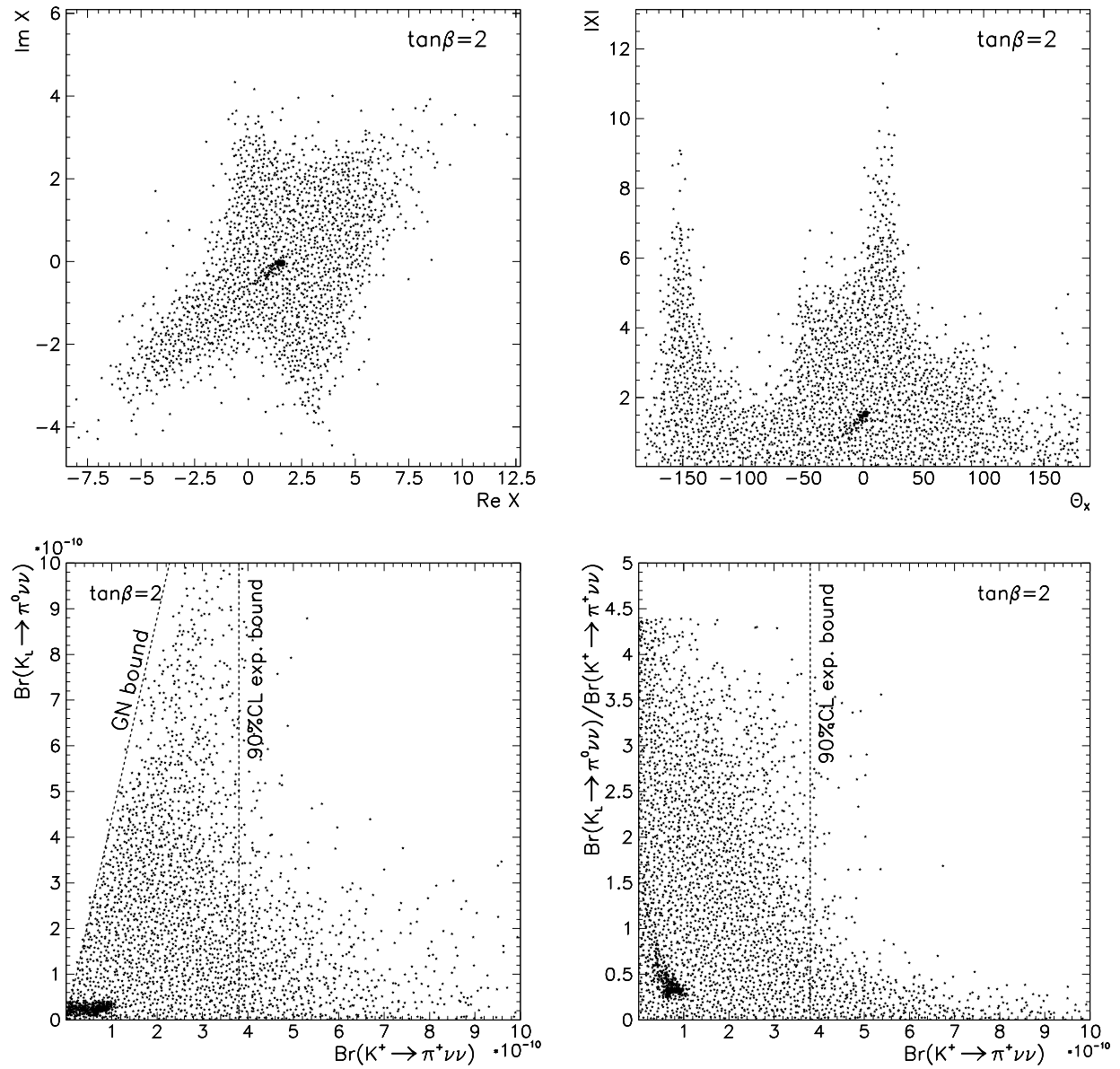- diagonal RR mixing slepton mass matrix $[M_E^2]_{RR}$, common for all generations (real)

Figure 3.9: Distributions of X, $Br(K^+ \to \pi^+\nu\bar{\nu})$ and $\mathcal{B}(K_L \to \pi^0\nu\bar{\nu})$ for $\tan\beta = 2$ in the 63-parameter scan.

- 9 independent diagonal mass parameters in squark mass matrices, 3 parameters for each of left, up-right and down-right mass matrix (all real)

- common sfermion LR mixing parameter A (real)

- 3 independent LL mass insertions in squark mass matrices: δ_{LL}^{12}, δ_{LL}^{13}, δ_{LL}^{32} (all complex)

- 6 independent RR mass insertions in squark mass matrices: δ_{DRR}^{12}, δ_{DRR}^{13}, δ_{DRR}^{32}, δ_{URR}^{12}, δ_{URR}^{13}, δ_{URR}^{32} (all complex)

- 12 independent LR up- and down-squark mass insertions δ_{DLR}^{12}, δ_{DLR}^{13}, δ_{DLR}^{32}, δ_{DLR}^{21}, δ_{DLR}^{31}, δ_{DLR}^{23}, δ_{ULR}^{12}, δ_{ULR}^{13}, δ_{ULR}^{32}, δ_{ULR}^{21}, δ_{ULR}^{31}, δ_{ULR}^{23} (all complex)

Altogether this gives 63 real degrees of freedom, more than half of the free parameters of the completely unconstrained (but R-parity-conserving) MSSM. For the MSSM mass parameters we use the same limits as given in table 3.1, with the additional requirement $|M_1| \geq 20$ GeV; for new complex parameters we assume their phase to vary completely freely. Of course, for any parameter point we still apply all experimental and theoretical constraints considered so far. Such an extensive scan was probably never reported before in the literature, so it is very interesting even to see if such a general MSSM version still retains any predictive power. The answer is positive – the results obtained for both analyzed decays, $K^+ \to \pi^+ \nu \bar{\nu}$ and $K^+ \to \pi^+ \nu \bar{\nu}$, remain qualitatively similar to those already discussed for the "constrained" scan case!

Plots equivalent to those shown in fig. 3.2 confirm the assumption that the dependence on most new parameters is weak (i.e. distributions are flat). Actually, in some cases like the left-handed stop and right-handed sbottom mass parameters they become even flatter than in fig. 3.2, as both discussed branching ratios do not depend directly on them (at least not strongly), and various experimental constraints can be satisfied varying additional parameters.

The allowed ranges for X and both branching ratios are extended somewhat in the 63-parameter scan, but not drastically, as illustrated in fig. 3.9. In general, as could be expected, it is easier to generate a θ_X in the full range, there are more points with large $Br(K^+ \to \pi^+ \nu \bar{\nu})$ and $\mathcal{B}(K_L \to \pi^0 \nu \bar{\nu})$ or their ratio, but in general all distributions are still well defined in shape, just a bit broader. Thus, the most important conclusion of this kind of analysis is the statement that even the almost fully general low-energy MSSM does not lose its predictive power and exploring it can still lead to reasonable and well defined results. Although it requires more effort in numerical computation, it also minimizes the possibility of overlooking some interesting scenarios which can be realized for particular MSSM parameter choices.

Chapter 4

QCD Corrections to $\bar{B} \to X_s l^+ l^-$

This chapter is devoted to the calculation of the two-loop QCD corrections to the matching conditions of the $b \to s l^+ l^-$ transition in the context of the "effective MSSM" introduced in sec. 2.5. To ensure the completeness of the calculated QCD corrections we furthermore assume that the down-squark mass matrix decomposes into 2×2 matrices for each generation and concentrate on the region $\tan \beta \le 10$. We review the low-energy effective Lagrangian relevant for this scenario and summarize our analytical findings for the two-loop Wilson coefficients in sec. 4.1. Details of the calculation can be found in the subsequent section. As an application, we present the formulae for the dilepton invariant mass distribution and the forward-backward asymmetry of the leptons in the decay $\bar{B} \to X_s l^+ l^-$ including all NNLO corrections and the phenomenological implications for both observables.

4.1 Two-Loop Matching Conditions

The framework of effective theories applied to electroweak decays is a convenient tool to resum QCD corrections to all orders using renormalization group methods [118–120]. The important point here is that the mass hierarchy of the SM and the considered extension – the "effective MSSM" – allows for integrating out the heavy degrees of freedom of masses $M_{\text{heavy}} \ge M_W$. The effect of the decoupled degrees of freedom will be contained in the Wilson coefficients of the QCD and QED gauge invariant low-energy effective theory with five active quark flavors.

Low-Energy Effective Lagrangian

The effective low-energy Lagrangian relevant to the inclusive decay $\bar{B} \to X_s l^+ l^-$ resulting from the SM and the "effective MSSM" has the following form,

$$\mathcal{L}_{\text{eff}} = \mathcal{L}_{\text{QED} \times \text{QCD}} + \mathcal{L}_{\text{physical}} + \mathcal{L}_{\text{evanescent}} + \mathcal{L}_{\text{EOM}} + \mathcal{L}_{\text{CT}} \tag{4.1}$$

The first term consists of kinetic terms of the light SM particles – the leptons and the five light quark flavors – as well as their QCD and QED interactions, while the second term is

given as follows [153–157],

$$\mathcal{L}_{\text{physical}} = \frac{4G_F}{\sqrt{2}} \left\{ \sum_{Q=u,c} \sum_{i=1}^{2} K_{Qb} K_{Qs}^* C_i^Q \mathcal{O}_i^Q + \sum_{Q=u,c,t} \sum_{i=3}^{10} K_{Qb} K_{Qs}^* C_i^Q \mathcal{O}_i \right\} \tag{4.2}$$

Here G_F is the Fermi constant and furthermore we refrain from using unitarity of the CKM matrix. This part consist of $\Delta B = -\Delta S = 1$ gauge-invariant local operators[1] up to dimension 6 built out of the light SM fields. It includes the current-current operators

$$\mathcal{O}_1^Q = (\bar{s}\gamma_\mu P_L T^a Q)(\bar{Q}\gamma^\mu P_L T^a b)$$

$$\mathcal{O}_2^Q = (\bar{s}\gamma_\mu P_L Q)(\bar{Q}\gamma^\mu P_L b) \tag{4.3}$$

the QCD penguin operators[2] [83, 158]

$$\mathcal{O}_3 = (\bar{s}\gamma_\mu P_L b)\sum_q (\bar{q}\gamma^\mu q)$$

$$\mathcal{O}_4 = (\bar{s}\gamma_\mu P_L T^a b)\sum_q (\bar{q}\gamma^\mu T^a q)$$

$$\mathcal{O}_5 = (\bar{s}\gamma_\mu \gamma_\nu \gamma_\rho P_L b)\sum_q (\bar{q}\gamma^\mu \gamma^\nu \gamma^\rho q)$$

$$\mathcal{O}_6 = (\bar{s}\gamma_\mu \gamma_\nu \gamma_\rho P_L T^a b)\sum_q (\bar{q}\gamma^\mu \gamma^\nu \gamma^\rho T^a q) \tag{4.4}$$

where the sum runs over all light quark flavors, the electro- and chromomagnetic moment operators[3]

$$\mathcal{O}_7 = \frac{e}{g_s^2} m_b (\bar{s}\sigma_{\mu\nu} P_R b) F^{\mu\nu}$$

$$\mathcal{O}_8 = \frac{1}{g_s} m_b (\bar{s}\sigma_{\mu\nu} P_R T^a b) G^{a\mu\nu} \tag{4.5}$$

where $\sigma^{\mu\nu} = \frac{1}{2}[\gamma^\mu, \gamma^\nu]$, and finally the semileptonic operators

$$\mathcal{O}_9 = \frac{e^2}{g_s^2} (\bar{s}\gamma_\mu P_L b)(\bar{l}\gamma^\mu l)$$

$$\mathcal{O}_{10} = \frac{e^2}{g_s^2} (\bar{s}\gamma_\mu P_L b)(\bar{l}\gamma^\mu \gamma_5 l) \tag{4.6}$$

The specific structure of the physical operators $\mathcal{O}_{1,...,10}$ is determined from the requirement that the effective theory reproduces the SM $\Delta B = -\Delta S = 1$ amplitudes of $b \to s+$(light particles) at the leading order in electroweak gauge couplings and up to $O[(\text{external momenta and light masses})^2/M_{\text{heavy}}^2])$, but to all orders in strong interactions. The same applies to the

---

[1]The operators conserve flavors other than B and S.

[2]Electroweak penguin operators arise first at $O(\alpha_{\text{em}})$ and are only relevant if QED corrections are considered. However, we will not include the higher order QED corrections, but rather use $\alpha_{\text{em}} = 1/133$ which yields results close to those obtained when including them, as was found in [86].

[3]The s-quark mass is neglected here, i.e. it is assumed to be negligibly small when compared to m_b.

extensions of the SM. It should be noted that the above given basis of physical operators results from the SM, however in extensions of the SM other physical operators could become relevant, too. In the MSSM scenario chosen here this is not the case for low values of $\tan \beta$ and the SM operator basis suffices.

We remark that the QCD penguin operators $\mathcal{O}_{3...6}$ are defined in such a way that problems connected with the treatment of γ_5 in $D \neq 4$ dimensions do not arise [158]. Consequently we are allowed to consistently use anticommuting γ_5 in dimensional regularization throughout the calculation.

In addition to the physical operators several non-physical operators have to be included in the matching procedure of the full and effective theories. The so-called EOM-vanishing operators that vanish by the QCD×QED equation of motion of the effective theory up to a total derivative are collected in the third term given in (4.1). They appear in intermediate steps of the off-shell calculation of the processes $b \to s\gamma$ and $b \to sg$ and contribute to the final results of Wilson coefficients of physical operators when going beyond LO matching. The so-called evanescent operators contained in the fourth term in (4.1) vanish algebraically in four dimensions, however in $D \neq 4$ dimensions they are indispensable and contribute to Wilson coefficients of physical operators. We use the same convention for the evanescent operators as introduced in the evaluation of the anomalous dimensions relevant to $b \to s\gamma$, $b \to sg$ and $b \to sl^+l^-$ of [83, 84]. All EOM and evanescent operators relevant for the two-loop matching presented here can be found in app. B.

The last term given (4.1) collects all counterterms to render the effective theory finite.

Two-Loop Matching Conditions

The Wilson coefficients at the matching scale μ_t can be perturbatively expanded in $\alpha_s(\mu_t)$ as follows,

$$C_i^Q = C_i^{Q(0)} + \frac{\alpha_s(\mu_t)}{4\pi} C_i^{Q(1)} + \frac{\alpha_s^2(\mu_t)}{(4\pi)^2} C_i^{Q(2)} + \dots, \qquad Q = u, c, t \qquad (4.7)$$

Contributions to order α_s^n to each Wilson coefficient originate from n-loop diagrams which follows from the particular convention of powers of the QCD gauge coupling g_s in the normalization of the operators $\mathcal{O}_{7,...,10}$ given in (4.5) and (4.6).

The result of the matching calculation of the Wilson coefficients of the physical operators $\mathcal{O}_{1...,10}$ can be summarized as follows. At the tree-level the only nonzero Wilson coefficient is

$$C_2^{c(0)} = -1 \qquad (4.8)$$

The one- and two-loop matching conditions in the "charm-sector" read as[4]

$$C_1^{c(1)} = -15 - 6L_W, \qquad\qquad C_2^{c(1)} = C_3^{c(1)} = 0$$

$$C_4^{c(1)} = \frac{7}{9} - \frac{2}{3}L_W, \qquad\qquad C_5^{c(1)} = C_6^{c(1)} = 0$$

---

[4]In the matching calculation we neglected all light particle masses except for linear effects in m_b in the determination of the Wilson coefficients corresponding to the electro- and chromomagnetic moment operators. In consequence the u-quark and c-quark sectors are equal, i.e. $C_i^u = C_i^c$.

$$C_7^{c(1)} = \frac{23}{36}, \qquad\qquad\qquad C_8^{c(1)} = \frac{1}{3}$$

$$C_9^{c(1)} = -\frac{1}{4\mathrm{s}_W^2} - \frac{38}{27} + \frac{4}{9}L_W, \qquad\qquad C_{10}^{c(1)} = \frac{1}{4\mathrm{s}_W^2} \qquad (4.9)$$

$$C_1^{c(2)} = [T_1]_t^1 + [T_1]_{\tilde{q}}^1 - \frac{7987}{72} - \frac{17}{3}\pi^2 - \frac{475}{6}L_W - 17L_W^2$$

$$C_2^{c(2)} = -\frac{127}{18} - \frac{4}{3}\pi^2 - \frac{46}{3}L_W - 4L_W^2$$

$$C_3^{c(2)} = \frac{680}{243} + \frac{20}{81}\pi^2 + \frac{68}{81}L_W + \frac{20}{27}L_W^2$$

$$C_4^{c(2)} = -\frac{950}{243} - \frac{10}{81}\pi^2 - \frac{124}{27}L_W - \frac{10}{27}L_W^2$$

$$C_5^{c(2)} = -\frac{68}{243} - \frac{2}{81}\pi^2 - \frac{14}{81}L_W - \frac{2}{27}L_W^2$$

$$C_6^{c(2)} = -\frac{85}{162} - \frac{5}{108}\pi^2 - \frac{35}{108}L_W - \frac{5}{36}L_W^2$$

$$C_7^{c(2)} = -\frac{713}{243} - \frac{4}{81}L_W, \qquad\qquad C_8^{c(2)} = -\frac{91}{324} + \frac{4}{27}L_W$$

$$C_9^{c(2)} = -\frac{1}{\mathrm{s}_W^2} - \frac{524}{729} + \frac{128}{243}\pi^2 + \frac{16}{3}L_W + \frac{128}{81}L_W^2, \qquad C_{10}^{c(2)} = \frac{1}{\mathrm{s}_W^2} \qquad (4.10)$$

with

$$L_W = \ln\frac{\mu_W^2}{M_W^2} \qquad\qquad (4.11)$$

and $\mu_W \sim O(M_W)$ being the renormalization scale in the "charm-sector". Due to the chosen renormalization prescription the first diagram given in fig. 4.2 with top quarks or squarks in the loops is completely "renormalized away", and thus the Wilson coefficient of $\mathcal{O}_2$ is not affected by virtual top quark or squark exchange. The second and third diagram shown in fig. 4.2 are the origin of the function [82]

$$[T_1]_t^1 = -(16x+8)\sqrt{4x-1}\,\mathrm{Cl}_2\left(2\arcsin\frac{1}{2\sqrt{x}}\right) + \left(16x + \tfrac{20}{3}\right)\ln x + 32x + \frac{112}{9} \quad (4.12)$$

where $x = m_t^2/M_W^2$, and of the function[5]

$$[T_1]_{\tilde{q}}^1 = \sum_{a=1}^{6}\sum_{q=u,d}\left\{2(4x_{\tilde{q}_a}-1)^{\frac{3}{2}}\,\mathrm{Cl}_2\left(2\arcsin\frac{1}{2\sqrt{x_{\tilde{q}_a}}}\right)\right.$$

$$\left. - 8\left(x_{\tilde{q}_a} - \frac{1}{3}\right)\ln x_{\tilde{q}_a} - 16x_{\tilde{q}_a}\right\} + \frac{208}{3} \qquad (4.13)$$

---

[5]Here we assumed $2m_{\tilde{q}_a} > M_W$ which is clearly fulfilled.

where $x_{\tilde{q}_a} = m_{\tilde{q}_a}^2/M_W^2$, both entering the Wilson coefficient of $\mathcal{O}_1$. The definition of the Clausen function $\mathrm{Cl}_2(x)$ can be found in app. C.

The one- and two-loop matching conditions in the "top-sector" read as

$$C_3^{t(1)} = 0, \qquad\qquad\qquad C_3^{t(2)} = [G_3]^1$$

$$C_4^{t(1)} = [E_4]^{(n-1)}$$

$$C_5^{t(1)} = 0, \qquad\qquad\qquad C_5^{t(2)} = -\frac{1}{10}[G_3]^1 + \frac{2}{15}[E_4]^0$$

$$C_6^{t(1)} = 0, \qquad\qquad\qquad C_6^{t(2)} = -\frac{3}{16}[G_3]^1 + \frac{1}{4}[E_4]^0$$

$$C_7^{t(1)} = -\frac{1}{2}[A_7]^{(n-1)}$$

$$C_8^{t(1)} = -\frac{1}{2}[F_8]^{(n-1)}$$

$$C_9^{t(1)} = \frac{1 - 4\mathrm{s}_W^2}{\mathrm{s}_W^2}[C_9^{\bar{l}l}]^{(n-1)} - \frac{1}{\mathrm{s}_W^2}[B_9^{\bar{l}l}]^{(n-1)} - [D_9^{\bar{l}l}]^{(n-1)}$$

$$C_{10}^{t(1)} = \frac{1}{\mathrm{s}_W^2}\left\{[B_{10}^{\bar{l}l}]^{(n-1)} - [C_9^{\bar{l}l}]^{(n-1)}\right\} \tag{4.14}$$

The index n corresponds to the number of loops in the diagrams which can be classified into LO ($n = 0$), NLO ($n = 1$) and NNLO ($n = 2$) contributions; see also the comment below (4.7). The various functions $[X_k]^n$ introduced in (4.14) indicate their origin when matching the $b \to s+$(light particles) Green functions of the full and effective theory,

- $[G_3]$: two-loop box-type diagrams of $b \to sq\bar{q}$ (see fig. 4.4)

- $[E_4]$: off-shell part of $b \to sg$, contributing to $b \to sq\bar{q}$ (see fig. 4.3)

- $[A_7]$: on-shell part of $b \to s\gamma$ (see fig. 4.3)

- $[F_8]$: on-shell part of $b \to sg$ (see fig. 4.3)

- $[B_{9,10}^{\bar{l}l}]$: box-type diagrams of $b \to l^+l^-$ (see fig. 4.5)

- $[C_9^{\bar{l}l}]$: Z penguin diagrams of $b \to l^+l^-$ (see fig. 4.3)

- $[D_9^{\bar{l}l}]$: off-shell part of $b \to s\gamma$, contributing to $b \to l^+l^-$ (see fig. 4.3)

Furthermore, each function $[X_k]^n$ receives contributions from different virtual particle exchange,

$$[X_k]^n = \sum_i = [X_k]_i^n \tag{4.15}$$

where the index i corresponds to

- $i = W$: "top quark – W boson" loops (SM)

- $i = H$: "top quark – charged Higgs boson" loops

- $i = C$: "chargino – up-squark" loops

receiving virtual gluon corrections at NNLO and further

- $i = Q$: "chargino – up-squark" loops containing the quartic squark-vertex[6]

which contribute only at NNLO. Discarding the contributions $\{H, C, Q\}$ in the sum of (4.15) one recovers the SM results, whereas discarding only $\{C, Q\}$ one obtains the results for the 2HDM of type II provided $\tan \beta$ is small. Not all of the functions $[X_k]^n$ are new but some have already been resented in the literature. To summarize:

- The contributions $[A_7]^1_i$, $[F_8]^1_i$, $[B_{10}^{\bar{l}l}]^1_i$, $[C_9^{\bar{l}l}]^1_i$ with $i = W, H, C, Q$ and $[B_9^{\bar{l}l}]^1_W$, $[D_9^{\bar{l}l}]^1_W$, $[G_3]^1_W$, $[E_4]^1_W$, $[T_1]^1_t$ have been calculated previously in [38,39,41,42,82,99–101,159–163] with the expressions listed in (4.12) and app. C.

- The contributions $[G_3]^1_i$, $[E_4]^1_i$, $[B_9^{\bar{l}l}]^1_i$, $[D_9^{\bar{l}l}]^1_i$ with $i = H, C, Q$ and $[T_1]^1_{\tilde{q}}$ have been calculated here for the first time with the expressions listed in (4.13) and app. C. The contributions with $i = H$ have been calculated already in [164] and very recently the same result has been obtained in [165].

Explicit expressions for the various functions $[X_k]^n$ can be found in app. C. We stress that all parameters appearing there are $\overline{\text{MS}}$ renormalized[7].

4.2   Details of the Calculation

The calculation of the Wilson coefficients will be performed working with background gauge bosons in dimensional regularization with fully anticommuting γ_5 and in an arbitrary R_ξ gauge for the gluon gauge parameter but in the t'Hooft-Feynman gauge for the W boson gauge parameter. A detailed description of the two-loop matching calculation for the $b \to s l^+ l^-$ transition within the SM can be found in [82]. We will follow their approach in calculating the supersymmetric contributions to the relevant Wilson coefficients.

In order to render the effective side finite we have to introduce renormalization constants for the low-energy effective couplings,

$$C_i^{Q,\text{bare}} = \sum_j Z_{ji} C_j^Q, \qquad\qquad Q = u, c, t \qquad\qquad (4.16)$$

which can be expanded in terms of the strong coupling constant as follows,

$$Z = \mathbb{1} + \sum_{k=1}^{\infty} \left(\frac{\alpha_s}{4\pi}\right)^k \delta Z^{(k)} = \mathbb{1} + \sum_{k=1}^{\infty} \sum_{l=0}^{k} \left(\frac{\alpha_s}{4\pi}\right)^k \frac{1}{\epsilon^l} \delta Z^{(k,l)} \qquad (4.17)$$

and is found in the $\overline{\text{MS}}$ scheme from the following two conditions which the n-loop effective theory amplitudes have to satisfy [42]:

---

[6]Strictly speaking these contributions originate from the part of the quartic squark vertex proportional to the strong coupling constant g_s.

[7]The expressions for the functions $[X_k]^n$ can also be found in [166].

- Renormalized amplitudes proportional to the Wilson coefficients coefficients of physical operators have to be finite in the limit $\epsilon \to 0$. Counterterms which make them finite can contain nothing but $1/\epsilon^k$ poles, with $1 \le k \le n$.

- Renormalized amplitudes proportional to the Wilson coefficients coefficients of evanescent operators have to vanish in the limit $\epsilon \to 0$. Counterterms which make them vanish can contain nothing but $1/\epsilon^k$ poles, with $0 \le k \le n-1$ if the are proportional to physical operators, and with $1 \le k \le n$ if the are proportional to evanescent operators

The Wilson coefficients $C_i^{(1)}$ can then be obtained by the matching procedure,

$$\mathcal{A}_{\text{MSSM}}^Q = i\frac{4G_F}{\sqrt{2}}K_{Qb}K_{Qs}^*\left[C_i^{Q(0)}\left(\delta\tilde{Z}^{(1)}\delta_{ij} + \delta Z_{ij}^{(1)}\right) + \frac{\alpha_s}{4\pi}C_i^{Q(1)}\delta_{ij}\right]\langle\mathcal{O}_j\rangle_{\text{tree}} \tag{4.18}$$

where $\mathcal{A}_{\text{MSSM}}$ is the relevant amplitude in the MSSM. Here, the sum over i and j extends over all physical, evanescent and EOM-vanishing operators present in the low-energy effective Lagrangian. Furthermore, $\delta\tilde{Z}^{(1)}$ summerizes $O(\alpha_s)$ renormalization constants of the strong coupling constant, quark fields and quark masses present in the local operators $\mathcal{O}_i$ in the $\overline{\text{MS}}$ scheme with five active quark flavors. Note that only tree-level diagrams contribute on the effective theory side since all light masses have been set equal to zero. The equation to be solved for $C_i^{(2)}$ reads

$$\mathcal{A}_{\text{MSSM}}^Q = i\frac{4G_F}{\sqrt{2}}K_{Qb}K_{Qs}^*\left[C_i^{Q(0)}\left(\delta\tilde{Z}^{(2)}\delta_{ij} + \delta Z_{ij}^{(2)} + \delta\tilde{Z}^{(1)}\delta Z_{ij}^{(1)}\right)\right.$$
$$\left. + \frac{\alpha_s}{4\pi}C_i^{Q(1)}\left(\delta\tilde{Z}^{(1)}\delta_{ij} + \delta Z_{ij}^{(2)}\right) + \frac{\alpha_s^2}{(4\pi)^2}C_i^{Q(2)}\delta_{ij}\right]\langle\mathcal{O}_j\rangle_{\text{tree}} \tag{4.19}$$

where $\delta\tilde{Z}^{(2)}$ summerizes now corresponding $O(\alpha_s^2)$ renormalization constants.

Having renormalized the effective theory side of the matching equation[8], let us proceed to renormalize the "effective MSSM" side. Since weak interactions produce flavor non-diagonal propagation in the down-quark sector we have to introduce matrix-valued field renormalization constants for the down-quark fields [167–169],

$$d_X^{\text{bare}} = \sqrt{Z_d^X}d_X = \sqrt{\mathbb{1} + \delta Z_d^X}d_X, \qquad\qquad d_X = P_X d \tag{4.20}$$

with $X = L, R$ and d being a three-component object in flavor space, in order to obtain diagonal down-quark mass matrices at $O(e^2)$ and $O(e^2g_s^2)$. These renormalized fields produce a non-diagonal counterterm for the down-quark kinetic term,

$$\mathcal{L}_{dd,}^{\text{CT},I\neq J} = i\bar{d}_I\left([\delta Z_d^L]_{IJ}^{c(1)} + [\delta Z_d^L]_{IJ}^{c(2)}\right)\slashed{\partial}P_L d_J$$
$$- \bar{d}_I\left([\delta Z_d^{LR}]_{IJ}^{m(1)} + [\delta Z_d^{LR}]_{IJ}^{m(2)}\right)P_L d_J - \bar{d}_I\delta Z_m^{(1)}[\delta Z_d^{LR}]_{IJ}^{m(1)}P_L d_J + (L \leftrightarrow R)$$
$$\tag{4.21}$$

---

[8]Needless to say that there remain infrared divergences which cancel in the matching equation against their counterparts contained in the "effective MSSM" amplitudes.

where we defined

$$[\delta Z_d^L]_{IJ}^c = \frac{1}{2}[\delta Z_d^L]_{IJ} + \frac{1}{2}[\delta Z_d^{L\dagger}]_{IJ}$$

$$[\delta Z_d^{LR}]_{IJ}^m = \frac{1}{2}[M_D]_{II}[\delta Z_d^L]_{IJ} + \frac{1}{2}[M_D]_{JJ}[\delta Z_d^{R\dagger}]_{IJ} \tag{4.22}$$

with δZ_m being the flavor diagonal one-loop quark mass renormalization constant in the $\overline{\text{MS}}$ scheme, and the renormalization constants $[\delta Z_d^R]^c$ and $[\delta Z_d^{RL}]^m$ can be obtained by substituting $L \leftrightarrow R$ in (4.22). The field renormalization constants introduced in (4.20) are uniquely fixed by the requirement that the renormalized one-loop and two-loop selfenergy for the $b \to s$ transition vanishes for $p^2 = 0$, where p is the incoming momentum of the b quark. Therefore non-diagonal propagation is not present in the renormalized theory in the approximation where terms of order $O[(\text{external momenta and light masses})/M_{\text{heavy}}])$ are neglected[9].

The relevant one-loop and two-loop counterterms at $O(e^2)$ and $O(e^2 g_s^2)$ for the $b \to s\gamma$, $b \to sg$ and the $b \to sZ$ matching calculations read[10]

$$\mathcal{L}_{dd\gamma}^{\text{CT},I \neq J} = \frac{1}{3}e\bar{d}_I \left([\delta Z_d^L]_{IJ}^{c(1)} + [\delta Z_d^L]_{IJ}^{c(2)}\right)\gamma^\mu P_L d_J A_\mu + (L \leftrightarrow R)$$

$$\mathcal{L}_{ddg}^{\text{CT},I \neq J} = -g_s\bar{d}_I \left([\delta Z_d^L]_{IJ}^{c(1)} + [\delta Z_d^L]_{IJ}^{c(2)}\right)\gamma^\mu T^a P_L d_J G_\mu^a + (L \leftrightarrow R)$$

$$\mathcal{L}_{ddZ}^{\text{CT},I \neq J} = \frac{e}{s_W c_W}\Bigg\{ \left(\frac{1}{2} - \frac{1}{3}s_W^2\right)\bar{d}_I \left([\delta Z_d^L]_{IJ}^{c(1)} + [\delta Z_d^L]_{IJ}^{c(2)}\right)\gamma^\mu P_L d_J$$

$$-\frac{1}{3}s_W^2 \bar{d}_I \left([\delta Z_d^R]_{IJ}^{c(1)} + [\delta Z_d^R]_{IJ}^{c(2)}\right)\gamma^\mu P_R d_J\Bigg\}Z_\mu \tag{4.23}$$

An additional complication arises in the MSSM because the strong interactions are no longer flavor blind which is the case in the SM. Here we have "squark–quark–gluino" and "quartic–squark" interactions leading to flavor transitions between quarks and squarks, and in our scenario, where the gluino is heavy and decoupled, only the latter interactions are relevant. They lead to off-diagonal field renormalization constants for up-squarks,

$$\tilde{u}_a^{\text{bare}} = [\sqrt{Z_{\tilde{u}}}]_{ab}\, \tilde{u}_b = [\sqrt{\mathbb{1} + \delta Z_{\tilde{u}}}]_{ab}\, \tilde{u}_b \tag{4.24}$$

which in turn affects the mixing matrix Γ^U [170],

$$\Gamma^{U(0)} = \left(\mathbb{1} + \delta\Gamma^U\right)\Gamma^U, \qquad\qquad \delta\Gamma^U = \frac{1}{4}\left(\delta Z_{\tilde{u}} - \delta Z_{\tilde{u}}^\dagger\right) \tag{4.25}$$

We will renormalize the matrix-valued field renormalization constants for up-squarks and hence the mixing matrix Γ^U in the $\overline{\text{MS}}$ scheme.

---

[9]Working in such a renormalization scheme, the Wilson coefficient of the operator N_{30} (cf. app. B) gets no contribution from the $b \to s$ matching. Alternatively one could simply require the $\gamma^\mu P_L$ term to vanish in the $b \to s\gamma$ and $b \to sg$ matching to determine $[\delta Z_d^L]^c$ directly. This is possible, because the $\gamma^\mu P_L$ term not proportional to external momenta or light masses on the effective side stems solely from N_{30}.

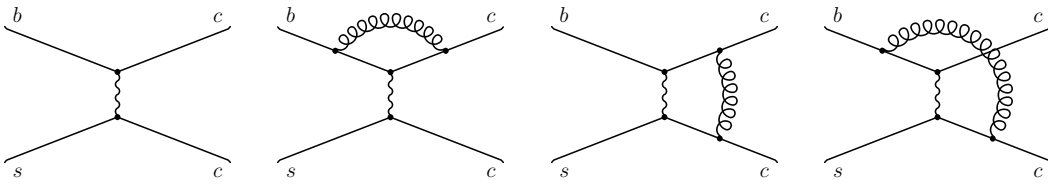[10]Note that $Z_{\hat{G}} = Z_g^{-2}$ since we work with a background field gluon.

Figure 4.1: Tree-level and one-loop contributions to $b \to sc\bar{c}$. The wiggly line denotes the W boson. Possible left-right and up-down reflected diagrams are not shown.

The $\overline{\text{MS}}$ counterterms for the effective couplings a_g and a_Y, defined by $\delta a_g = a_g + \delta a_g$ and $\delta a_Y = a_Y + \delta a_Y$, read

$$\delta a_g = -\frac{2}{\epsilon}\frac{\alpha_s}{4\pi}\,a_g, \qquad\qquad \delta a_Y = \frac{2}{\epsilon}\frac{\alpha_s}{4\pi}\,a_Y \qquad\qquad (4.26)$$

They are needed to cancel divergences stemming from gluon corrections to the "chargino–upsquark–downquark" vertex in the "effective MSSM".

All remaining QCD counterterms in the "effective MSSM" will be $\overline{\text{MS}}$ renormalized except for those were the top quark and squarks contribute to light-quark and gluon propagators. The corresponding renormalization constants will be determined in the MOM scheme at $q^2 = 0$, where q is the four-momentum of the light-quark or the gluon.

Matching $b \to s\bar{c}c$

The diagrams contributing to the $b \to sc\bar{c}$ amplitudes within the MSSM are depicted in figs. 4.1 and 4.2. Here we neglected diagrams with charged Higgs boson exchange instead of the W boson being an excellent approximation for low values of $\tan\beta$. All diagrams have been calculated for vanishing external momenta and light quark masses set equal to zero. The appearing infrared divergences, which we regularize dimensionally, cancel when matching with the "effective MSSM".

Our renormalization scheme is fixed by the following observations. The Lagrangian $\mathcal{L}_{\text{QED}\times\text{QCD}}$ given in (4.1) is taken in its canonical form, i.e. we drop only terms including the top quark and squarks, and will be renormalized in the $\overline{\text{MS}}$ scheme. We want the full theory side, the "effective MSSM", to have fields and parameters being equal to those present in the low-energy effective Lagrangian, and hence we have to "renormalize away" all light particle Green function with the top quark and squarks in the loops[11]. More precisely this means that the propagators of light particles are subtracted in the MOM scheme at $q^2 = 0$, i.e. terms of order $O[(\text{external momenta and light masses})/m_t])$ are neglected. In the case at hand this renormalization affects the gluon field renormalization constant $\delta Z_G^{(1)}$ at the one-loop level, which in turn affects the strong coupling constant renormalization constant $\delta Z_g^{(1)}$, and furthermore the light quark field QCD renormalization constant $\delta Z_q^{(2)}$ at the two-loop level. We remark that we have to include infinite, finite and $O(\epsilon)$ terms in these renormalization

---

[11]This means in particular that the strong coupling constant α_s being the same in both theories is the $\overline{\text{MS}}$ renormalized one with five active flavors
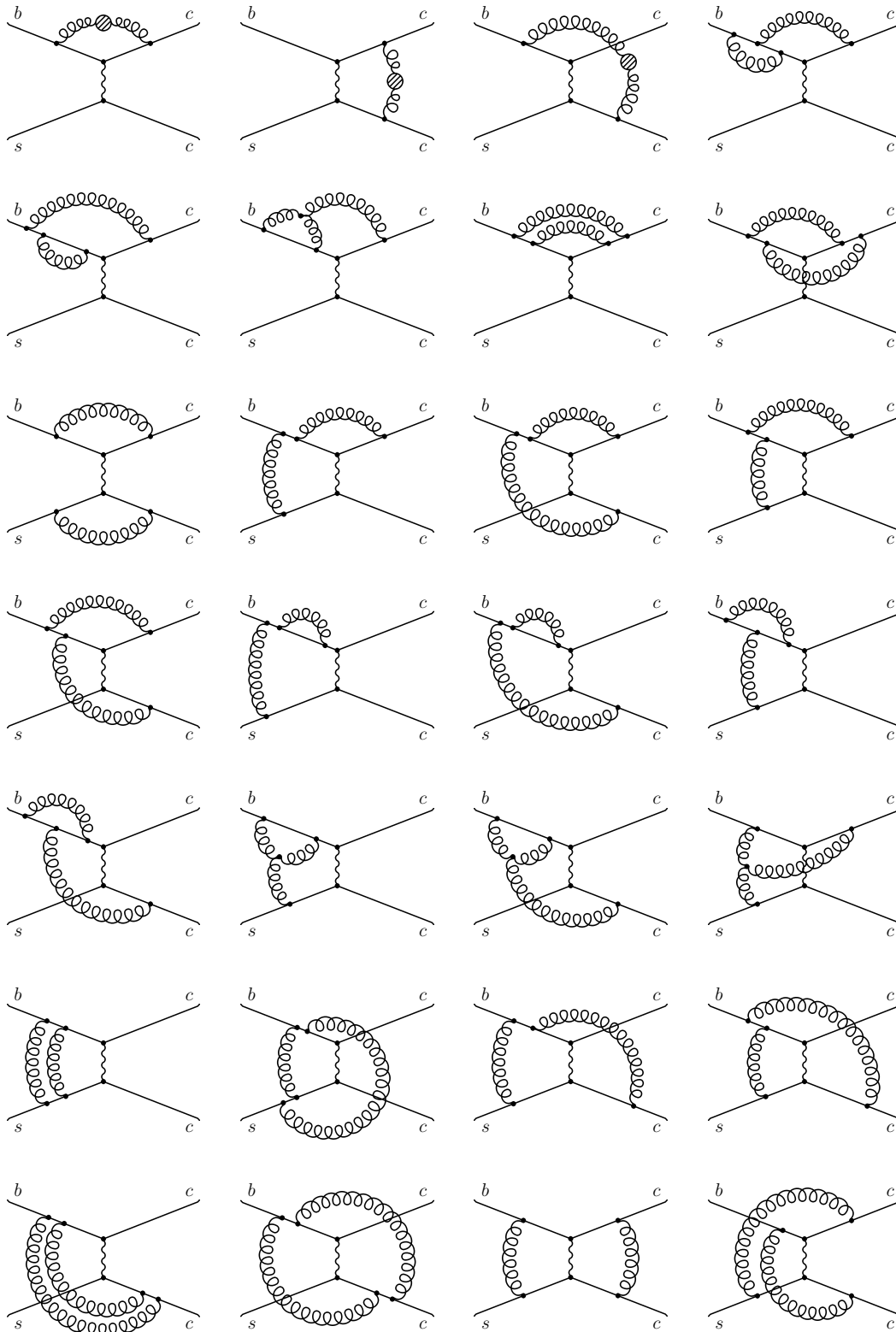
Figure 4.2: Two-loop contributions to $b \to sc\bar{c}$. The wiggly line denotes the W boson. Shaded blobs stand for self-energy insertions. Possible left-right and up-down reflected diagrams are not shown.
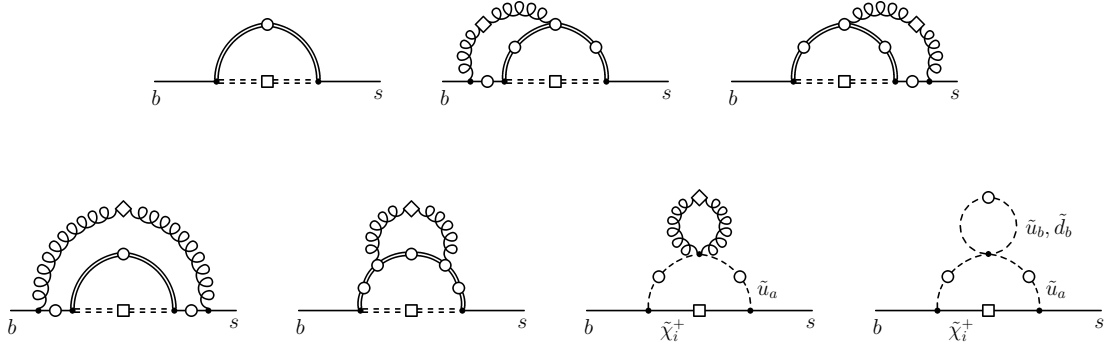
Figure 4.3: One-loop and two-loop contributions to $b \to s\gamma$, $b \to sZ$ and $b \to sg$. The circle indicates the positions where photons, Z bosons or gluons can be emitted, whereas the square (diamond) indicates the positions where only photons and Z bosons (gluons) can be emitted. The double plain line represents up-type quarks and squarks, and the double dashed line W, G, H bosons and charginos.

constants. All other QCD renormalization constant are taken in the $\overline{\text{MS}}$ scheme with five active flavors.

For the $b \to sc\bar{c}$ transition this means that no top quark and squark loop contribution remaines in the "light quark – W boson" effective vertex after renormalization, and hence the first diagram shown in fig. 4.2 gives no contribution to $C_2^{c(2)}$. The next two diagrams giving non-vanishing contributions to $C_1^{c(2)}$ are the origin of the functions $[T_1]_t$ and $[T_1]_{\tilde{q}}$ given in (4.12) and (4.13), respectively.

Matching $b \to s\gamma$ and $b \to sg$

Here, we neglect all light quark masses except for linear terms in m_b in the diagrams of the "effective MSSM" shown in fig. 4.3. In consequence all loop-diagrams on the effective side are equal to zero, and the EOM-vanishing gauge-invariant operators given app. C are sufficient as long as we work with background photon and gluon fields. There is no need to introduce EOM-vanishing gauge-variant operators in the matching procedure[12].

All possible Lorentz structures we encountered in the $b \to s\gamma$ and $b \to sg$ off-shell matching calculation are collected in

$$S_{X_i}^{\mu} \in \{ \gamma^{\mu} P_X, \, \slashed{k}\gamma^{\mu} P_X, \, \gamma^{\mu}\slashed{k} P_X, \, \slashed{p}\gamma^{\mu} P_X, \, \gamma^{\mu}\slashed{p} P_X,$$

$$k^{\mu}\slashed{k} P_X, \, k^{\mu}\slashed{p} P_X, \, p^{\mu}\slashed{k} P_X, \, p^{\mu}\slashed{p} P_X, \, (kp)\gamma^{\mu} P_X, \, k^2\gamma^{\mu} P_X, \, p^2\gamma^{\mu} P_X \} \quad (4.27)$$

where $X = L, R$ and $i = 1, \ldots, 13$. In terms of these 26 Lorenz structures, the off-shell

---

[12]However, they are necessary to determine the renormalization constants Z of the Wilson coefficients entering the matching equation.
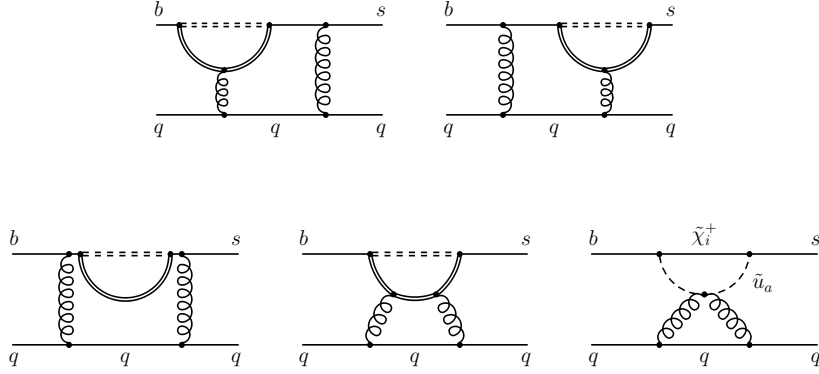
Figure 4.4: Two-loop 1PI contributions to $b \to sq\bar{q}$. The double plain line represents up-type quarks and squarks, and the double dashed line W, G, H bosons and charginos. Diagrams with crossed gluon lines are not shown.

$b \to s\gamma$ amplitudes in the "effective MSSM" can be written as

$$\mathcal{A}^Q_{\text{MSSM}} = i \frac{4G_F}{\sqrt{2}} K_{Qb} K^*_{Qs} \sum_{i=1}^{13} \left(a^Q_{L_i} S^\mu_{L_i} + a^Q_{R_i} S^\mu_{R_i} \right) \varepsilon^*_\mu \, \delta_{\alpha\beta} \tag{4.28}$$

where α and β are color indices, and ε_μ is the polarization vector of the photon. The amplitude of the effective theory is given by

$$\mathcal{A}^Q_{\text{effective}} = i \frac{4G_F}{\sqrt{2}} K_{Qb} K^*_{Qs} \left\{ \sum_{i=7,8} C^Q_i \langle \mathcal{O}_i \rangle_{\text{tree}} + \sum_{i=30}^{36} C^Q_{N_i} \langle N_i \rangle_{\text{tree}} \right\} \tag{4.29}$$

Matching the amplitudes of both theories yields the Wilson coefficients of the operators $\mathcal{O}_7$, $N_{32,33}$ and $N_{35,36}$, for example

$$C^Q_7 = \frac{g^2_s}{ie} \left[\frac{1}{m_b} a^Q_{R_3} + \frac{1}{4} a^Q_{L_9} \right] \tag{4.30}$$

The determination of the Wilson coefficients of the operators $\mathcal{O}_8$ and $N_{31,34}$ from the off-shell $b \to sg$ amplitudes is completely analogous. The Wilson coefficients of the operators N_{32} and N_{33} can be determined from both decays which provides a check of our calculation. Furthermore, since not all coefficients $a^Q_{X_i}$ are independent from each other, we obtain further non-trivial relations between the $a^Q_{X_i}$ which provides a an additional check of the calculation.

Matching $b \to sq\bar{q}$ and $b \to sl^+l^-$

The $b \to s\bar{q}q$ decay receives two contributions from the "effective MSSM". First the off-shell part of the $b \to sg$ matching, and second 1PI diagrams emerging here for the first time at two-loops and being depicted in fig. 4.4. The former contribution enters the matching
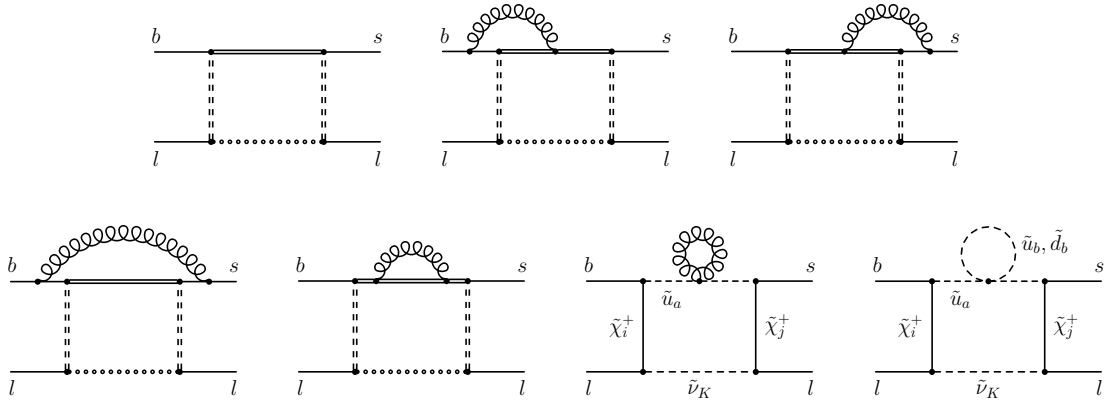
Figure 4.5: One- and two-loop contributions to $b \to sl^+l^-$. The double plain line represents up-type quarks and squarks, the double dashed line W, G, H bosons and charginos, and the double dotted line neutrinos and sneutrinos.

equation via the operator N_{31}

$$\mathcal{A}^Q_{\text{MSSM}} = i\frac{4G_F}{\sqrt{2}}K_{Qb}K^*_{Qs}(C^Q_4 + C^Q_{N_{31}})\langle\mathcal{O}_4\rangle_{\text{tree}} \tag{4.31}$$

where $\mathcal{A}^Q_{\text{MSSM}}$ is the amplitude in the "effective MSSM" resulting from considering only the diagrams shown in fig. 4.4. This matching equation has of course to be understood only schematically. Needless to say that one also has to consider evanescent operators and counterterms on the effective side.

The matching of the $b \to sl^+l^-$ decay is performed complete analogously. We have three contributions, the off-shell $b \to s\gamma$ part, the Z-penguins and the box-type diagrams displayed in fig. 4.5. The off-shell photonic amplitudes enter the matching equation again via the operator N_{36},

$$\mathcal{A}^Q_{\text{MSSM}} = i\frac{4G_F}{\sqrt{2}}K_{Qb}K^*_{Qs}(C^Q_9 - C^Q_{N_{36}})\langle\mathcal{O}_9\rangle_{\text{tree}} \tag{4.32}$$

where $\mathcal{A}^Q_{\text{MSSM}}$ is the amplitude in the MSSM including only Z-penguins (cf. fig. 4.3) and box-type diagrams shown in figure 4.5. Again, evanescent operators and counterterms have been suppressed in this matching equation.

4.3 Renormalization Group Evolution

The evolution of the Wilson coefficients from the matching scale μ_t down to the low-energy scale μ_b is governed by

$$\mu\frac{d}{d\mu}\vec{C}(\mu) = \gamma^T\vec{C}^Q_j(\mu) \tag{4.33}$$

where γ is the so-called anomalous dimension matrix corresponding to the operators $\mathcal{O}_{1\ldots10}$ which can be perturbatively expanded as

$$\gamma(g_s) = \frac{\alpha_s}{4\pi}\gamma^{(0)} + \frac{\alpha_s^2}{(4\pi)^2}\gamma^{(1)} + \frac{\alpha_s^3}{(4\pi)^3}\gamma^{(2)} + \ldots \tag{4.34}$$

Neglecting the running of the electromagnetic coupling constant the general solution of (4.33) can be written as

$$\vec{C}(\mu) = U(\mu, \mu_t)\,\vec{C}(\mu_t) \tag{4.35}$$

with $U(\mu, \mu_0)$ being the evolution-matrix. It is given by

$$U(\mu, \mu_t) = T_{g_s}\exp\left\{\int_{g_s(\mu_t)}^{g_s(\mu)} dg_s'\frac{\gamma^T(g_s')}{\beta_s(g_s')}\right\}$$

$$= U^{(0)}(\mu, \mu_t) + \frac{\alpha_s}{4\pi}U^{(1)}(\mu, \mu_t) + \frac{\alpha_s^2}{(4\pi)^2}U^{(2)}(\mu, \mu_t) + \ldots \tag{4.36}$$

where T_{g_s} denotes ordering of the coupling constants $g_s(\mu)$ in such a way that their value increase from right to left, and $\beta(g_s)$ is the QCD beta function,

$$\beta(g_s) = -g_s\left\{\frac{\alpha_s}{4\pi}\beta_0 + \frac{\alpha_s^2}{(4\pi)^2}\beta_1 + \frac{\alpha_s^3}{(4\pi)^3}\beta_2 + \ldots\right\} \tag{4.37}$$

The leading order evolution matrix reads

$$U^{(0)}(\mu, \mu_t) = V\mathrm{diag}(\eta_s^{a_i})V^{-1} \tag{4.38}$$

which depends on the matrix V and the so-called magic numbers that are obtained via diagonalization of $\gamma^{(0)T}$,

$$[\gamma_D^{(0)}]_{ij} = [V^{-1}\gamma^{(0)T}V]_{ij} = 2\beta_0\,a_i\,\delta_{ij} \tag{4.39}$$

Furthermore, we defined $\eta_s = \alpha_s(\mu_t)/\alpha_s(\mu)$. The perturbative solution of (4.33) relevant for the NNLO QCD corrections we discussed in sec. 4.1 is given by

$$\vec{C}(\mu) = U^{(0)}\vec{C}^{(0)}(\mu_t) + \frac{\alpha_s(\mu_t)}{4\pi}\left\{\left[\eta_s^{-1}J_1U^{(0)} - U^{(0)}J_1\right]\vec{C}^{(0)}(\mu_t) + U^{(0)}\vec{C}^{(1)}(\mu_0)\right\}$$

$$+ \frac{\alpha_s^2(\mu_t)}{(4\pi)^2}\left\{\left[\eta_s^{-2}J_2U^{(0)} - \eta_s^{-1}J_1U^{(0)}J_1 - U^{(0)}(J_2 - J_1^2)\right]\vec{C}^{(0)}(\mu_t)\right.$$

$$\left. + \left[\eta_s^{-1}J_1U^{(0)} - U^{(0)}J_1\right]\vec{C}^{(1)}(\mu_t) + U^{(0)}\vec{C}^{(2)}(\mu_t)\right\} \tag{4.40}$$

where the arguments of the evolution matrix $U(\mu, \mu_t)$ have been omitted to avoid unnecessary clutter. Furthermore, $J_1 = VS_1V^{-1}$ and $J_2 = VS_2V^{-1}$ with S_1 and S_2 given by

$$[S_1]_{ij} = \frac{\beta_1}{2\beta_0^2}[\gamma_D^{(0)}]_{ii}\delta_{ij} - \frac{[V^{-1}\gamma^{(1)T}V]_{ij}}{2\beta_0 + [\gamma_D^{(0)}]_{ii} - [\gamma_D^{(0)}]_{jj}}$$

$$[S_2]_{ij} = \frac{\beta_2}{4\beta_0^2}[\gamma_D^{(0)}]_{ii}\delta_{ij} - \frac{[V^{-1}\gamma^{(2)T}V]_{ij}}{4\beta_0 + [\gamma_D^{(0)}]_{ii} - [\gamma_D^{(0)}]_{jj}}$$

$$+ \sum_k \frac{2\beta_0 + [\gamma_D^{(0)}]_{ii} - [\gamma_D^{(0)}]_{kk}}{4\beta_0 + [\gamma_D^{(0)}]_{ii} - [\gamma_D^{(0)}]_{jj}}\left([S_1]_{ik}[S_1]_{kj} - \frac{\beta_1}{\beta_0}[S_1]_{ij}\delta_{jk}\right) \tag{4.41}$$

The derivation of (4.40) up to NLO is shown in great detail in [119], which can be generalized to include the $O(\alpha_s^2)$ term in a straightforward way [171].

4.4 Effective Wilson Coefficients

In the following we will summarize the perturbative calculation of the matrix elements at the parton level $b \to sl^+l^-$ within the effective theory at the low-energy scale $\mu_b \sim O(m_b)$. At this scale the usually rescaled operators and Wilson coefficients

$$\widetilde{\mathcal{O}}_i = \frac{\alpha_s(\mu_b)}{4\pi}\mathcal{O}_i, \qquad\qquad \widetilde{C}_i(\mu_b) = \frac{4\pi}{\alpha_s(\mu_b)}C_i(\mu_b) \tag{4.42}$$

for $i = 7, 8, 9, 10$ are used. The matrix elements at the low-energy scale with single insertions of physical operators are proportional to the tree-level matrix elements of $\widetilde{\mathcal{O}}_7$ and $\widetilde{\mathcal{O}}_9$, and it has become customary to take them into account by the introduction of the effective Wilson coefficients

$$\widetilde{C}_7^{Q\text{eff}} = \frac{4\pi}{\alpha_s(\mu_b)}C_7^Q(\mu_b) + \mathcal{M}_{7,1}^{Q,\{1,2\}} + \mathcal{M}_{7,1}^{Q,\{3...6\}} + \mathcal{M}_{7,2}^{Q,\{1,2\}} + \mathcal{M}_{7,2}^{Q,\{3...6\}} + \mathcal{M}_{7,2}^{Q,8}$$

$$\widetilde{C}_9^{Q\text{eff}} = \frac{4\pi}{\alpha_s(\mu_b)}C_9^Q(\mu_b) + \mathcal{M}_{9,1}^{Q,\{1,2\}} + \mathcal{M}_{9,1}^{Q,\{3...6\}} + \mathcal{M}_{9,2}^{Q,\{1,2\}} + \mathcal{M}_{9,2}^{Q,\{3...6\}} + \mathcal{M}_{9,2}^{Q,8}$$

$$\widetilde{C}_{10}^{Q\text{eff}} = \frac{4\pi}{\alpha_s(\mu_b)}C_{10}^Q(\mu_b) \tag{4.43}$$

At the LO the only operator mediating $b \to sl^+l^-$ is $\widetilde{\mathcal{O}}_9$ which receives a non-zero Wilson coefficient at the scale μ_b when solving the renormalization group equation due to the mixing of the four-quark operators into $\widetilde{\mathcal{O}}_9$.

The low-energy matrix elements at the NLO are given by [78, 79, 82]

$$\mathcal{M}_{7,1}^{Q,\{1,2\}} = \mathcal{M}_{9,1}^{Q,\{1,2\}} = 0$$

$$\mathcal{M}_{7,1}^{Q,\{3...6\}} = -\frac{1}{3}C_3^Q(\mu) - \frac{4}{9}C_4^Q(\mu) - \frac{20}{3}C_5^Q(\mu) - \frac{80}{9}C_6^Q(\mu)$$

$$\mathcal{M}_{9,1}^{u,\{1,2\}} = \sum_{i=1}^{2}C_i^Q(\mu)\gamma_{i9}^{Q(0)}\ln\frac{m_b}{\mu} + \left(\frac{4}{3}C_1^c(\mu) + C_2^c(\mu)\right)h(0,\hat{s})$$

$$\mathcal{M}_{9,1}^{c,\{1,2\}} = \sum_{i=1}^{2} C_i^Q(\mu)\gamma_{i9}^{Q(0)} \ln\frac{m_b}{\mu} + \left(\frac{4}{3}C_1^c(\mu) + C_2^c(\mu)\right) h(z_c,\hat{s})$$

$$\mathcal{M}_{9,1}^{Q,\{3...6\}} = \sum_{i=3}^{6} C_i^Q(\mu)\gamma_{i9}^{Q(0)} \ln\frac{m_b}{\mu} + \left(6C_3^Q(\mu) + 60C_5^Q(\mu)\right) h(z_c,\hat{s})$$

$$- \left(\frac{7}{2}C_3^Q(\mu) + \frac{2}{3}C_4^Q(\mu) + 38C_5^Q(\mu) + \frac{32}{3}C_6^Q(\mu)\right) h(1,\hat{s})$$

$$- \left(\frac{1}{2}C_3^Q(\mu) + \frac{2}{3}C_4^Q(\mu) + 8C_5^Q(\mu) + \frac{32}{3}C_6^Q(\mu)\right) h(0,\hat{s})$$

$$+ \frac{4}{3}C_3^Q(\mu) + \frac{64}{9}C_5^Q(\mu) + \frac{64}{27}C_6^Q(\mu) \tag{4.44}$$

where $z_c = m_c^2/m_b^2$ and $h_1(z_c,\hat{s})$ being the loop function

$$h(z_c,\hat{s}) = -4\int_0^1 dx\, x(1-x)\ln[z_Q^2 - x(1-x)\hat{s} - i\rho] \tag{4.45}$$

Defining $y = 4z_c^2/\hat{s}$, we find as its solution in accordance with [79]

$$h(z_c,\hat{s}) = \frac{2}{9}(5+3y) - \frac{2}{3}\ln z_c^2 - \frac{1}{3}(2+y)\sqrt{|1-y|} \begin{cases} \left[\ln\left(\frac{1+\sqrt{1-y}}{1-\sqrt{1-y}}\right) - i\pi\right], & y < 1 \\ 2\arctan\frac{1}{\sqrt{y-1}}, & y > 1 \end{cases}$$

$$h(0,\hat{s}) = -\frac{2}{3}(\ln\hat{s} - i\pi) + \frac{10}{9} \tag{4.46}$$

The matrix elements originate from one-loop diagrams with single insertions of the operators $\mathcal{O}_{1...6}$ and from virtual gluon corrections to the operator $\widetilde{\mathcal{O}}_9$ in the $b \to sl^+l^-$ transition. Infrared singularities arising in the latter calculation cancel once the gluon bremsstrahlung corrections of the process $b \to sgl^+l^-$ to the operator $\widetilde{\mathcal{O}}_9$ are taken into account, summarized in the function $\omega_{99}(\hat{s})$, where $\hat{s} = s/m_b^2$ [cf. (4.49)].

At the NNLO level, the matrix elements read [87, 88, 90]

$$\mathcal{M}_{7,2}^{t,\{1,2\}} = \mathcal{M}_{9,2}^{t,\{1,2\}} = 0$$

$$\mathcal{M}_{7,2}^{Q,\{1,2\}} = -\frac{\alpha_s(\mu)}{4\pi}\sum_{Q=u,c}\left(C_1^{c(0)}(\mu)F_{Q,1}^{(7)}(\hat{s}) + C_2^{c(0)}(\mu)F_{Q,2}^{(7)}(\hat{s})\right)$$

$$\mathcal{M}_{7,2}^{Q,8} = -\frac{\alpha_s(\mu)}{4\pi}A_8^{Q(0)}(\mu)F_8^{(7)}(\hat{s})$$

$$\mathcal{M}_{9,2}^{Q,\{1,2\}} = -\frac{\alpha_s(\mu)}{4\pi}\sum_{Q=u,c}\left(C_1^{c(0)}(\mu)F_{Q,1}^{(9)}(\hat{s}) + C_2^{c(0)}(\mu)F_{Q,2}^{(9)}(\hat{s})\right)$$

$$\mathcal{M}_{9,2}^{Q,8} = -\frac{\alpha_s(\mu)}{4\pi}A_8^{Q(0)}(\mu)F_8^{(9)}(\hat{s}) \tag{4.47}$$

and originate from infrared finite virtual corrections to the matrix elements of the operators $\mathcal{O}_{1,2}$ and $\mathcal{O}_8$ represented in the functions $F_i^{(j)}$, and from virtual and bremsstrahlungs corrections to the matrix elements of $\mathcal{O}_{7,9,10}$. The latter suffer from infrared and and collinear singularities which cancel when combined at the parton level of differential decay rates yielding the functions $\omega_{77}(\hat{s})$, $\omega_{79}(\hat{s})$ and $\omega_{99}(\hat{s})$ [cf. (4.49)]. The functions $F_i^{(j)}$ for low values of $\hat{s}$, which involves an expansion in the ratios m_c/m_b, $\sqrt{s}/m_b$ and $\sqrt{s}/2m_c$, can be found in [87,88,90], together with the auxiliary quantity $A_8^{Q(0)}$. The calculation valid for all dilepton invariant masses s can be found in [91,92]. The matrix elements involving single insertions of the operators $\mathcal{O}_{3\ldots 6}$ have not been calculated yet and are expected to be negligibly small[13]. However, a complete NNLO computation of $\bar{B} \to X_s l^+ l^-$ should include these corrections as well. As far as the two-loop $O(\alpha_s^2)$ matrix element of $\mathcal{O}_9$ is concerned, we will use the approximate formula given in [86].

4.5 Differential Decay Distributions

In this section we provide the formulae of some differential decay distributions of the decay $\bar{B} \to X_s l^+ l^-$. These are the dilepton invariant mass spectrum and the differential forward-backward asymmetry with respect to the dilepton invariant mass s of the lepton pair. They are given in terms of the Wilson coefficients at the low-energy scale,

$$\widetilde{C}_i^{\mathrm{eff}} = \widetilde{C}_i^{t,\mathrm{eff}} + \frac{K_{cs}^* K_{cb}}{K_{ts}^* K_{tb}} \widetilde{C}_i^{c,\mathrm{eff}} + \frac{K_{us}^* K_{ub}}{K_{ts}^* K_{tb}} \widetilde{C}_i^{u,\mathrm{eff}} \tag{4.48}$$

A rather precise determination of the dilepton invariant mass spectrum seems to be possible once the values of s are restricted to be below or above these resonances. Then the calculation can be performed using perturbative methods whereas non-perturbative corrections can be addressed within the framework of Heavy Quark Expansion (HQE) predicting the leading contribution of the inclusive decay $\bar{B} \to X_s l^+ l^-$ to be the matrix elements of the quark-level transition $b \to s l^+ l^-$ whereas non-perturbative corrections of the type $(\Lambda_{\mathrm{QCD}}/m_b)^n$ can be taken systematically into account. However, this method is not applicable over the whole kinematical range of s and in this work we will restrict the analysis to the so-called low-s region [82] below the $c\bar{c}$-resonances[14].

The dilepton invariant mass spectrum at the parton level reads [97]

$$\frac{d\Gamma(b \to s l^+ l^-)}{d\hat{s}} = \left(\frac{\alpha_{\mathrm{em}}}{4\pi}\right)^2 \frac{G_F^2 (m_b^{\mathrm{pole}})^5 \left|K_{ts}^* K_{tb}\right|^2}{48\pi^3} (1 - \hat{s})^2$$

$$\times \left\{ (1 + 2\hat{s}) \left(\left|\widetilde{C}_9^{\mathrm{eff}}\right|^2 + \left|\widetilde{C}_{10}^{\mathrm{eff}}\right|^2 \right) [1 + \frac{2\alpha_s}{\pi} \omega_{99}(\hat{s})] \right.$$

$$\left. + 4 \left(1 + \frac{2}{\hat{s}}\right) \left|\widetilde{C}_7^{\mathrm{eff}}\right|^2 [1 + \frac{2\alpha_s}{\pi} \omega_{77}(\hat{s})] + 12\mathrm{Re}\left(\widetilde{C}_7^{\mathrm{eff}} \widetilde{C}_9^{\mathrm{eff}*}\right) [1 + \frac{2\alpha_s}{\pi} \omega_{79}(\hat{s})] \right\}$$

---

[13]The analogous corrections to $\bar{B} \to X_s\gamma$ are 1% [80,81].

[14]However, contrary to the semileptonic decays $\bar{B} \to X_{u,c} l \bar{\nu}_l$ and the radiative decay $\bar{B} \to X_s\gamma$ this method is not applicable in the endpoint region of the spectrum as pointed out in [172]. Here other approaches have to be used such as for example heavy hadron chiral perturbation theory (HHχPT) by summing over the kinematically allowed exclusive channels to reliably estimate the magnitude of the endpoint decay spectrum.

$$+ \frac{d\Gamma^{\text{Brems,A}}}{d\hat{s}} + \frac{d\Gamma^{\text{Brems,B}}}{d\hat{s}} \tag{4.49}$$

The functions $\omega_{ij}(\hat{s})$ summarize the virtual and real QCD corrections to the matrix elements of the operators $\widetilde{\mathcal{O}}_{7,9,10}$ [87,88,96] discusses in the previous section, whereas the terms $d\Gamma^{\text{Brems,A}}/d\hat{s}$ and $d\Gamma^{\text{Brems,B}}/d\hat{s}$ result from infrared finite bremsstrahlungs corrections due to interferences between $\mathcal{O}_8$ and $\mathcal{O}_{7,\dots 10}$ and between $\mathcal{O}_{1,2}$ and $\mathcal{O}_{1,2,7,\dots 10}$, respectively [89]. In the numerical analysis we follow [86] concerning the QCD corrections. However, we will not include the higher order QED corrections discussed there, but rather use $\alpha_{\text{em}} = 1/133$ which yields results close to those obtained when including them, as was found in [86].

To obtain the hadronic differential decay rate $d\Gamma(\bar{B} \to X_s l^+ l^-)/d\hat{s}$ within HQE, $(\Lambda_{\text{QCD}}/m_b)^n$ corrections have to be added to the partonic differential decay rate $d\Gamma(b \to s l^+ l^-)/d\hat{s}$ given in (4.49) [172–177]. These corrections were calculated up to the order $n = 3$ [176,177] and turn out to be small compared to the leading perturbative contribution – however, still involving poorly known matrix elements of the HQET for $n = 3$. In the numerical analysis we will only include the corrections with $n = 2$. We also include the $(\Lambda_{\text{QCD}}/m_c)^2$ corrections of [74] in order to take effects related to the tails of $c\bar{c}$ resonances in the low-s region into account. Their size was found to be similar to the that of the $\Lambda_{\text{QCD}}^2/m_b^2$ corrections. Both type of corrections can also be found in [93].

The partially integrated branching ratio $\mathcal{B}(\bar{B} \to X_s l^+ l^-)$ of the low-s region is

$$\mathcal{B}(\bar{B} \to X_s l^+ l^-) = \mathcal{N} \int_{q_{\text{min}}^2}^{q_{\text{max}}^2} \frac{d\Gamma(\bar{B} \to X_s l^+ l^-)}{d\hat{s}} \frac{d(q^2)}{m_b^2} \tag{4.50}$$

with the boundaries chosen to be $q_{\text{min}}^2 = 1 \, \text{GeV}^2$ and $q_{\text{max}}^2 = 6 \, \text{GeV}^2$. Commonly the semileptonic decay $\bar{B} \to X_c l \nu$ is used as normalization because the factor $(m_b^{\text{pole}})^5$ – the origin of large uncertainties – cancels in the ratio,

$$\mathcal{N} = \frac{\mathcal{B}(\bar{B} \to X_c l \nu_l)}{\Gamma(\bar{B} \to X_c l \nu_l)} \tag{4.51}$$

An alternative proposed in [178] reduces the uncertainty due to the charm quark mass present in the decay rate $\Gamma(\bar{B} \to X_c l \nu_l)$ owing to a normalization on the charmless semileptonic decay $\bar{B} \to X_u l \nu_l$ in combination with the decay $\bar{B} \to X_c l \nu_l$. The application of this method to the decay $\bar{B} \to X_s l^+ l^-$ can be found in [86,179],

$$\mathcal{N} = \frac{1}{C} \left| \frac{K_{ub}}{K_{cb}} \right|^2 \frac{\mathcal{B}(\bar{B} \to X_c l \nu_l)}{\Gamma(\bar{B} \to X_u l \nu_l)} \tag{4.52}$$

with $C = 0.581 \pm 0.017$, and will be used in the numerical analysis.

The so-called un-normalized forward-backward asymmetry is defined as

$$\bar{\mathcal{A}}_{\text{FB}}(\hat{s}) = \mathcal{N} \int_{-1}^{1} \frac{d^2\Gamma(\bar{B} \to X_s l^+ l^-)}{d\hat{s} \, dz} \text{sgn}(z) \, dz \tag{4.53}$$

where $z = \cos\theta$ and θ is the angle between the positively charged lepton and the b quark in the dilepton center of mass frame. Again the normalization is commonly chosen to be the semileptonic decay $\bar{B} \to X_c l \nu_l$, however also the alternative of the combination of the decays

$\bar{B} \to X_{u,c} l \nu_l$ [86] can be applied. The so-called normalized forward-backward asymmetry is given by the ratio

$$\mathcal{A}_{\text{FB}}(\hat{s}) = \int_{-1}^{1} \frac{d^2\Gamma(\bar{B} \to X_s l^+ l^-)}{d\hat{s}\,dz} \text{sgn}(z)\,dz \left/ \frac{d\Gamma(\bar{B} \to X_s l^+ l^-)}{d\hat{s}} \right. \tag{4.54}$$

The numerator at the parton level of the forward-backward asymmetries introduced in (4.53) and (4.54) is

$$\int_{-1}^{1} \frac{d^2\Gamma(b \to s l^+ l^-)}{d\hat{s}\,dz} \text{sgn}(z)\,dz = -\left(\frac{\alpha_{\text{em}}}{4\pi}\right)^2 \frac{G_F^2 (m_b^{\text{pole}})^5 |K_{ts}^* K_{tb}|^2}{48\pi^3}(1-\hat{s})^2$$

$$\times \left[3\hat{s}\,\text{Re}(\widetilde{C}_9^{\text{eff}} \widetilde{C}_{10}^{\text{eff}*}) \left(1 + \frac{2\alpha_s}{\pi} f_{910}(\hat{s})\right) \right.$$

$$\left. + 6\,\text{Re}(\widetilde{C}_7^{\text{eff}} \widetilde{C}_{10}^{\text{eff}*}) \left(1 + \frac{2\alpha_s}{\pi} f_{710}(\hat{s})\right) - \mathcal{A}_{\text{FB}}^{\text{Brems}}(\hat{s}) \right] \tag{4.55}$$

The functions $f_{i10}(\hat{s})$ summarize virtual and real QCD corrections [96,97]. The real QCD corrections $\mathcal{A}_{\text{FB}}^{\text{Brems}}(\hat{s})$ are infrared finite [98] and their contribution does not exceed 1% in the SM. In the following they will be neglected. As in the case of the dilepton invariant mass spectrum the non-perturbative contributions $(\Lambda_{\text{QCD}}/m_b)^n$ have to be added to pass from the partonic quantity $d^2\Gamma(b \to s l^+ l^-)/d\hat{s}\,dz$ to the hadronic quantity $d^2\Gamma(\bar{B} \to X_c l \nu)/d\hat{s}\,dz$. They can be found in [172,174,176,177] whereas the $(\Lambda_{\text{QCD}}/m_c)^2$ corrections are given in [74].

4.6 Phenomenological Implications

In what follows we will investigate the phenomenological implications of the MSSM corrections for the branching ratio, the dilepton invariant mass distribution and the forward-backward asymmetry. As far as the SM parameters are concerned we will take the values as given in [86] throughout the numerical analysis.

MSSM Parameters and Constraints

At the present, neither squark masses nor elements of squark mixing matrices have been measured, and thus in the numerical analysis we would like to vary the $O(\alpha_s)$ corrected fundamental parameters of the MSSM [146,147], taken to be in the super-CKM basis, rather then the squark masses and mixing matrices of the "effective MSSM". The latter are determined from the former in matching the "effective MSSM" with the full MSSM, and hence have to be understood as $\overline{\text{MS}}$ renormalized quantities at the scale $\mu_{\tilde{g}}$.

We refrain here from shifting the up-squark masses and mixing matrices of the "effective MSSM" into the on-shell scheme in order to avoid the appearance of large logarithms "$\ln(\mu_{\tilde{g}}/m_{\tilde{u}_a})$", as can be seen by inspection of (C.5). Then the next step is to integrate out successively all other particles with masses much smaller than $M_{\tilde{g}}$ and much larger than m_t when going to smaller scales using NLO renormalization group equations between all occurring matching scales. In our analysis, however, we integrate out all sparticles other than the gluino in one step with the top quark, taking into account the LO renormalization group
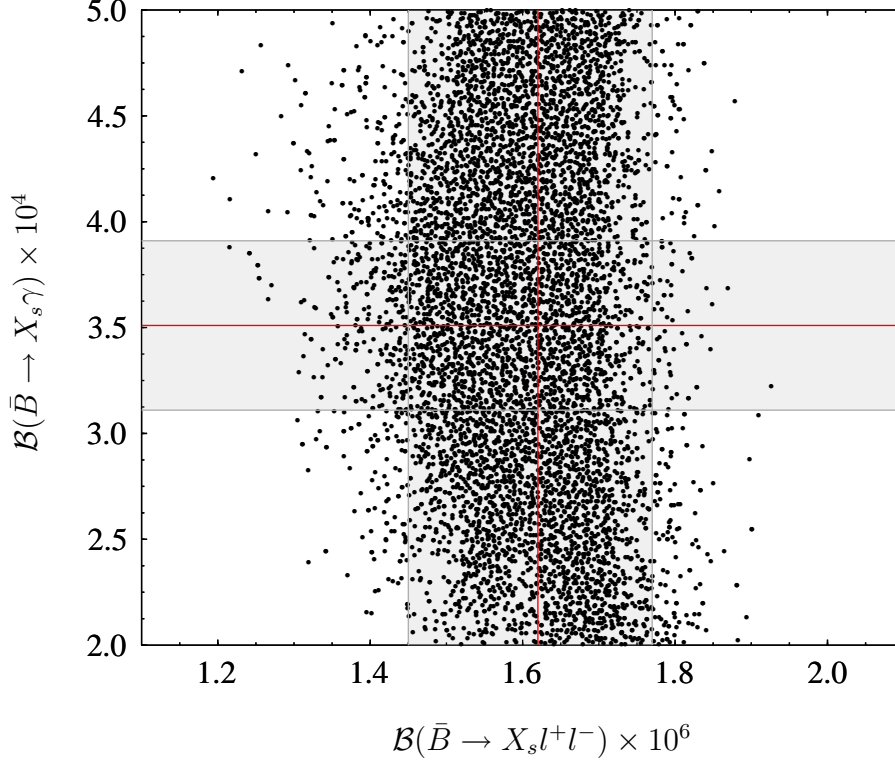
Figure 4.6: $\mathcal{B}(\bar{B} \to X_s \gamma)$ versus $\mathcal{B}(\bar{B} \to X_s l^+ l^-)$ for randomly chosen points in the parameter space of the MSSM scenario. The three vertical lines indicate the SM prediction of $\mathcal{B}(\bar{B} \to X_s l^+ l^-)$ [86] and the three horizontal lines the one for $\mathcal{B}(\bar{B} \to X_s \gamma)$ [80, 178].

running between $\mu_{\tilde{g}}$ and μ_t for up-squark masses and their mixing matrices Γ^U. Due to the quartic QCD-interaction of the scalar squarks the LO renormalization group equations of masses and mixing matrices are coupled and found to be

$$\mu \frac{d}{d\mu} m_{\tilde{u}_a}^2 = \frac{\alpha_s}{4\pi} \left[-8 m_{\tilde{u}_a}^2 + \frac{8}{3} \sum_{b=1}^{6} P_{ab}^U m_{\tilde{u}_b}^2 P_{ba}^U \right]$$

$$\mu \frac{d}{d\mu} \Gamma_{ab}^U = \frac{\alpha_s}{4\pi} \frac{8}{3} \sum_{e=1}^{6} \sum_{\substack{c=1 \\ c \neq a}}^{6} P_{ae}^U \frac{m_{\tilde{u}_e}^2}{m_{\tilde{u}_a}^2 - m_{\tilde{u}_c}^2} P_{ec}^U \Gamma_{cb}^U \qquad (4.56)$$

with

$$P^U = \Gamma^U \mathbb{1}_{6\times 6}^{\text{LR}} \Gamma^{U\dagger}, \qquad\qquad \mathbb{1}_{6\times 6}^{\text{LR}} = \text{diag}(1, 1, 1, -1, -1, -1) \qquad (4.57)$$

The down-squark mixing matrix Γ^D still retains its 2×2 block structure after scaling it down from $\mu_{\tilde{g}}$ to μ_t using LO renormalization group equations, and thus neutralino contributions are absent in $b \to s+$(light particle) decays in LO electroweak interactions at the scale μ_t.
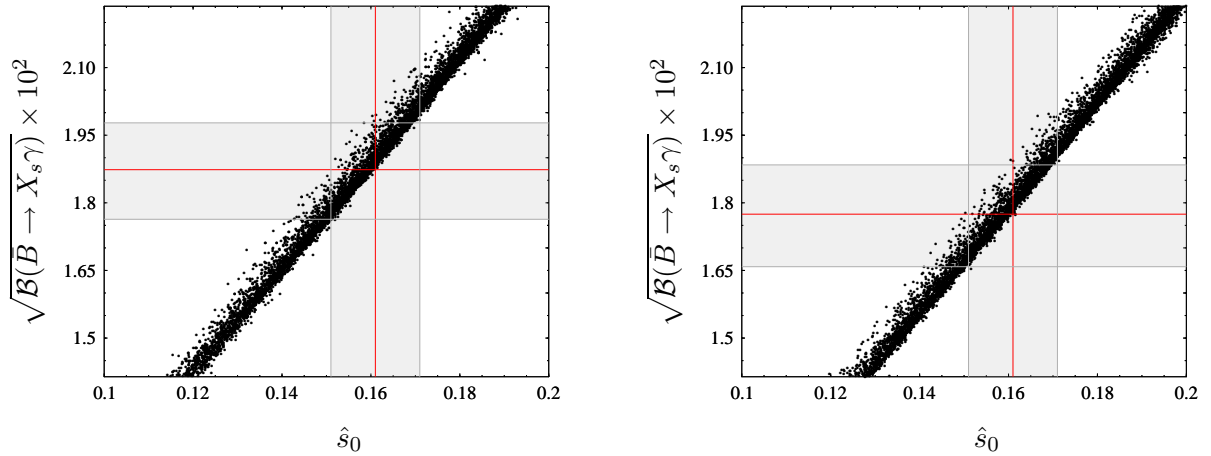
Figure 4.7: $\sqrt{\mathcal{B}(\bar{B} \to X_s \gamma)}$ versus $\hat{s}_0$, the position of zero of the normalized $\bar{\mathcal{A}}_{\mathrm{FB}}(\hat{s})$ for randomly chosen points in the parameter space of the MSSM scenario. The three vertical lines indicate the SM prediction of $\hat{s}_0$ [86, 92] and the three horizontal lines the one for $\mathcal{B}(\bar{B} \to X_s \gamma)$ [80, 178]. In the left plot the $\overline{\mathrm{MS}}$ charm quark mass is used for $\mathcal{B}(\bar{B} \to X_s \gamma)$, whereas in the right plot m_c^{pole}, resulting in a smaller prediction.

Having scaled the squarks masses and mixing matrices down to the scale μ_t the heavy SM particles and the remaining (apart from the gluino) sparticles have to be integrated out. Here we could either stay in the $\overline{\mathrm{MS}}$ renormalization scheme or shift the squarks masses and mixing matrices into the on-shell scheme as discussed in app. C. However, using the Wilson coefficients in terms of on-shell quantities one needs of course on-shell input parameters. In our approach we have $\overline{\mathrm{MS}}$ quantities at the scale μ_t, and shifting them to their on-shell values with the help of (C.5) only reproduced our numerical results in the $\overline{\mathrm{MS}}$ scheme if all squark masses are close in size. More properly one should integrate out squarks stepwise if their mass splittings are large, and then shift to the on-shell scheme at the appropriate scale for each squark. We chose to integrate out all squarks at one scale, and hence we refrain from working in the on-shell scheme in our numerical analysis.

The fundamental parameters of the MSSM relevant for our numerical analysis are

- the charged Higgs mass M_{H^+} and $\tan\beta$ in the Higgs sector,

- μ and M_2 that parameterize the chargino sector,

- the gluino mass $M_{\tilde{g}} \sim O(\mu_{\tilde{g}})$,

- the soft supersymmetry breaking scalar masses $[M_D^2]_{LL}$, $[M_U^2]_{RR}$,

- the soft supersymmetry breaking trilinear couplings $A_U = (M_U)^{-1}[M_U^2]_{LR}$,

with $[M_D^2]_{LL}$, $[M_U^2]_{RR}$ and A_U assumed to be real and diagonal matrices. We remark that the up-type squark squared mass matrix $[M_U^2]_{RR}$ cannot be decomposed into three 2×2 block-matrices for an arbitrary diagonal $[M_D^2]_{LL}$ due to (2.70) [145].
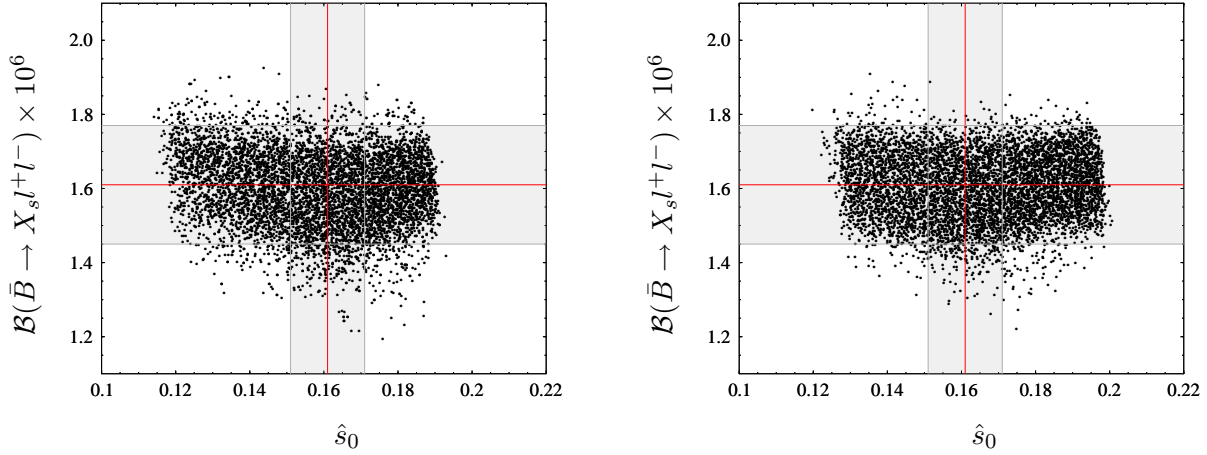
Figure 4.8: $\mathcal{B}(\bar{B} \to X_s l^+ l^-)$ versus $\hat{s}_0$, the position of zero of the normalized $\bar{\mathcal{A}}_{\mathrm{FB}}(\hat{s})$ for randomly chosen points in the parameter space of the MSSM scenario. The three vertical lines indicate the SM prediction of $\hat{s}_0$ [86, 92] and the three horizontal lines the one for $\mathcal{B}(\bar{B} \to X_s l^+ l^-)$ [86].

The decoupling of the gluino requires that the masses of all other sparticles should be lighter compared to the gluino mass and consequently effects of order $M_{\mathrm{sparticle}}/M_{\tilde{g}}$ can be neglected. This provides an upper bound on the sparticle spectrum which is chosen to be $\sim 600\,\mathrm{GeV}$. Further lower bounds have to be fulfilled on sparticle masses by direct searches from [180]

- $m_{\chi^+} \geq 94\,\mathrm{GeV}$ for the chargino masses,

- $m_{\tilde{u}_a} \geq 100\,\mathrm{GeV}$ for the 2 lightest up-squarks whereas the remaining squarks are required to be heavier than $250\,\mathrm{GeV}$.

Due to the matching of box-diagrams contributing to $b \to s l^+ l^-$ the Wilson coefficients also depend on the masses of sneutrinos. As such contributions are rather small we fix their masses to be degenerate, with values in the range of 100 to $300\,\mathrm{GeV}$. Also the down-squarks are approximated by a common mass of about 300 to $500\,\mathrm{GeV}$, as they only appear in the function $[T_1]_{\tilde{q}}^1$, which effect is negligibly small.

A very important constraint on new physics models is the total inclusive branching ratio for $\bar{B} \to X_s \gamma$. It has been shown within scenarios of the MSSM [99, 100] that the NLO QCD corrections of one-loop diagrams with virtual sparticles can become important and comparable to the present experimental uncertainty of $\mathcal{B}(\bar{B} \to X_s \gamma)$. Also a correlation between the $\bar{B} \to X_s \gamma$ and the $\bar{B} \to X_s l^+ l^-$ decays is obvious because both involve the Wilson coefficient $\tilde{C}_7$. However, the issue of theoretical uncertainties in $\mathcal{B}(\bar{B} \to X_s \gamma)$ is not settled yet. Two main points arise here. First the choice of the renormalization scheme of the charm quark mass m_c in the 2-loop matrix elements of the four-quark operators is still a large theoretical uncertainty of 11% [178]. It can only be solved by the calculation of NNLO corrections to $\mathcal{B}(\bar{B} \to X_s \gamma)$ as anticipated in [181, 182]. The second point is concerned with
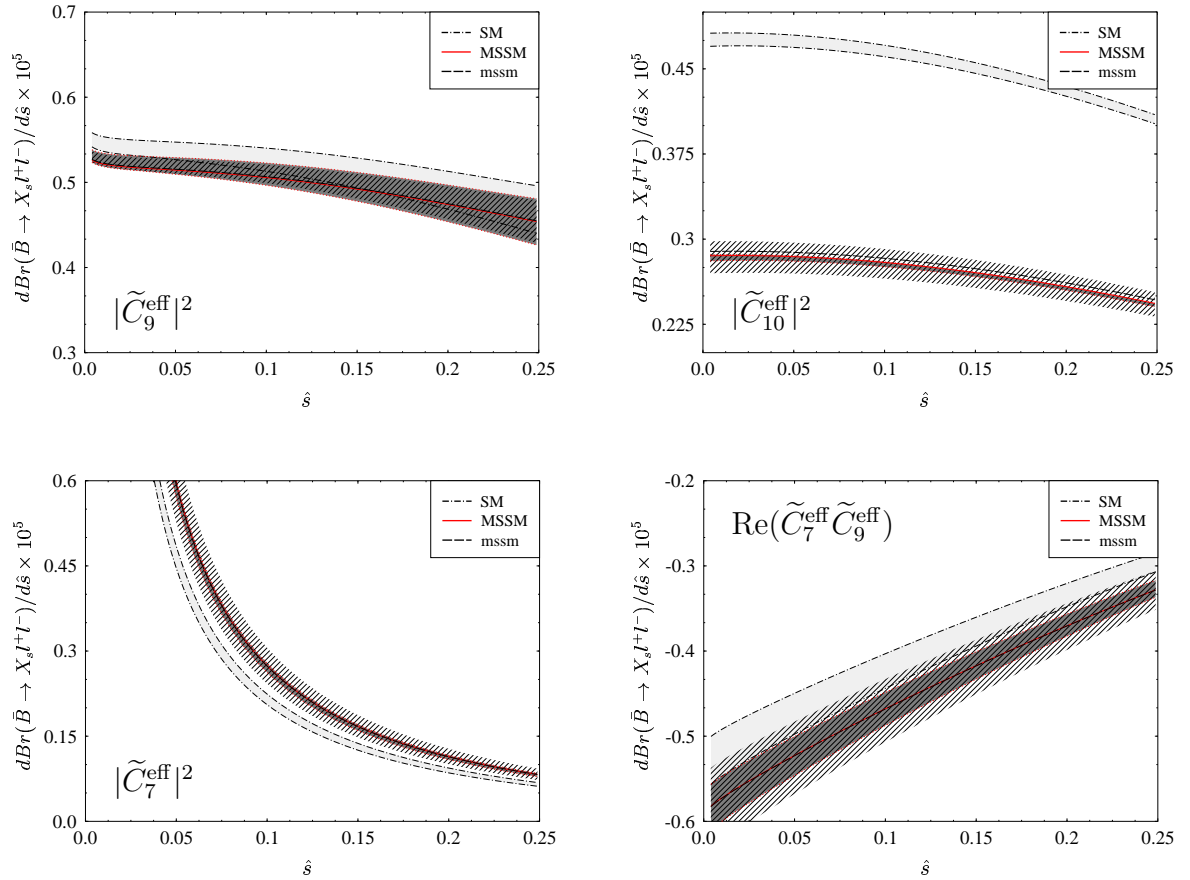
Figure 4.9: Various contributions to the differential branching ratio for fixed MSSM parameter point "P1" compared to the SM result and the partial MSSM result as functions of $\hat{s}$.

the model-dependences entering the results of $\mathcal{B}(\bar{B} \to X_s \gamma)$ measurements when extrapolating to the lower end of the photon energy spectrum in the experimental analysis. In [183] a total inclusive branching ratio $\mathcal{B}(\bar{B} \to X_s \gamma) = (3.34 \pm 0.38) \times 10^{-4}$ with a photon energy cut $E_0 > m_b/20$ was quoted. A very recent analysis of the Belle Collaboration [184] uses the full inclusive spectrum between $1.8 < E_\gamma < 2.8 \, \text{GeV}$, without invoking theoretical models of the photon-spectrum. The necessity to introduce the photon energy cut in theoretical calculations in order to avoid model-dependent experimental results was also raised very recently in [185]. The method proposed there results in larger uncertainties of the theoretical prediction of the order of 25%. In our numerical analysis the most recent SM calculations [80,178] will be used, however with $E_0 > m_b/20$, and the rather conservative interval

$$2.0 \times 10^{-4} \leq \mathcal{B}(\bar{B} \to X_s \gamma) \leq 5.0 \times 10^{-4} \tag{4.58}$$

to show the correlations with the $\bar{B} \to X_s l^+ l^-$ observables.

Results

We find that the branching ratio $\mathcal{B}(\bar{B} \to X_s l^+ l^-)$ receives only small corrections within the considered MSSM scenario. This is illustrated in fig. 4.6 where for randomly chosen points of
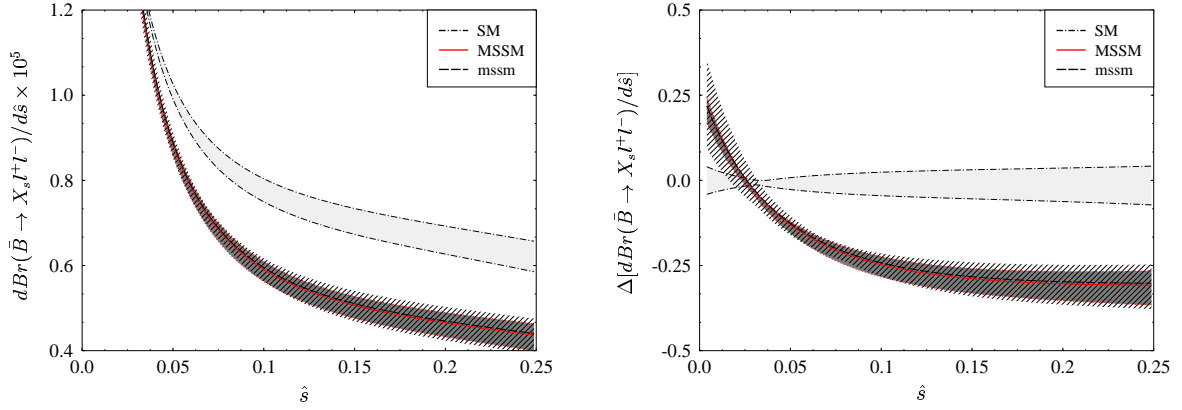
Figure 4.10: The differential branching ratio for fixed MSSM parameter point "P1" compared to the SM result and the partial MSSM result as a function of $\hat{s}$ (left plot). The relative size compared to the SM is given in the right plot.

the MSSM parameter space, fulfilling the lower sparticle mass bounds, the resulting $\mathcal{B}(\bar{B} \to X_s \gamma)$ versus $\mathcal{B}(\bar{B} \to X_s l^+ l^-)$ is shown. The vertical lines correspond to the SM prediction of $\mathcal{B}(\bar{B} \to X_s l^+ l^-)$ and the corresponding estimate of the theoretical uncertainty [86]. The horizontal lines indicate the SM prediction and theoretical uncertainties of $\mathcal{B}(\bar{B} \to X_s \gamma)$ [80, 178]. Deviations are possible from the SM central value $\mathcal{B}(\bar{B} \to X_s l^+ l^-) \sim 1.60 \times 10^{-6}$ up to $\pm(15 - 20)\%$ respecting the experimental bound from $\mathcal{B}(\bar{B} \to X_s \gamma)$. Therefore the observable $\mathcal{B}(\bar{B} \to X_s l^+ l^-)$ of the low-s region will not serve as a good candidate allowing to distinguish the SM and the considered MSSM scenario in view of the present theoretical uncertainties. The reason is the smallness of the MSSM contributions to $\widetilde{C}_9^{\text{eff}}$ and $\widetilde{C}_{10}^{\text{eff}}$ which dominate in the expression for $\mathcal{B}(\bar{B} \to X_s l^+ l^-)$ in the low-s region. Although $\widetilde{C}_7^{\text{eff}}$ could receive a larger MSSM contribution its magnitude is strongly constraint by the measured value of $\mathcal{B}(\bar{B} \to X_s \gamma)$.[15] Furthermore, the contribution to $|\widetilde{C}_7^{\text{eff}}|^2$ to the differential branching ratio falls like $1/\hat{s}$ and therefore only dominates for values of $\hat{s} \lesssim 0.05$ which coincides with the lower end of our integration range. The interplay between various contribution to the differential branching ratio within the SM is depicted in fig. 4.9. There also a specific point in the space of supersymmetric parameters with significant corrections to $\widetilde{C}_{10}^{\text{eff}}$ is shown.

The position of the zero of the forward-backward asymmetry $\hat{s}_0$ represents a more sensitive observable than $\mathcal{B}(\bar{B} \to X_s l^+ l^-)$ in the considered MSSM scenario. In fig. 4.7 we plot $\sqrt{\mathcal{B}(\bar{B} \to X_s \gamma)}$ versus $\hat{s}_0$ of the normalized $\bar{\mathcal{A}}_{\text{FB}}(\hat{s})$ for randomly chosen points of the MSSM parameter space. There the vertical lines correspond to the SM prediction of $\hat{s}_0$ and its uncertainties [86, 92] and the horizontal lines as in fig. 4.6 to the SM prediction of $\mathcal{B}(\bar{B} \to X_s \gamma)$. We note that the points in both plots in fig. 4.7 are clustered along a straight line, exhibiting very clearly the correlation between the value of $Br(B \to X_s \gamma)$ and $\hat{s}_0$ within models with minimal flavor violation as pointed out in [186].

The straight lines in fig. 4.7 are to a very good approximation model independent within the class of models with minimal flavor violation. Only different points on them correspond

---

[15]It should be stressed that this is a quite loose terminology since for the LO expression of the radiative decay $\mathcal{B}(\bar{B} \to X_s \gamma)$ the initial Wilson coefficients of the two operators $\mathcal{O}_7$ and $\mathcal{O}_8$ enter. At the NLO this becomes even more involved.

"P1"	$M_{H^+} = 440.11\,\text{GeV}$, $\tan\beta = 5.01$, $\mu = -122.87\,\text{GeV}$, $M_2 = 184.56\,\text{GeV}$
	$A_U = \text{diag}(370.29,\ 79.60,\ 535.71)\,\text{GeV}$
	$M_{D_L} = \text{diag}(299.63,\ 127.20,\ 454.43)\,\text{GeV}$
	$M_{U_R} = \text{diag}(219.96,\ 519.91,\ 167.68)\,\text{GeV}$
"P2"	$M_{H^+} = 248.34\,\text{GeV}$, $\tan\beta = 2.56$, $\mu = 192.83\,\text{GeV}$, $M_2 = 489.68\,\text{GeV}$
	$A_U = \text{diag}(-419.30,\ 525.64,\ -540.81)\,\text{GeV}$
	$M_{D_L} = \text{diag}(339.09,\ 128.18,\ 393.52)\,\text{GeV}$
	$M_{U_R} = \text{diag}(232.08,\ 351.41,\ 234.77)\,\text{GeV}$
"P3"	$M_{H^+} = 451.74\,\text{GeV}$, $\tan\beta = 4.89$, $\mu = -540.06\,\text{GeV}$, $M_2 = 582.50\,\text{GeV}$
	$A_U = \text{diag}(-375.95,\ -324.59,\ -497.23)\,\text{GeV}$
	$M_{D_L} = \text{diag}(503.97,\ 281.42,\ 264.06)\,\text{GeV}$
	$M_{U_R} = \text{diag}(444.06,\ 186.86,\ 417.40)\,\text{GeV}$

Table 4.1: **Three selected points.** All values are taken at the scale $\mu_{\tilde{g}} = M_{\tilde{g}} = 1\,\text{TeV}$, and the down-squarks and sneutrinos are assumed to have masses about 300 and $250\,\text{GeV}$, respectively.

to different models and/or different sets of parameters in a given model. On the other hand the position of these lines depends on the parameters of the low energy theory, in particular on the charm quark mass that enters sensitively the evaluation of $Br(B \to X_s\gamma)$ [178] but is practically irrelevant for $\hat{s}_0$. In the left plot in fig. 4.7 we used the $\overline{\text{MS}}$ mass $\overline{m}_c(m_c)$ and in the right plot the m_c^{pole} mass, that results in a different straight line. The SM prediction for $\mathcal{B}(\bar{B} \to X_s\gamma)$ is lower in the right plot than in the left plot. It is clear that the usefulness of the correlation between the values of $Br(B \to X_s\gamma)$ and $\hat{s}_0$ in testing the MSSM will depend on the progress in NNLO calculations for $B \to X_s\gamma$ that should significantly decrease the sensitivity due to the choice of m_c.

As seen in fig. 4.7, in addition to dense points in the ballpark of SM expectations, there are values of $Br(B \to X_s\gamma)$ and $\hat{s}_0$ within the MSSM that are larger and smaller than the SM predictions. This should be contrasted with the result in a model with one universal extra dimension in which only smaller values of $Br(B \to X_s\gamma)$ and $\hat{s}_0$ were possible [186].

In fig. 4.8 we show $Br(\bar{B} \to X_s l^+ l^-)$ versus $\hat{s}_0$. In the left plot the $\overline{\text{MS}}$ definition was used for the charm quark mass in the evaluation of $\mathcal{B}(\bar{B} \to X_s\gamma)$ whereas in the right plot the pole-mass definition. As a consequence the allowed range of the position of the zero of $\bar{\mathcal{A}}_{\text{FB}}(\hat{s})$ becomes shifted a bit towards higher values. The comparison of figs. 4.7 and 4.8 shows that the position of $\hat{s}_0$ is much more sensitive to the Wilson coefficient C_7 and consequently to $Br(B \to X_s\gamma)$ than to $Br(\bar{B} \to X_s l^+ l^-)$ itself.

In fig. 4.9 we show the four main contributions due to $|\widetilde{C}_{7,9,10}^{\text{eff}}|^2$ and $\text{Re}(\widetilde{C}_7^{\text{eff}}\widetilde{C}_9^{\text{eff}*})$ to the differential branching ratio, see (4.49), as functions of $\hat{s}$ for the fixed MSSM parameter point "P1" given in table 4.1. Each plot shows the SM (light grey band) and the MSSM contribution. To demonstrate the reduction of the renormalization scale dependence μ_t we show the MSSM result when including all calculated corrections (dark grey band – "MSSM") and the partial MSSM result (shaded bend – "mssm") obtained by discarding all contributions with $n = 2$ and $i = \{H, C, Q\}$ to the functions $[X_k]_i^n$ in (4.15), but not to the SM. The bands are
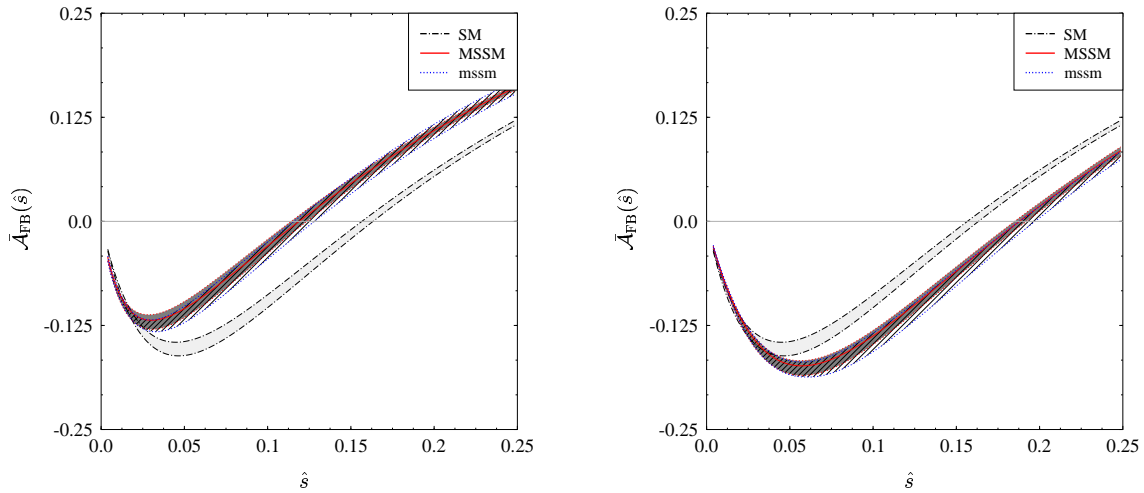
Figure 4.11: Normalized forward-backward asymmetry $\bar{\mathcal{A}}_{\mathrm{FB}}(\hat{s})$ versus $\hat{s}$ in the low-$\hat{s}$ region for two (left, right) fixed MSSM-parameter points "P2" and "P3" compared with the SM prediction.

obtained by varying the renormalization scale $\mu_t \in [120, 300]\,\mathrm{GeV}$ and the low-energy scale $\mu_b \in [2.5, 10]\,\mathrm{GeV}$. Large deviations from the SM appear in the contribution $|\widetilde{C}_{10}^{\mathrm{eff}}|^2$ mainly due to the Z-penguin function $[C_9^{l\bar{l}}]$ which is suppressed in $|\widetilde{C}_9^{\mathrm{eff}}|^2$ as can be seen in (4.14). The inclusion of the NNLO matching conditions in the MSSM reduces the renormalization scale dependence to comparable size as obtained in the SM calculation.

The sum of this four separate contributions (and the bremsstrahlung contributions) adds up to the final differential branching ratio shown in fig. 4.10 in the left plot. As before the bands are obtained by variation of the renormalization scales μ_t and μ_b. The reduction due to MSSM contributions is roughly -30% for values of $\hat{s} > 0.15$ as can be seen in the right plot of fig. 4.10 where the relative size compared to the SM result (obtained for $\mu_t = 120\,\mathrm{GeV}$ and $\mu_b = 5\,\mathrm{GeV}$) is given by the quantity $\Delta Q = Q/Q_{\mathrm{SM}} - 1$. Thus the shape and magnitude of the dilepton invariant mass distribution provides in certain regions of $\hat{s}$ a more sensitive observable then the integrated branching ratio itself in the search for deviations from the SM prediction, depending on the MSSM parameter point. It should be noted that the very small scale dependence around values of $\hat{s} \sim 0.05$ are due to accidental cancellations between the 4 separate contributions in (4.49).

In fig. 4.11 we show the normalized forward-backward asymmetry $\bar{\mathcal{A}}_{\mathrm{FB}}(\hat{s})$ for the low-s region. The left plot illustrates the result for the fixed MSSM-parameter point "P2" and the right plot for "P3" that are given in table 4.1. The SM result is shown in both plots for comparison. Again the bands are obtained by varying the renormalization scales μ_t and μ_b as in figs. 4.9 and 4.10. Due to the strong correlation of the position of the zero $\hat{s}_0$ and $\mathcal{B}(\bar{B} \to X_s \gamma)$ in the considered MSSM-scenarios further shifts to the left or right (as shown in the two plots) of $\hat{s}_0$ are unlikely.

In fig. 4.12 the fundamental MSSM parameters μ and $[A_U]_{33}$ are shown versus the position of the zero of $\bar{\mathcal{A}}_{\mathrm{FB}}(\hat{s})$, $\hat{s}_0$, for the sample of random MSSM points given in fig. 4.7. The lower and upper bounds of $\hat{s}_0$ present in both plots are evidently due to the strong correlation to $\mathcal{B}(\bar{B} \to X_s \gamma)$. The "hole" in the μ distribution for values $|\mu| < 100\,\mathrm{GeV}$ comes of course
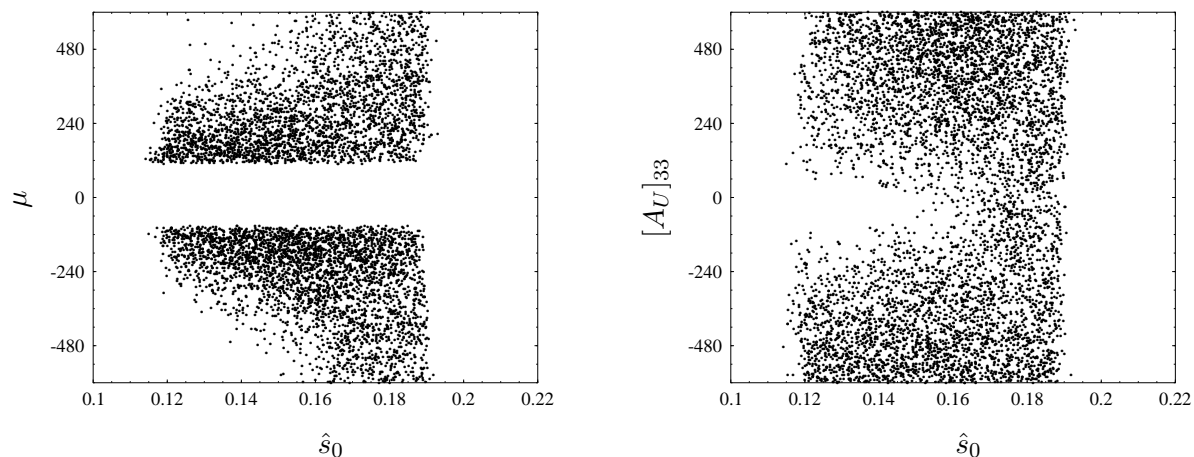
Figure 4.12: Correlation between $\hat{s}_0$ and parameters μ and $[A_U]_{33}$ produced in our scan over MSSM input parameters. The distributions for the other soft-breaking parameters are flat.

from the bound on the lightest chargino mass. As can be seen for small values of $\hat{s}_0$ also smaller values of μ are preferred. The allowed values of $[A_U]_{33}$ versus $\hat{s}_0$ generated during our random scan are shown in the right plot. Almost no bounds are found here, only towards smaller values of $\hat{s}_0$ very small values of $[A_U]_{33}$ seem to be excluded. We could not find such correlations for all other soft-supersymmetry breaking parameters.

Chapter 5

Conclusions and Outlook

The first topic of this thesis was concerned with an analysis of the rare decays $K^+ \to \pi^+ \nu\bar{\nu}$ and $K_L \to \pi^0 \nu\bar{\nu}$ in the context of the general MSSM with conserved R-parity. We briefly reviewed the effective Hamiltonian relevant for these decays, and presented the corresponding branching ratios in a form particularly suitable for our numerical analysis. The function X entering these observables has been calculated in the mass eigenstates basis for all particles of the MSSM in order to take all sources of flavor violation in the squark sector into account. This generalizes earlier work [44, 64, 65] where the mass-insertion approximation was used exclusively in calculating the X function, and only those flavor changing entries in the squark mass-squared matrices assumed to be the most important have been considered.

As a consequence, in our numerical analysis we had to consider a huge space of MSSM parameters, 16 in the constraint scan and 63 in the extended scan, which to our knowledge has been presented here for the first time. To find the possible large deviations of the function X from its SM prediction, we used a random scan based on an adaptation of the Monte Carlo integration algorithm VEGAS [66–68] rather than a random generation of points with a uniform distribution. The advantage of such a scan is its ability to find the maximal allowed regions of the parameter space and the extremal values of observables in a reasonable time.

Concerning the individual contributions to the function X, we find in agreement with [44,64,65] that chargino-mediated diagrams are always strongly dominant, typically one order of magnitude larger than the neutralino contributions, whereas gluino-mediated diagrams are fully negligible. However, unlike these authors we find that in addition to chargino-mediated Z penguins, chargino box-type diagrams can be important and even dominant for light charged slepton masses, as seen in fig. 3.4.

The answers to the questions posed in the introduction are as follows:

- The phase θ_X can be as large as found in [48, 49]. In fact as seen in fig. 3.7 one finds typically $-160° \leq \theta_X \leq 50°$ with a slightly increased range for the extended scan as seen in fig. 3.9. However, among the allowed values of $|X|$, it is not easy to find simultaneously $|X| \approx 2.2$ and $\theta_X \approx -85°$ as found in [48, 49][1]. Indeed, for $\theta_X \approx -85°$ the allowed value of $|X|$ in the constrained scan is typically lower than its SM value of 1.53 and only in the extended scan can it reach $|X| \approx 2.0$. On the other hand for $-50° \leq \theta_X \leq 50°$, one can have $|X|$ as high as 7. A similar situation is found for $\theta_X = -(150 \pm 10)°$ with $|X|$ reaching values as high as 8.

---

[1]See also the footnote on p. 4.

- As seen in figs. 3.6, 3.8 and 3.9, the branching ratio $\mathcal{B}(K^+ \to \pi^+ \nu\bar{\nu})$ can be naturally obtained in the ball park of the central experimental value given in (2), and simultaneously, $\mathcal{B}(K_L \to \pi^0 \nu\bar{\nu})$ can be enhanced by an order of magnitude over the SM expectation with the ratio of both branching ratios of $K_L \to \pi^0 \nu\bar{\nu}$ and $K^+ \to \pi^+ \nu\bar{\nu}$ reaching the bound given in (4). Comparing figs. 3.6 and 3.7 we observe that the experimental bound given in (2) has a significant impact on the maximal allowed values of $|X|$ with essentially no impact on θ_X. This is not surprising as $K^+ \to \pi^+ \nu\bar{\nu}$ is a CP-conserving decay. Clearly an improved upper bound on $\mathcal{B}(K_L \to \pi^0 \nu\bar{\nu})$ should have an important impact on the allowed values of θ_X.

Finally, we would like to mention that the numerical analysis of the extended scan can be used to put bounds on the allowed magnitude of the mass-insertions present in the squark mass-squared matrices, without resorting to the simplifying assumptions made in the literature. There, the bounds on the mass-insertions coming from various experimental results were obtained by the approximate procedure of requiring that each individual term in the mass-insertion expansion at most saturates the measured value. This neglects of course the possibility of significant cancellations between contributions from different terms in the expansion and also the interference with the SM contribution that is always present. In our approach, we use the exact results and hence we are able to "derive" improved bounds on the mass-insertions. The results of such an analysis, including additional experimental constraints not considered here, will, however, be presented elsewhere.

The second topic of this thesis was devoted to the presentation of a complete NNLO QCD analysis of the semileptonic inclusive decay $\bar{B} \to X_s l^+ l^-$ $(l = e, \mu)$. This calculation was motivated by the fact that in the SM the corresponding observables suffer from sizable renormalization scale uncertainties which are reduced considerably at NNLO. Consequently, in order to have a chance to reveal supersymmetric effects in this decay, it is essential to reduce the renormalization scale uncertainties in the MSSM as well. And in the light of the improving precision in measuring the branching ratio $\mathcal{B}(\bar{B} \to X_s l^+ l^-)$ at Belle and BaBar in ongoing experiments, this decay channel provides a valuable source of information of new physics scenarios complementary to those coming from the radiative decay $\bar{B} \to X_s \gamma$.[2]

As a first step in this challenging enterprise we have assumed that the down-squark mass-squared matrix decomposes into 2×2 matrices for each generation, that the gluino is heavy and decouples from the theory, and furthermore we concentrated on region within the MSSM parameter space with $\tan\beta \leq 10$. Within this special scenario we determined the squark masses and mixing matrices present in the "effective MSSM" with a decoupled gluino from the $O(\alpha_s)$ corrected squark mass-squared matrices present in the "full MSSM" including the gluino when matching both theories at the scale $\mu_{\tilde{g}} \sim O(M_{\tilde{g}})$. The resulting effective Lagrangian was then scaled down using renormalization group techniques to the scale μ_t where all remaining sparticles, assumed to be much lighter than the gluino, together with the Higgs bosons, the W bosons and the top quark have been integrated out. At the NNLO level in QCD, the latter matching procedure required the calculation of two-loop Wilson coefficients, some of which were already present in the literature and some of which have never been calculated before[3]. We calculated these Wilson coefficients in the $\overline{\text{MS}}$ and on-shell

---

[2]In the very recent work [187] it has been pointed out that the measured branching ratio $\mathcal{B}(\bar{B} \to X_s l^+ l^-)$ already indicates that the sign of $\widetilde{C}_7^{\text{eff}}$ is unlikely to be different than in the SM, an information which cannot be extracted from $\mathcal{B}(\bar{B} \to X_s \gamma)$ alone.

[3]We have re-calculated all contributions relevant for the NNLO QCD analysis of the decay $\bar{B} \to X_s l^+ l^-$

scheme for squark masses and mixing matrices. While the latter has the advantage that all contributions involving "quartic QCD interactions" of squarks are absent, it introduces large logarithms once we allow for larger splittings in the squark mass spectrum, and therefore makes predictions following from perturbation theory unreliable. Hence, in our numerical analysis we worked throughout with $\overline{\text{MS}}$ renormalized parameters in the squark sector.

Solving known renormalization group equations for Wilson coefficients in order to scale our findings down from the hight-energy scale μ_t to the low-energy scale μ_b, and including known low-energy matrix elements up to the NNLO level, we were able to calculate with this accuracy the branching ratio for $\bar{B} \to X_s l^+ l^-$ in the low-s region, the corresponding dilepton invariant mass distribution and the forward-backward asymmetry.

Our main findings are as follows:

- As seen in figs. 4.9, 4.10 and 4.11, the μ dependence present in all quantities of interest at NLO is visibly reduced at NNLO depending on the magnitude of the MSSM contribution for the particular MSSM parameter point, and it is typically of the same size as the one of the corresponding SM result.

- Supersymmetric effects in the branching ratio amount only to at most 20% (cf. fig. 4.6), and consequently in view of theoretical uncertainties in this quantity it will be very difficult to see them unless experimental and theoretical uncertainties will be significantly reduced. In this respect the dilepton invariant mass distribution can offer in certain regions of $\hat{s}$ the possibility to distinguish the supersymmetric effects from the SM prediction. Such effects can reach up to 30% depending on the MSSM parameters and the value of $\hat{s}$, as seen in fig. 4.10.

- The best chance to observe supersymmetric effects in this decays is through the forward-backward asymmetry. We find that the position of the zero $\hat{s}_0$ in this asymmetry can be significantly shifted both downwards and upwards relatively to the SM expectation (cf. fig. 4.11). These shifts are accompanied by shifts in $\mathcal{B}(\bar{B} \to X_s \gamma)$ as shown in fig. 4.7. As the predictions for $\hat{s}_0$ is theoretically rather clean, accurate measurements could be able to detect a possible departure from the SM prediction one day.

The next step is of course an analysis with a more general scenario than considered here. On could for example relax our first assumption and consider an arbitrary down-squark mass-squared matrix, which makes it necessary to calculate also diagrams with virtual neutralino contributions. Such contributions are, however, typically smaller than chargino-mediated diagrams, and therefore we do not expect large deviations from our findings. More promising in this respect is to relax our second or third assumption. But once the gluino is assumed to be relatively light, or that $\tan\beta$ is large, unavoidably new operators besides those relevant for the SM have to be taken into account. For example, considering the $b \to s l^+ l^-$ transition at large values for $\tan\beta$, neutral Higgs boson contributions give rise to scalar operators and the corresponding anomalous dimensions turns out to be a 54×54 matrix. In [188] only a subset of the relevant operators and only their one-loop mixing has been considered in a model-independent analysis of radiative and semileptonic B decays[4]. As already in the SM

---

already present in the literature since some results have never been checked by another group.

[4]The one-loop mixing of gluino-induced non-SM operators in the framework of the MSSM for the $b \to s\gamma$ transition has been presented in [189].

the magnitude of the NLO contributions is of the same size as the LO contribution, it is desirable to extend the analysis of [188] to the NLO, which requires the calculation of the two-loop $54{\times}54$ anomalous dimension matrix and the one-loop low-energy matrix elements of the corresponding operators. Such a calculation is essential to arrive at reasonable estimates for the branching ratios and forward-backward asymmetries for the decays $\bar{B} \to X_s l^+ l^-$ and $\bar{B} \to K^{(*)} l^+ l^-$ in the presence of new scalar operators, and will be postponed to another publication.

Part III

Appendices

Appendix A

Matching Conditions for $d \to s\nu\bar{\nu}$

In this appendix we collect the contributions to the functions X_L and X_R introduced in (3.3) within the general MSSM in the mass eigenstates basis for particles and sparticles. They can can be divided into two classes, generated by box-type and Z penguin diagrams:

$$K_{3I}K_{3J}^*[X_{L,R}]_{JIKL} = \sum_{i=W,H,C,N,G} \left\{ [B_{L,R}^i]_{JIKL} + [P_{L,R}^i]_{JI}\delta_{KL} \right\} \tag{A.1}$$

where W denotes the SM contribution and H, C, N ,G diagrams with virtual charged Higgs boson, chargino, neutralino and gluino exchange, respectively. This formula corresponds to a generalization of (3.3) to[1]

$$\tilde{\mathcal{H}}_{\text{eff}}^{(t)} = \sum_{K,L=1}^{3} K_{3I}K_{3J}^* \left\{ [X_L]_{JIKL}(\bar{d}_J P_L d_I)(\bar{\nu}_K P_L \nu_L) \right.$$

$$\left. + [X_R]_{JIKL}(\bar{d}_J P_R d_I)_{V+A}(\bar{\nu}_K P_L \nu_L) \right\} \tag{A.2}$$

where for $K \to \pi\nu\bar{\nu}$ decays one should use $I = 1, J = 2$ and K, L are neutrino flavor indices. In general the $X_{L,R}$ quantities defined in (A.1) carry lepton flavor indices. Only in the case when the lepton flavor number is conserved in the slepton sector and the left- and right-slepton flavor diagonal mass parameters are identical for all three generations, the $X_{L,R}$ are to a good approximation (neglecting small terms proportional to the lepton Yukawa couplings) universal, as assumed in (3.3). The relation between the $X_{L,R}$ of (3.3) and of (A.2) is given by

$$[X_{L,R}]_{21KL} = X_{L,R}\,\delta_{KL} \tag{A.3}$$

In the numerical analysis presented in sec. 3.3 we assume the above mentioned simple flavor conserving structure of the slepton sector and use the definition given in (A.3).

Defining further

$$x_t = \frac{m_t^2}{M_W^2}, \qquad\qquad y_t = \frac{m_t^2}{M_{H^+}^2} \tag{A.4}$$

---

[1]Note that the subscript L on X_L and P_L refers to the chirality structure of the quark current and hence is no summation index.

the non-vanishing box contributions read[2]

$$[B_L^W]_{JIKL} = -K_{3I}K_{3J}^* \, 4 f_1(x_t) \, \delta_{KL}$$

$$[B_R^H]_{JIKL} = -K_{3I}K_{3J}^* \frac{m_{d_I} m_{d_J} m_{e_K}^2 \tan^4 \beta}{4 M_W^2 M_{H^+}^2} f_1(y_t) \, \delta_{KL}$$

$$[B_L^C]_{JIKL} = -\frac{M_W^2 \mathrm{s}_W^4}{2e^4} [X_j^{N_L \dagger}]_{Kb} [X_i^{N_L}]_{bL} [X_j^{U_L \dagger}]_{Ja} [X_i^{U_L}]_{aI} \, m_{\tilde{\chi}_i^+} m_{\tilde{\chi}_j^+} D_0(m_{\tilde{\chi}_i^+}^2, m_{\tilde{\chi}_j^+}^2, m_{\tilde{u}_a}^2, m_{\tilde{e}_b}^2)$$

$$[B_R^C]_{JIKL} = \frac{M_W^2 \mathrm{s}_W^4}{4e^4} [X_j^{N_L \dagger}]_{Kb} [X_i^{N_L}]_{bL} [X_j^{U_R \dagger}]_{Ja} [X_i^{U_R}]_{aI} D_2(m_{\tilde{\chi}_i^+}^2, m_{\tilde{\chi}_j^+}^2, m_{\tilde{u}_a}^2, m_{\tilde{e}_b}^2)$$

$$[B_L^N]_{JIKL} = -\frac{M_W^2 \mathrm{s}_W^4}{4e^4} [Z_j^{D_L \dagger}]_{Ja} [Z_i^{D_L}]_{aI}$$

$$\times \left\{ [Z_i^{N_L \dagger}]_{KN} [Z_j^{N_L}]_{NL} D_2(m_{\tilde{\chi}_i^0}^2, m_{\tilde{\chi}_j^0}^2, m_{\tilde{d}_a}^2, m_{\tilde{\nu}_N}^2) \right.$$

$$\left. + 2[Z_j^{N_L \dagger}]_{KN} [Z_i^{N_L}]_{NL} m_{\tilde{\chi}_i^0} m_{\tilde{\chi}_j^0} D_0(m_{\tilde{\chi}_i^0}^2, m_{\tilde{\chi}_j^0}^2, m_{\tilde{d}_a}^2, m_{\tilde{\nu}_N}^2) \right\}$$

$$[B_R^N]_{JIKL} = \frac{M_W^2 \mathrm{s}_W^4}{4e^4} [Z_j^{D_L \dagger}]_{Ja} [Z_i^{D_L}]_{aI}$$

$$\times \left\{ [Z_j^{N_L \dagger}]_{KN} [Z_i^{N_L}]_{NL} D_2(m_{\tilde{\chi}_i^0}^2, m_{\tilde{\chi}_j^0}^2, m_{\tilde{d}_a}^2, m_{\tilde{\nu}_N}^2) \right.$$

$$\left. + 2[Z_i^{N_L \dagger}]_{KN} [Z_j^{N_L}]_{NL} m_{\tilde{\chi}_i^0} m_{\tilde{\chi}_j^0} D_0(m_{\tilde{\chi}_i^0}^2, m_{\tilde{\chi}_j^0}^2, m_{\tilde{d}_a}^2, m_{\tilde{\nu}_N}^2) \right\} \tag{A.5}$$

while the non-vanishing penguin contributions read

$$[P_L^W]_{JI} = K_{3I}K_{3J}^* f_2(x_t)$$

$$[P_L^H]_{JI} = -K_{3I}K_{3J}^* \frac{\cot^2 \beta M_{H^+}^2}{2 M_W^2} y_t f_1(y_t)$$

$$[P_R^H]_{JI} = K_{3I}K_{3J}^* \frac{m_{d_I} m_{d_J} \tan^2 \beta}{2 M_W^2} f_1(y_t)$$

$$[P_L^C]_{JI} = \frac{\mathrm{s}_W^2}{8e^2} [X_j^{U_L \dagger}]_{Ja} [X_i^{U_L}]_{bI}$$

$$\times \left\{ 2 U_{i1}^* U_{j1} \delta_{ab} \, m_{\tilde{\chi}_i^+} m_{\tilde{\chi}_j^+} C_0(m_{\tilde{u}_b}^2, m_{\tilde{\chi}_i^+}^2, m_{\tilde{\chi}_j^+}^2) \right.$$

$$\left. - V_{j1}^* V_{i1} \delta_{ab} \, C_2(m_{\tilde{u}_b}^2, m_{\tilde{\chi}_i^+}^2, m_{\tilde{\chi}_j^+}^2) + (\Gamma^{U_L} \Gamma^{U_L \dagger})_{ab} \delta_{ij} \, C_2(m_{\tilde{\chi}_i^+}^2, m_{\tilde{u}_a}^2, m_{\tilde{u}_b}^2) \right\}$$

---

[2]Summation over all indices other than J, I, K and L is understood. All box and penguin contributions presented here can also be found in [190].

$$[P_R^C]_{JI} = \frac{\mathrm{s}_W^2}{8e^2}[X_j^{U_L\,\dagger}]_{Ja}[X_i^{U_L}]_{bI}$$

$$\times \left\{ 2V_{j1}^*V_{i1}\delta_{ab}\, m_{\tilde\chi_i^+}m_{\tilde\chi_j^+}C_0(m_{\tilde u_b}^2, m_{\tilde\chi_i^+}^2, m_{\tilde\chi_j^+}^2) \right.$$

$$\left. - U_{i1}^*U_{j1}\delta_{ab}\, C_2(m_{\tilde u_b}^2, m_{\tilde\chi_i^+}^2, m_{\tilde\chi_j^+}^2) - (\Gamma^{U_R}\Gamma^{U_R\dagger})_{ab}\delta_{ij}\, C_2(m_{\tilde\chi_i^+}^2, m_{\tilde u_a}^2, m_{\tilde u_b}^2) \right\}$$

$$[P_L^N]_{JI} = \frac{\mathrm{s}_W^2}{8e^2}[Z_j^{D_L\,\dagger}]_{Ja}[Z_i^{D_L}]_{bI}$$

$$\times \left\{ (\Gamma^{D_R}\Gamma^{D_R\dagger})_{ab}\delta_{ij}\, C_2(m_{\tilde\chi_i^0}^2, m_{\tilde d_a}^2, m_{\tilde d_b}^2) \right.$$

$$+ (N_{j4}^*N_{i4} - N_{j3}^*N_{i3})\delta_{ab}\, C_2(m_{\tilde d_b}^2, m_{\tilde\chi_i^0}^2, m_{\tilde\chi_j^0}^2)$$

$$\left. + 2(N_{j4}N_{i4}^* - N_{j3}N_{i3}^*)\delta_{ab}\, m_{\tilde\chi_i^0}m_{\tilde\chi_j^0}C_0(m_{\tilde d_b}^2, m_{\tilde\chi_i^0}^2, m_{\tilde\chi_j^0}^2) \right\}$$

$$[P_R^N]_{JI} = -\frac{\mathrm{s}_W^2}{8e^2}[Z_j^{D_L\,\dagger}]_{Ja}[Z_i^{D_L}]_{bI}$$

$$\times \left\{ (\Gamma^{D_L}\Gamma^{D_L\dagger})_{ab}\delta_{ij}\, C_2(m_{\tilde\chi_i^0}^2, m_{\tilde d_a}^2, m_{\tilde d_b}^2) \right.$$

$$+ (N_{j4}N_{i4}^* - N_{j3}N_{i3}^*)\delta_{ab}\, C_2(m_{\tilde d_b}^2, m_{\tilde\chi_i^0}^2, m_{\tilde\chi_j^0}^2)$$

$$\left. + 2(N_{j4}^*N_{i4} - N_{j3}^*N_{i3})\delta_{ab}\, m_{\tilde\chi_i^0}m_{\tilde\chi_j^0}C_0(m_{\tilde d_b}^2, m_{\tilde\chi_i^0}^2, m_{\tilde\chi_j^0}^2) \right\}$$

$$[P_L^G]_{JI} = \frac{g_s^2\,\mathrm{s}_W^2}{3e^2}(\Gamma^{D_R}\Gamma^{D_R\dagger})_{ab}[\Gamma^{D_L\dagger}]_{Ja}[\Gamma^{D_L}]_{bI}C_2(M_{\tilde g}^2, m_{\tilde d_b}^2, m_{\tilde d_a}^2)$$

$$[P_R^G]_{JI} = -\frac{g_s^2\,\mathrm{s}_W^2}{3e^2}(\Gamma^{D_L}\Gamma^{D_L\dagger})_{ab}[\Gamma^{D_R\dagger}]_{Ja}[\Gamma^{D_R}]_{bI}C_2(M_{\tilde g}^2, m_{\tilde d_b}^2, m_{\tilde d_a}^2) \tag{A.6}$$

For the definitions of the couplings $X^{U_{L,R}}$, $X^{N_{L,R}}$, $Z^{D_{L,R}}$ and $Z^{N_{L,R}}$ we refer the reader to [191, 192][3]. The loop functions appearing in these Wilson coefficients are given by

$$f_1(x) = \frac{x}{4(1-x)} + \frac{x\ln x}{4(1-x)^2}$$

$$f_2(x) = \frac{x(6-x)}{8(1-x)} + \frac{x(2+3x)\ln x}{8(1-x)^2}$$

$$C_0(x,y,z) = -\frac{y}{(x-y)(z-y)}\ln\frac{y}{x} + (y\leftrightarrow z)$$

$$C_2(x,y,z) = \frac{2}{4-D} + \log 4\pi - \gamma_E + \ln\frac{\mu^2}{x} + 1 - \left\{ \frac{y^2}{(x-y)(z-y)}\ln\frac{y}{x} + (y\leftrightarrow z) \right\}$$

---

[3]We remark that in [192] the couplings $X^{N_{L,R}}$ and $Z^{N_{L,R}}$ are denoted by $X^{L_{L,R}}$ and $Z^{L_{L,R}}$, respectively.

$$D_0(x, y, z, t) = \frac{-y}{(y-x)(y-z)(y-t)} \ln \frac{y}{x} + (y \leftrightarrow z) + (y \leftrightarrow t)$$

$$D_2(x, y, z, t) = \frac{-y^2}{(y-x)(y-z)(y-t)} \ln \frac{y}{x} + (y \leftrightarrow z) + (y \leftrightarrow t) \tag{A.7}$$

The infinite and μ-dependent terms in C_2 always cancels out in flavor off-diagonal penguins after summation over squark, chargino and neutralino mixing matrices. We recall that $f_1(x) = B_0(x)$ and $f_2(x) = C_0(x)$ in the notation of [118, 120].

Appendix B

Non-Physical Operators for $b \to sl^+l^-$

The effective low-energy Lagrangian relevant for the $\bar{B} \to X_s l^+l^-$ decay consists of several operators which can be divided into two classes, namely physical and non-physical operators. In the following we will discuss the non-physical operators relevant for two-loop QCD corrections to the $\bar{B} \to X_s l^+l^-$ decay. These are the so-called evanescent operators, i.e. algbraically vanishing in four dimensions, and the EOM-vanishing operators, i.e. vanishing by the QED×QCD equations of motion. The effect of these non-physical operators is twofold. First, in the matching calculation they contribute to the Wilson coefficients of physical operators. Second, in calculating the anomalous dimension of the physical operators they are necessary to remove the divergences of all possible 1PI Green functions with single insertions of physical operators.

B.1   Evanescent operators

All evanescent operators we encountered in the two-loop QCD calculations are collected in

$$
\mathcal{L}_{\text{evanescent}} = \frac{4G_F}{\sqrt{2}} \Bigg\{ \sum_{Q=u,c} \sum_{i=1}^{2} K_{Qb} K_{Qs}^* \left(C_{E_{1i}}^Q E_{1i}^Q + C_{E_{2i}}^Q E_{2i}^Q \right)
$$
$$
+ \sum_{Q=u,c,t} K_{Qb} K_{Qs}^* \Bigg\{ \sum_{i=5}^{6} \left(C_{E_{1i}}^Q E_{1i} + C_{E_{2i}}^Q E_{2i} \right) + C_{E_{19}}^Q E_{19} \Bigg\}
$$
$$
+ K_{tb} K_{ts}^* \Bigg\{ \sum_{i=1}^{2,5} \left(C_{E_i^{LL}}^t E_i^{LL} + C_{E_i^{LR}}^t E_i^{LR} \right)
$$
$$
+ C_{E_3^{LL}}^t E_3^{LL} + C_{E_4^{LR}}^t E_4^{LR} + (L \leftrightarrow R) \Bigg\} \Bigg\} \tag{B.1}
$$

Their explicit form defines what the $\overline{\text{MS}}$ scheme means in the effective theory. Introducing the short-hand notation $\gamma_{\mu_1 \ldots \mu_n} = \gamma_{\mu_1} \cdots \gamma_{\mu_n}$ those relevant for the $b \to s\bar{q}q$ transitions read

as [82, 83, 158]

$$E_{11}^Q = (\bar{s}\gamma_{\mu\nu\rho}P_L T^a Q)(\bar{Q}\gamma^{\mu\nu\rho}P_L T^a b) - 16\,\mathcal{O}_1^Q$$

$$E_{12}^Q = (\bar{s}\gamma_{\mu\nu\rho}P_L q)(\bar{Q}\gamma^{\mu\nu\rho}P_L b) - 16\,\mathcal{O}_2^Q$$

$$E_{15} = (\bar{s}\gamma_{\mu\nu\rho\lambda\sigma}P_L b)\sum_q (\bar{q}\gamma^{\mu\nu\rho\lambda\sigma}q) - 20\,\mathcal{O}_5 + 64\,\mathcal{O}_3$$

$$E_{16} = (\bar{s}\gamma_{\mu\nu\rho\lambda\sigma}P_L T^a b)\sum_q (\bar{q}\gamma^{\mu\nu\rho\lambda\sigma}T^a q) - 20\,\mathcal{O}_6 + 64\,\mathcal{O}_4$$

$$E_{21}^Q = (\bar{s}\gamma_{\mu\nu\rho\lambda\sigma}P_L T^a Q)(\bar{Q}\gamma^{\mu\nu\rho\lambda\sigma}P_L T^a b) - 256\,\mathcal{O}_1^Q - 20\,E_{11}^Q$$

$$E_{22}^Q = (\bar{s}\gamma_{\mu\nu\rho\lambda\sigma}P_L Q)(\bar{Q}\gamma^{\mu\nu\rho\lambda\sigma}P_L b) - 256\,\mathcal{O}_2^Q - 20\,E_{12}^Q$$

$$E_{25} = (\bar{s}\gamma_{\mu\nu\rho\lambda\sigma\kappa\delta}P_L b)\sum_q (\bar{q}\gamma^{\mu\nu\rho\lambda\sigma\kappa\delta}q) - 336\,\mathcal{O}_5 + 1280\,\mathcal{O}_3$$

$$E_{26} = (\bar{s}\gamma_{\mu\nu\rho\lambda\sigma\kappa\delta}P_L T^a b)\sum_q (\bar{q}\gamma^{\mu\nu\rho\lambda\sigma\kappa\delta}T^a q) - 336\,\mathcal{O}_6 + 1280\,\mathcal{O}_4 \tag{B.2}$$

where the sum over q runs over all light quark flavors participating the effective theory.

For the $b \to sl^+l^-$ two-loop matching within the SM one needs

$$E_{19} = \frac{e^2}{g^2}(\bar{s}\gamma_{\mu\nu\rho}P_L b)(\bar{l}\gamma^{\mu\nu\rho}P_L l) - 8\,\mathcal{O}_9 + 8\,\mathcal{O}_{10} \tag{B.3}$$

We remark that the definition of this evanescent operator is irrelevant for QCD corrections because it does not appear in the calculation of the anomalous dimension matrix.

All of these evanescent operators can be shown to vanish in four dimensions by means of the identity

$$\gamma_\mu\gamma_\nu\gamma_\rho = g_{\mu\nu}\gamma_\rho + g_{\mu\rho}\gamma_\nu + g_{\nu\rho}\gamma_\mu + i\epsilon_{\alpha\mu\nu\rho}\gamma^\alpha\gamma_5 \tag{B.4}$$

The appearance of γ_5 in this identity exhibits the reason why we have to introduce evanescent operators in $D \neq 4$ dimensions.

The matching of $b \to sl^+l^-$ within the considered scenario of the MSSM requires the introduction of

$$E_1^{LL} = (\bar{s}P_L l)(\bar{l}P_L b) + \tfrac{1}{2}(\bar{s}P_L b)(\bar{l}P_L l) + \tfrac{1}{8}(\bar{s}\sigma_{\mu\nu}P_L b)(\bar{l}\sigma^{\mu\nu}P_L l)$$

$$E_1^{LR} = (\bar{s}P_L l)(\bar{l}P_R b) + \tfrac{1}{2}(\bar{s}\gamma_\mu P_R b)(\bar{l}\gamma^\mu P_L l)$$

$$E_2^{LL} = (\bar{s}\gamma_\mu P_L l)(\bar{l}\gamma^\mu P_L b) - (\bar{s}\gamma_\mu P_L b)(\bar{l}\gamma^\mu P_L l)$$

$$E_2^{LR} = (\bar{s}\gamma_\mu P_L l)(\bar{l}\gamma^\mu P_R b) + 2(\bar{s}P_R b)(\bar{l}P_L l)$$

$$E_3^{LL} = (\bar{s}\sigma_{\mu\nu}P_L l)(\bar{l}\sigma^{\mu\nu}P_L b) + 6(\bar{s}P_L b)(\bar{l}P_L l) - \tfrac{1}{2}(\bar{s}\sigma_{\mu\nu}P_L b)(\bar{l}\sigma^{\mu\nu}P_L l)$$

$$E_4^{LR} = (\bar{s}\gamma_{\mu\nu}P_L l)(\bar{l}\gamma^{\mu\nu}P_R b) - 4(\bar{s}P_L l)(\bar{l}P_R b)$$

$$E_5^{LL} = (\bar{s}\gamma_{\mu\nu\rho}P_L l)(\bar{l}\gamma^{\mu\nu\rho}P_L b) - 16(\bar{s}\gamma_\mu P_L l)(\bar{l}\gamma^\mu P_L b)$$

$$E_5^{LR} = (\bar{s}\gamma_{\mu\nu\rho}P_L l)(\bar{l}\gamma^{\mu\nu\rho}P_R b) - 4(\bar{s}\gamma_\mu P_L l)(\bar{l}\gamma^\mu P_R b) \tag{B.5}$$

and those obtained by the substitution $L \leftrightarrow R$. The first five operators are so-called Fierz-vanishing evanescent operators. They can be shown to vanish by observing that $\{\mathbb{1}, \gamma^\mu, \gamma_5, \gamma^\mu \gamma_5, \sigma^{\mu\nu}\}$ is a basis for complex 4×4 matrices. It is again the appearance of γ_5 in this set that makes it necessary to introduce evanescent operators.

For the calculation of the two-loop anomalous dimension matrix only $E_{11,12,15,16}$ and $E_{21,22,25,26}$ are relevant. However, the definition of the operators $E_{21,22,25,26}$ is not unique because we can for example add any multiple of ϵ times any physical operator to them without affecting the one-loop and two-loop anomalous dimensions. This is contrary to what happens if such a redefinition is applied to the operators $E_{11,12,15,16}$. However, the evanescent operators $E_{21,22,25,26}$ become more important at the three-loop level [84, 193].

B.2 EOM-vanishing operators

All EOM-vanishing operators we need are given in

$$\mathcal{L}_{\text{EOM}} = \frac{4G_F}{\sqrt{2}} \sum_{Q=u,c,t} K_{Qb} K_{Qs}^* \left\{ \sum_{i=1}^{6} C_{N_{3i}}^Q N_{3i} + \sum_{i=0}^{3} C_{N_{5(2i+1)}}^Q N_{5(2i+1)} \right\} \tag{B.6}$$

Here, we have to consider both gauge-invariant and gauge-variant operators.

Using the properties of the covariant derivatives

$$D_\mu = \partial_\mu + ieQ_f + ig_s G_\mu^a T^a, \qquad\qquad D_\nu^{ab} = \delta^{ab}\partial_\nu + g_s f^{abc} G_\nu^c \tag{B.7}$$

where Q_f is the electric charge of fermion f on which D_μ acts, the gauge-invariant EOM-vanishing operators can be chosen to be [82, 161]

$$N_{30} = \frac{i}{g_s^2} M_W^2 (\bar{s} \slashed{D} P_L b)$$

$$N_{31} = \frac{1}{g_s} (\bar{s} \gamma^\mu P_L T^a b) D_{ab}^\nu G_{\mu\nu}^b + \mathcal{O}_4$$

$$N_{32} = \frac{1}{g_s^2} m_b (\bar{s} \slashed{D} \slashed{D} P_R b)$$

$$N_{33} = \frac{i}{g_s^2} (\bar{s} \slashed{D} \slashed{D} \slashed{D} P_L b)$$

$$N_{34} = \frac{i}{g_s} \left[(\bar{s} \overleftarrow{\slashed{D}} \sigma^{\mu\nu} P_L T^a b) G_{\mu\nu}^a - G_{\mu\nu}^a (\bar{s} T^a \sigma^{\mu\nu} \slashed{D} P_L b) \right] + \mathcal{O}_8$$

$$N_{35} = \frac{ie}{g_s^2} \left[(\bar{s} \overleftarrow{\slashed{D}} \sigma^{\mu\nu} P_L b) F_{\mu\nu} - F_{\mu\nu} (\bar{s} \sigma^{\mu\nu} \slashed{D} P_L b) \right] + \mathcal{O}_7$$

$$N_{36} = \frac{e}{g_s^2} (\bar{s} \gamma^\mu P_L b) \partial^\nu F_{\mu\nu} - \mathcal{O}_9 \tag{B.8}$$

where we neglected the strange quark mass.

In the above given equation $\mathcal{O}_9$ is redefined so that it contains a sum over all the light charged fermions f weighted by their electric charges Q_f,

$$\mathcal{O}_9 = -\frac{e^2}{g_s^2} (\bar{s} \gamma_\mu P_L b) \sum_f Q_f (\bar{f} \gamma^\mu f) \tag{B.9}$$

Such a redefinition of $\mathcal{O}_9$ does not alter its Wilson coefficient at leading order in electroweak interactions.

Strictly speaking N_{31} is no EOM-vanishing operator. However, we will adopt a renormalization prescription on the full theory side such that its Wilson coefficient gets no contribution, and thus we put it here with the other gauge-invariant operators.

We note that the operators $\mathcal{O}_{1\ldots10}$ and $N_{30\ldots36}$ close off-shell under QCD corrections up to evanescent operators [82, 153–157] if one works with background gluons and photons.

The gauge-variant EOM-vanishing operators relevant for the calculation of the two-loop anomalous dimension matrix are given by [84]

$$
\begin{aligned}
N_{51} &= -\frac{i}{g_s} m_b \left[\bar{s}(\overleftarrow{\slashed{D}} \slashed{G}^a T^a - \slashed{G}^a T^a \slashed{D}) P_R b \right] \\
N_{53} &= -\frac{1}{g_s} \left[\bar{s}(\overleftarrow{\slashed{D}}\overleftarrow{\slashed{D}} \slashed{G}^a T^a - \slashed{G}^a T^a \slashed{D}\slashed{D}) P_L b + i m_b (\bar{s}\slashed{G}^a T^a \slashed{D} P_R b) \right] \\
N_{55} &= -\frac{1}{g_s} \left[\bar{s}(\overleftarrow{\slashed{D}}\overleftarrow{D}_\mu G^{a\mu} T^a - G^{a\mu} T^a D_\mu \slashed{D}) P_L b + i m_b (\bar{s} G^{a\mu} T^a D_\mu P_R b) \right] \\
N_{57} &= \frac{1}{g_s} \left[(\bar{s} \overleftarrow{\slashed{D}} \slashed{G}^a T^a \slashed{D} P_L b) + i m_b (\bar{s} \overleftarrow{\slashed{D}} \slashed{G}^a T^a P_R b) \right]
\end{aligned}
\tag{B.10}
$$

where we again neglected the strange quark mass.

They are necessary in the calculation of the anomalous dimension matrix of the physical operators beyond LO in order to remove the divergences of all possible 1PI Greens functions with single insertions of operators even if one works with background gluons and photons.

Appendix C

Matching Conditions for $b \to sl^+l^-$

This appendix summarizes the matching results relevant for $\bar{B} \to X_s l^+ l^-$ in the SM and the considered scenario of the MSSM as introduced in sec. 2.5. It provides the formulae for the functions $[X_k]_i^n$ introduced in (4.15). We define the mass ratios

$$x = \frac{m_t^2}{M_W^2}, \qquad y = \frac{m_t^2}{M_{H^+}^2}, \qquad x_{ij} = \frac{m_{\tilde{\chi}_i^+}^2}{m_{\tilde{\chi}_j^+}^2}, \qquad y_{ai} = \frac{m_{\tilde{u}_a}^2}{m_{\tilde{\chi}_i^+}^2}, \qquad v_{Ki} = \frac{m_{\tilde{\nu}_K}^2}{m_{\tilde{\chi}_i^+}^2} \qquad \text{(C.1)}$$

and introduce the abbreviations

$$L_t = \ln \frac{\mu_t^2}{m_t^2}, \qquad\qquad L_{\tilde{u}_a} = \ln \frac{\mu_t^2}{m_{\tilde{u}_a}^2}, \qquad\qquad \kappa = \frac{s_W^2}{e^2 K_{tb} K_{ts}^*} \qquad \text{(C.2)}$$

The integral representations for the dilogarithm $\text{Li}_2(z)$ and the Clausen function $\text{Cl}_2(x)$ are as follows,

$$\text{Li}_2(z) = -\int_0^z dt \frac{\ln(1-t)}{t}$$

$$\text{Cl}_2(x) = \text{Im}\left[\text{Li}_2\left(e^{ix}\right)\right] = -\int_0^x d\theta \ln|2\sin(\theta/2)| \qquad \text{(C.3)}$$

As a consequence of the adopted renormalization procedure outlined in sec. 4.2, all masses of quarks and squarks, as well as the mixing matrix Γ^U and the effective couplings $X_i^{U_L}$ and $X_i^{U_R}$ appearing in this appendix are $\overline{\text{MS}}$ quantities. The masses of particles which do not interact strongly are not renormalized and thus might be interpreted as their tree-level masses. For the definition of the couplings $X_i^{N_L}$ and $X_i^{N_R}$ we refer the reader to [101].

To obtain the Wilson coefficients in terms of on-shell masses and mixing matrices for squarks, the following steps should be performed:

1. Remove the contributions due to strong quartic squark couplings, i.e. the contributions with the index $i = Q$ in the functions $[X_k]^n$.

2. Make the following shift of the up-squark mass in the contributions with the index $i = \tilde{\chi}$:

$$m_{\tilde{u}_a}^2(\mu_t) = (m_{\tilde{u}_a}^{\text{pole}})^2 \left\{ 1 - \frac{\alpha_s(m_{\tilde{u}_a}^{\text{pole}})}{4\pi} \frac{4}{3} \left[7 + 6\ln\left(\frac{\mu_t}{m_{\tilde{u}_a}^{\text{pole}}}\right) \right] \right\} \qquad \text{(C.4)}$$

Observe that this shift involves only the gluonic corrections, since the contributions due to strong quartic squark couplings have already been considered in step 1.

These two steps are a direct consequence of the application of the full scheme shift from the $\overline{\text{MS}}$ to the on-shell scheme given by

$$m_{\tilde{u}_a}^2(\mu_t) = (m_{\tilde{u}_a}^{\text{pole}})^2 \left\{ 1 - \frac{\alpha_s(\mu_t)}{4\pi} \frac{4}{3} \left[7 + 6 \ln \left(\frac{\mu_t}{m_{\tilde{u}_a}^{\text{pole}}} \right) \right] \right.$$

$$\left. + \frac{\alpha_s(\mu_t)}{4\pi} \frac{4}{3} \sum_{b=1}^{6} \frac{P_{ab}^U (m_{\tilde{u}_b}^{\text{pole}})^2 P_{ba}^U}{(m_{\tilde{u}_a}^{\text{pole}})^2} \left[1 + 2 \ln \left(\frac{\mu_t}{m_{\tilde{u}_b}^{\text{pole}}} \right) \right] \right\}$$

$$\Gamma_{ab}^U(\mu_t) = \Gamma_{ab}^U + \frac{\alpha_s(\mu_t)}{4\pi} \frac{4}{3} \sum_{e=1}^{6} \sum_{\substack{c=1 \\ c \neq a}}^{6} \frac{P_{ae}^U (m_{\tilde{u}_e}^{\text{pole}})^2 P_{ec}^U}{(m_{\tilde{u}_a}^{\text{pole}})^2 - (m_{\tilde{u}_c}^{\text{pole}})^2} \left[1 + 2 \ln \left(\frac{\mu_t}{m_{\tilde{u}_e}^{\text{pole}}} \right) \right] \Gamma_{cb}^U \qquad \text{(C.5)}$$

On the left hand side of these equations the squark masses and the mixing matrix are running $\overline{\text{MS}}$ parameters, whereas on the right hand side they take their on-shell values. The couplings a_g and a_Y [cf. (2.79)] present in $X_i^{U_L}$ and $X_i^{U_R}$ are still $\overline{\text{MS}}$ renormalized in the on-shell scheme for squarks.

C.1 Standard Model Contributions

The evaluation of Feynman diagrams contributing to $b \to s+$(light particles) Green functions within the SM mediated by "top quark – W boson" loops yields the functions denoted by the index $i = W$ in (4.15). We find

$$[E_4]_W^0 = \frac{-9x^2+16x-4}{6(1-x)^4} \ln x + \frac{-7x^3-21x^2+42x+4}{36(1-x)^3}$$

$$[A_7]_W^0 = \frac{-3x^3+2x^2}{2(1-x)^4} \ln x + \frac{22x^3-153x^2+159x-46}{36(1-x)^3}$$

$$[F_8]_W^0 = \frac{3x^2}{2(1-x)^4} \ln x + \frac{5x^3-9x^2+30x-8}{12(1-x)^3}$$

$$[B_9^{\bar{l}l}]_W^0 = [B_{10}^{\bar{l}l}]_W^0 = \frac{x}{4(1-x)^2} \ln x + \frac{1}{4(1-x)}$$

$$[C_9^{\bar{l}l}]_W^0 = \frac{3x^2+2x}{8(1-x)^2} \ln x + \frac{-x^2+6x}{8(1-x)}$$

$$[D_9^{\bar{l}l}]_W^0 = \frac{-3x^4+30x^3-54x^2+32x-8}{18(1-x)^4} \ln x + \frac{-47x^3+237x^2-312x+104}{108(1-x)^3} \qquad \text{(C.6)}$$

$$[G_3]_W^1 = \frac{10x^4-100x^3+30x^2+160x-40}{27(1-x)^4} \text{Li}_2\left(1 - \frac{1}{x}\right) + \frac{30x^3-42x^2-332x+68}{81(1-x)^4} \ln x$$

$$+ \frac{-6x^3-293x^2+161x+42}{81(1-x)^3} + \left[\frac{90x^2-160x+40}{27(1-x)^4} \ln x + \frac{35x^3+105x^2-210x-20}{81(1-x)^3} \right] L_t$$

$$[E_4]_W^1 = \frac{515x^4-614x^3-81x^2-190x+40}{54(1-x)^4} \text{Li}_2\left(1 - \frac{1}{x}\right)$$

$$+ \frac{-1030x^4+435x^3+1373x^2+1950x-424}{108(1-x)^5}\ln x + \frac{-29467x^4+45604x^3-30237x^2+66532x-10960}{1944(1-x)^4}$$

$$+ \left[\frac{-1125x^3+1685x^2+380x-76}{54(1-x)^5}\ln x + \frac{133x^4-2758x^3-2061x^2+11522x-1652}{324(1-x)^4}\right]L_t$$

$$[A_7]_W^1 = \frac{32x^4+244x^3-160x^2+16x}{9(1-x)^4}\mathrm{Li}_2\left(1-\tfrac{1}{x}\right)$$

$$+ \frac{-774x^4-2826x^3+1994x^2-130x+8}{81(1-x)^5}\ln x + \frac{-94x^4-18665x^3+20682x^2-9113x+2006}{243(1-x)^4}$$

$$+ \left[\frac{-12x^4-92x^3+56x^2}{3(1-x)^5}\ln x + \frac{-68x^4-202x^3-804x^2+794x-152}{27(1-x)^4}\right]L_t$$

$$[F_8]_W^1 = \frac{4x^4-40x^3-41x^2-x}{3(1-x)^4}\mathrm{Li}_2\left(1-\tfrac{1}{x}\right)$$

$$+ \frac{-144x^4+3177x^3+3661x^2+250x-32}{108(1-x)^5}\ln x + \frac{-247x^4+11890x^3+31779x^2-2966x+1016}{648(1-x)^4}$$

$$+ \left[\frac{17x^3+31x^2}{(1-x)^5}\ln x + \frac{-35x^4+170x^3+447x^2+338x-56}{18(1-x)^4}\right]L_t$$

$$[B_9^{\bar{l}l}]_W^1 = [B_{10}^{\bar{l}l}]_W^1 = \frac{-2x}{(1-x)^2}\mathrm{Li}_2\left(1-\tfrac{1}{x}\right)$$

$$+ \frac{-x^2+17x}{3(1-x)^3}\ln x + \frac{13x+3}{3(1-x)^2} + \left[\frac{2x^2+2x}{(1-x)^3}\ln x + \frac{4x}{(1-x)^2}\right]L_t$$

$$[C_9^{\bar{l}l}]_W^1 = \frac{-x^3-4x}{(1-x)^2}\mathrm{Li}_2\left(1-\tfrac{1}{x}\right)$$

$$+ \frac{3x^3+14x^2+23x}{3(1-x)^3}\ln x + \frac{4x^3+7x^2+29x}{3(1-x)^2} + \left[\frac{8x^2+2x}{(1-x)^3}\ln x + \frac{x^3+x^2+8x}{(1-x)^2}\right]L_t$$

$$[D_9^{\bar{l}l}]_W^1 = \frac{380x^4-1352x^3+1656x^2-784x+256}{81(1-x)^4}\mathrm{Li}_2\left(1-\tfrac{1}{x}\right)$$

$$+ \frac{304x^4+1716x^3-4644x^2+2768x-720}{81(1-x)^5}\ln x + \frac{-6175x^4+41608x^3-66723x^2+33106x-7000}{729(1-x)^4}$$

$$+ \left[\frac{648x^4-720x^3-232x^2-160x+32}{81(1-x)^5}\ln x + \frac{-352x^4+4912x^3-8280x^2+3304x-880}{243(1-x)^4}\right]L_t \qquad \text{(C.7)}$$

The functions $[X_k]_W^1$ have been first calculated in the following papers: $[A_7]_W^1$ and $[F_8]_W^1$ in [100, 159–162], $[B_9^{\bar{l}l}]_W^1$ and $[C_9^{\bar{l}l}]_W^1$ in [38, 39, 41, 42] and $[G_3]_W^1$, $[E_4]_W^1$ and $[D_9^{\bar{l}l}]_W^1$ in [82].

C.2   Charged Higgs Boson Contributions

The evaluation of Feynman diagrams contributing to $b \to s+$(light particles) Green functions within the MSSM (but also 2HDM of type II) mediated by "top quark – charged Higgs boson" loops and denoted by the index $i = H$ in (4.15) yields

$$[E_4]_H^0 = \cot^2\beta\left\{\frac{3y^2-2y}{6(y-1)^4}\ln y + \frac{7y^3-29y^2+16y}{36(y-1)^3}\right\}$$

$$[A_7]_H^0 = \frac{-3y^2+2y}{3(y-1)^3}\ln y + \frac{5y^2-3y}{6(y-1)^2} + \cot^2\beta\left\{\frac{-3y^3+2y^2}{6(y-1)^4}\ln y + \frac{8y^3+5y^2-7y}{36(y-1)^3}\right\}$$

$$[F_8]_H^0 = \frac{y}{(y-1)^3}\ln y + \frac{y^2-3y}{2(y-1)^2} + \cot^2\beta\left\{\frac{y^2}{2(y-1)^4}\ln y + \frac{y^3-5y^2-2y}{12(y-1)^3}\right\}$$

$$[B_9^{\bar{l}l}]_H^0 = [B_{10}^{\bar{l}l}]_H^0 = 0$$

$$[C_9^{\bar{l}l}]_H^0 = \frac{M_{H^+}^2}{8M_W^2} \cot^2\beta \left\{ \frac{-y^2}{(y-1)^2} \ln y + \frac{y^2}{y-1} \right\}$$

$$[D_9^{\bar{l}l}]_H^0 = \cot^2\beta \left\{ \frac{-3y^4+6y^2-4y}{18(y-1)^4} \ln y + \frac{47y^3-79y^2+38y}{108(y-1)^3} \right\} \qquad\qquad \text{(C.8)}$$

$$[G_3]_H^1 = \cot^2\beta \left\{ \frac{10y^4+30y^2-20y}{27(y-1)^4} \mathrm{Li}_2\left(1-\frac{1}{y}\right) + \frac{30y^3-66y^2-56y}{81(y-1)^4} \ln y \right.$$
$$\left. + \frac{6y^3-187y^2+213y}{81(y-1)^3} + \left[\frac{-30y^2+20y}{27(y-1)^4} \ln y + \frac{-35y^3+145y^2-80y}{81(y-1)^3} \right] L_t \right\}$$

$$[E_4]_H^1 = \cot^2\beta \left\{ \frac{515y^4-906y^3+99y^2+182y}{54(y-1)^4} \mathrm{Li}_2\left(1-\frac{1}{y}\right) \right.$$
$$+ \frac{1030y^4-2763y^3-15y^2+980y}{108(y-1)^5} \ln y + \frac{-29467y^4+68142y^3-6717y^2-18134y}{1944(y-1)^4}$$
$$\left. + \left[\frac{-375y^3-95y^2+182y}{54(y-1)^5} \ln y + \frac{133y^4-108y^3+4023y^2-2320y}{324(y-1)^4} \right] L_t \right\}$$

$$[A_7]_H^1 = \frac{-64y^3+224y^2-96y}{9(y-1)^3} \mathrm{Li}_2\left(1-\frac{1}{y}\right) + \frac{-28y^3+256y^2-132y}{9(y-1)^4} \ln y$$
$$+ \frac{16y^3-104y^2+56y}{3(y-1)^3} + \left[\frac{24y^3+112y^2-64y}{9(y-1)^4} \ln y + \frac{32y^3-188y^2+84y}{9(y-1)^3} \right] L_t$$
$$+ \cot^2\beta \left\{ \frac{-32y^4+148y^3-72y^2}{9(y-1)^4} \mathrm{Li}_2\left(1-\frac{1}{y}\right) + \frac{-126y^4+1614y^3-926y^2+14y}{81(y-1)^5} \ln y \right.$$
$$\left. + \frac{1202y^4-7569y^3+5436y^2-797y}{243(y-1)^4} + \left[\frac{12y^4+92y^3-56y^2}{9(y-1)^5} \ln y + \frac{28y^4-270y^3+36y^2+62y}{27(y-1)^4} \right] L_t \right\}$$

$$[F_8]_H^1 = \frac{-17y^3+25y^2-36y}{3(y-1)^3} \mathrm{Li}_2\left(1-\frac{1}{y}\right) + \frac{-34y^3+7y^2-165y}{6(y-1)^4} \ln y$$
$$+ \frac{29y^3-44y^2+143y}{4(y-1)^3} + \left[\frac{-34y^2-38y}{3(y-1)^4} \ln y + \frac{7y^3-16y^2+81y}{3(y-1)^3} \right] L_t$$
$$+ \cot^2\beta \left\{ \frac{-13y^4+17y^3-30y^2}{3(y-1)^4} \mathrm{Li}_2\left(1-\frac{1}{y}\right) + \frac{-468y^4+321y^3-2155y^2-2y}{108(y-1)^5} \ln y \right.$$
$$\left. + \frac{4451y^4-7650y^3+18153y^2-1130y}{648(y-1)^4} + \left[\frac{-17y^3-31y^2}{3(y-1)^5} \ln y + \frac{7y^4-18y^3+261y^2+38y}{18(y-1)^4} \right] L_t \right\}$$

$$[B_9^{\bar{l}l}]_H^1 = [B_{10}^{\bar{l}l}]_H^1 = 0$$

$$[C_9^{\bar{l}l}]_H^1 = \frac{M_{H^+}^2}{8M_W^2} \cot^2\beta \left\{ \frac{-8y^3+16y^2}{(y-1)^2} \mathrm{Li}_2\left(1-\frac{1}{y}\right) \right.$$
$$\left. + \frac{-24y^3+88y^2}{3(y-1)^3} \ln y + \frac{32y^3-96y^2}{3(y-1)^2} + \left[\frac{16y^2}{(y-1)^3} \ln y + \frac{8y^3-24y^2}{(y-1)^2} \right] L_t \right\}$$

$$[D_9^{\bar{l}l}]_H^1 = \cot^2\beta \left\{ \frac{380y^4-528y^3+72y^2+128y}{81(y-1)^4} \mathrm{Li}_2\left(1-\frac{1}{y}\right) \right.$$
$$+ \frac{596y^4-672y^3+64y^2+204y}{81(y-1)^5} \ln y + \frac{-6175y^4+9138y^3-3927y^2-764y}{729(y-1)^4}$$

$$+ \left[\frac{432y^4 - 456y^3 + 40y^2 + 128y}{81(y-1)^5} \ln y + \frac{-352y^4 - 972y^3 + 1944y^2 - 1052y}{243(y-1)^4} \right] L_t \right\} \tag{C.9}$$

The following functions $[X_k]^1_H$ have been calculated previously: $[A_7]^1_H$ and $[F_8]^1_H$ in [100, 161, 163] and $[B^{\bar{l}l}_{10}]^1_H$ and $[C^{\bar{l}l}_9]^1_H$ in [101]. The function $[D^{\bar{l}l}_9]^1_H$ has been calculated in [164] and confirmed in [165]. The results for the functions $[G_3]^1_H$ and $[E_4]^1_H$ are *new*. Note that $[B^{\bar{l}l}_9]^1_H$ and $[B^{\bar{l}l}_{10}]^1_H$ vanish due to the approximation of vanishing lepton masses.

C.3   Chargino-Squark Contributions

The evaluation of Feynman diagrams contributing to $b \to s +$ (light particles) Green functions within the MSSM mediated by "chargino – up squark" loops and denoted by the index $i = C$ in (4.15) yields[1]

$$[E_4]^0_C = \frac{\kappa M_W^2}{m_{\tilde{\chi}_i^+}^2} [X_i^{U_L \dagger}]_{2a} [X_i^{U_L}]_{a3} \, h_4^{(0)}(y_{ai})$$

$$[A_7]^0_C = \frac{\kappa M_W^2}{m_{\tilde{\chi}_i^+}^2} \left\{ [X_i^{U_L \dagger}]_{2a} [X_i^{U_L}]_{a3} \, h_1^{(0)}(y_{ai}) + \frac{m_{\tilde{\chi}_i^+}}{m_b} [X_i^{U_L \dagger}]_{2a} [X_i^{U_R}]_{a3} \, h_2^{(0)}(y_{ai}) \right\}$$

$$[F_8]^0_C = \frac{\kappa M_W^2}{m_{\tilde{\chi}_i^+}^2} \left\{ [X_i^{U_L \dagger}]_{2a} [X_i^{U_L}]_{a3} \, h_5^{(0)}(y_{ai}) + \frac{m_{\tilde{\chi}_i^+}}{m_b} [X_i^{U_L \dagger}]_{2a} [X_i^{U_R}]_{a3} \, h_6^{(0)}(y_{ai}) \right\}$$

$$[B^{\bar{l}l}_{9,10}]^0_C = \mp \frac{\kappa M_W^2 s_W^2}{4e^2 m_{\tilde{\chi}_i^+}^2} [X_j^{U_L \dagger}]_{2a} [X_i^{U_L}]_{a3}$$

$$\times \left\{ [X_i^{N_L \dagger}]_{lK} [X_j^{N_L}]_{Kl} f_5^{(0)}(x_{ji}, y_{ai}, v_{Ki}) \mp 2 [X_i^{N_R \dagger}]_{lK} [X_j^{N_R}]_{Kl} \sqrt{x_{ji}} f_6^{(0)}(x_{ji}, y_{ai}, v_{Ki}) \right\}$$

$$[C^{\bar{l}l}_9]^0_C = -\frac{\kappa}{8} [X_j^{U_L \dagger}]_{2b} [X_i^{U_L}]_{a3}$$

$$\times \left\{ (\Gamma^{U_L} \Gamma^{U_L \dagger})_{ba} f_4^{(0)}(y_{ai}, y_{bi}) \delta_{ij} \right.$$

$$\left. + \left[2 U_{i1}^* U_{j1} \sqrt{x_{ji}} f_3^{(0)}(x_{ji}, y_{ai}) - V_{i1} V_{j1}^* f_4^{(0)}(x_{ji}, y_{ai}) \right] \delta_{ab} \right\}$$

$$[D^{\bar{l}l}_9]^0_C = \frac{\kappa M_W^2}{m_{\tilde{\chi}_i^+}^2} [X_i^{U_L \dagger}]_{2a} [X_i^{U_L}]_{a3} \, h_3^{(0)}(y_{ai}) \tag{C.10}$$

$$[G_3]^1_C = \frac{\kappa M_W^2}{m_{\tilde{\chi}_i^+}^2} [X_i^{U_L \dagger}]_{2a} [X_i^{U_L}]_{a3} \, h_7^{(1)}(y_{ai}, L_{\tilde{u}_a})$$

$$[E_4]^1_C = \frac{\kappa M_W^2}{m_{\tilde{\chi}_i^+}^2} [X_i^{U_L \dagger}]_{2a} [X_i^{U_L}]_{a3} \, h_4^{(1)}(y_{ai}, L_{\tilde{u}_a})$$

---

[1] Summation over all indices other than l is of course understood. Also note that m_b is the b quark mass and hence the subscript is no summation index.

$$[A_7]_C^1 = \frac{\kappa M_W^2}{m_{\tilde\chi_i^+}^2} \left\{ [X_i^{U_L \dagger}]_{2a}[X_i^{U_L}]_{a3} \, h_1^{(1)}(y_{ai}, L_{\tilde u_a}) + \frac{m_{\tilde\chi_i^+}}{m_b}[X_i^{U_L \dagger}]_{2a}[X_i^{U_R}]_{a3} \, h_2^{(1)}(y_{ai}, L_{\tilde u_a}) \right\}$$

$$[F_8]_C^1 = \frac{\kappa M_W^2}{m_{\tilde\chi_i^+}^2} \left\{ [X_i^{U_L \dagger}]_{2a}[X_i^{U_L}]_{a3} \, h_5^{(1)}(y_{ai}, L_{\tilde u_a}) + \frac{m_{\tilde\chi_i^+}}{m_b}[X_i^{U_L \dagger}]_{2a}[X_i^{U_R}]_{a3} \, h_6^{(1)}(y_{ai}, L_{\tilde u_a}) \right\}$$

$$[B_{9,10}^{\bar l l}]_C^1 = \mp \frac{\kappa M_W^2 s_W^2}{4e^2 m_{\tilde\chi_i^+}^2}[X_j^{U_L \dagger}]_{2a}[X_i^{U_L}]_{a3}$$

$$\times \left\{ [X_i^{N_L \dagger}]_{lK}[X_j^{N_L}]_{Kl}\tilde f_8^{(1)}(x_{ji}, y_{ai}, v_{Ki}, L_{\tilde u_a}) \right.$$

$$\left. \mp 2[X_i^{N_R \dagger}]_{lK}[X_j^{N_R}]_{Kl}\sqrt{x_{ji}}\tilde f_9^{(1)}(x_{ji}, y_{ai}, v_{Ki}, L_{\tilde u_a}) \right\}$$

$$[C_9^{\bar l l}]_C^1 = -\frac{\kappa}{8}[X_j^{U_L \dagger}]_{2b}[X_i^{U_L}]_{a3}$$

$$\times \left\{ (\Gamma^{U_L}\Gamma^{U_L \dagger})_{ba}\tilde f_5^{(1)}(y_{ai}, y_{bi}, L_{\tilde u_a})\delta_{ij} \right.$$

$$\left. + \left[2U_{i1}^* U_{j1}\sqrt{x_{ji}}\tilde f_3^{(1)}(x_{ji}, y_{ai}, L_{\tilde u_a}) - V_{i1}V_{j1}^*\tilde f_4^{(1)}(x_{ji}, y_{ai}, L_{\tilde u_a}) \right] \delta_{ab} \right\}$$

$$[D_9^{\bar l l}]_C^1 = \frac{\kappa M_W^2}{m_{\tilde\chi_i^+}^2}[X_i^{U_L \dagger}]_{2a}[X_i^{U_L}]_{a3} \, h_3^{(1)}(y_{ai}, L_{\tilde u_a}) \tag{C.11}$$

All auxiliary functions introduced here can be found in app. C.5. The following functions $[X_k]_C^1$ have been calculated previously: $[A_7]_C^1$ and $[F_8]_C^1$ in [99, 100] and $[B_{10}^{\bar l l}]_C^1$ and $[C_9^{\bar l l}]_C^1$ in [101]. The results for the functions $[G_3]_C^1$, $[E_4]_C^1$, $[B_9^{\bar l l}]_C^1$ and $[D_9^{\bar l l}]_C^1$ are *new*.

C.4 Quartic Squark-Vertex Contributions

The evaluation of Feynman diagrams contributing to $b \rightarrow s+$(light particles) Green functions within the MSSM mediated by "chargino – up squark" loops containing the quartic squark vertex[2] instead of gluon corrections and denoted by the index $i = Q$ in (4.15) yields

$$[G_3]_Q^1 = 0$$

$$[E_4]_Q^1 = \frac{\kappa M_W^2}{m_{\tilde\chi_i^+}^2} \, P_{ab}^U \, y_{bi} \, P_{bc}^U \, (1 + L_{\tilde u_b}) \, [X_i^{U_L \dagger}]_{2a}[X_i^{U_L}]_{c3} \, q_6^{(1)}(y_{ai}, y_{ci})$$

$$[A_7]_Q^1 = \frac{\kappa M_W^2}{m_{\tilde\chi_i^+}^2} \, P_{ab}^U \, y_{bi} \, P_{bc}^U \, (1 + L_{\tilde u_b})$$

---

[2]Strictly speaking these matching contributions originate from the part of the quartic squark vertex proportional to the strong coupling constant g_s.

$$\times \left\{ [X_i^{U_L\,\dagger}]_{2a}[X_i^{U_L}]_{c3}\,\tilde{q}_1^{(1)}(y_{ai},y_{ci}) + \frac{m_{\tilde{\chi}_i^+}}{m_b}[X_i^{U_L\,\dagger}]_{2a}[X_i^{U_R}]_{c3}\,\tilde{q}_3^{(1)}(y_{ai},y_{ci}) \right\}$$

$$[F_8]_Q^1 = \frac{\kappa M_W^2}{m_{\tilde{\chi}_i^+}^2}\,P_{ab}^U y_{bi}\,P_{bc}^U\,(1+L_{\tilde{u}_b})$$

$$\times \left\{ [X_i^{U_L\,\dagger}]_{2a}[X_i^{U_L}]_{c3}\,q_2^{(1)}(y_{ai},y_{ci}) + \frac{m_{\tilde{\chi}_i^+}}{m_b}[X_i^{U_L\,\dagger}]_{2a}[X_i^{U_R}]_{c3}\,q_4^{(1)}(y_{ai},y_{ci}) \right\}$$

$$[B_{9,10}^{\bar{l}l}]_Q^1 = \pm\frac{\kappa M_W^2 s_W^2}{3e^2 m_{\tilde{\chi}_i^+}^2}\,P_{ab}^U\,y_{bi}\,P_{bc}^U\,(1+L_{\tilde{u}_b})\,[X_j^{U_L\,\dagger}]_{2a}[X_i^{U_L}]_{c3}$$

$$\times \left\{ [X_i^{N_L\,\dagger}]_{lK}[X_j^{N_L}]_{Kl}f_9^{(0)}(x_{ji},y_{ai},y_{ci},v_{Ki}) \right.$$

$$\left. \mp 2[X_i^{N_R\,\dagger}]_{lK}[X_j^{N_R}]_{Kl}\sqrt{x_{ji}}f_{10}^{(0)}(x_{ji},y_{ai},y_{ci},v_{Ki}) \right\}$$

$$[C_9^{\bar{l}l}]_Q^1 = \frac{\kappa}{6}P_{ab}^U\,y_{bi}\,P_{bc}^U\,(1+L_{\tilde{u}_b})\,[X_j^{U_L\,\dagger}]_{2d}[X_i^{U_L}]_{e3}$$

$$\times \left\{ (\Gamma^{U_L}\Gamma^{U_L\,\dagger})_{gf}\left[f_5^{(0)}(y_{ei},y_{fi},y_{gi})\delta_{af}\delta_{ce}\delta_{dg} + f_5^{(0)}(y_{di},y_{ei},y_{gi})\delta_{ad}\delta_{cg}\delta_{ef} \right]\delta_{ij} \right.$$

$$\left. + \left[2U_{i1}^*U_{j1}\sqrt{x_{ji}}f_6^{(0)}(x_{ji},y_{ai},y_{ci}) - V_{i1}V_{j1}^*f_5^{(0)}(x_{ji},y_{ai},y_{ci}) \right]\delta_{ad}\delta_{ce}\delta_{f1}\delta_{g1} \right\}$$

$$[D_9^{\bar{l}l}]_Q^1 = \frac{\kappa M_W^2}{m_{\tilde{\chi}_i^+}^2}\,P_{ab}^U\,y_{bi}\,P_{bc}^U\,(1+L_{\tilde{u}_b})\,[X_i^{U_L\,\dagger}]_{2a}[X_i^{U_L}]_{c3}\,q_5^{(1)}(y_{ai},y_{ci}) \tag{C.12}$$

All auxiliary functions introduced here can be found in app. C.5. The following functions $[X_k]_Q^1$ have been calculated previously: $[A_7]_Q^1$ and $[F_8]_Q^1$ in [100] and $[B_{10}^{\bar{l}l}]_Q^1$ and $[C_9^{\bar{l}l}]_Q^1$ in [101]. The result for the functions $[G_3]_Q^1$, $[E_4]_Q^1$, $[B_9^{\bar{l}l}]_C^1$ and $[D_9^{\bar{l}l}]_Q^1$ are *new*.

C.5   Auxiliary Functions

Here we present explicit formulae for the loop functions $h_i^{(0)}$, $f_i^{(0)}$, $h_i^{(1)}$, $f_i^{(1)}$, $\tilde{f}_i^{(1)}$, $q_i^{(1)}$ and $\tilde{q}_i^{(1)}$ introduced in app. C.3 and C.4. They read

$$h_1^{(0)}(x) = \frac{3x^2-2x}{3(x-1)^4}\ln x + \frac{-8x^2-5x+7}{18(x-1)^3}$$

$$h_2^{(0)}(x) = \frac{-6x^2+4x}{3(x-1)^3}\ln x + \frac{7x-5}{3(x-1)^2}$$

$$h_3^{(0)}(x) = \frac{-6x^3+9x^2-2}{9(x-1)^4}\ln x + \frac{52x^2-101x+43}{54(x-1)^3}$$

$$h_4^{(0)}(x) = \frac{-1}{3(x-1)^4}\ln x + \frac{2x^2-7x+11}{18(x-1)^3}$$

$$h_5^{(0)}(x) = \frac{-x}{(x-1)^4}\ln x + \frac{-x^2+5x+2}{6(x-1)^3}$$

$$h_6^{(0)}(x) = \frac{2x}{(x-1)^3} \ln x + \frac{-x-1}{(x-1)^2} \tag{C.13}$$

$$f_3^{(0)}(x,y) = \frac{x \ln x}{(x-1)(x-y)} + \frac{y \ln y}{(y-1)(y-x)}$$

$$f_4^{(0)}(x,y) = \frac{x^2 \ln x}{(x-1)(x-y)} + \frac{y^2 \ln y}{(y-1)(y-x)} \tag{C.14}$$

$$f_5^{(0)}(x,y,z) = \frac{x^2 \ln x}{(x-1)(x-y)(x-z)} + (x \leftrightarrow y) + (x \leftrightarrow z)$$

$$f_6^{(0)}(x,y,z) = \frac{x \ln x}{(x-1)(x-y)(x-z)} + (x \leftrightarrow y) + (x \leftrightarrow z) \tag{C.15}$$

$$f_9^{(0)}(x,y,z,w) = \frac{x^2 \ln x}{(x-1)(x-y)(x-z)(x-w)} + (x \leftrightarrow y) + (x \leftrightarrow z) + (x \leftrightarrow w)$$

$$f_{10}^{(0)}(x,y,z,w) = \frac{x \ln x}{(x-1)(x-y)(x-z)(x-w)} + (x \leftrightarrow y) + (x \leftrightarrow z) + (x \leftrightarrow w) \tag{C.16}$$

$$h_1^{(1)}(x,y) = \frac{-48x^3 - 104x^2 + 64x}{9(x-1)^4} \mathrm{Li}_2\left(1 - \frac{1}{x}\right) + \frac{-378x^3 - 1566x^2 + 850x + 86}{81(x-1)^5} \ln x$$
$$+ \frac{2060x^3 + 3798x^2 - 2664x - 170}{243(x-1)^4} + \left[\frac{12x^3 - 124x^2 + 64x}{9(x-1)^5} \ln x + \frac{-56x^3 + 258x^2 + 24x - 82}{27(x-1)^4}\right] y$$

$$h_2^{(1)}(x,y) = \frac{224x^2 - 96x}{9(x-1)^3} \mathrm{Li}_2\left(1 - \frac{1}{x}\right) + \frac{-24x^3 + 352x^2 - 128x - 32}{9(x-1)^4} \ln x$$
$$+ \frac{-340x^2 + 132x + 40}{9(x-1)^3} + \left[\frac{-24x^3 + 176x^2 - 80x}{9(x-1)^4} \ln x + \frac{-28x^2 - 108x + 64}{9(x-1)^3}\right] y$$

$$h_3^{(1)}(x,y) = \frac{32x^3 + 120x^2 - 384x + 128}{81(x-1)^4} \mathrm{Li}_2\left(1 - \frac{1}{x}\right)$$
$$+ \frac{-108x^4 + 1058x^3 - 898x^2 - 1098x + 710}{81(x-1)^5} \ln x + \frac{-304x^3 - 13686x^2 + 29076x - 12062}{729(x-1)^4}$$
$$+ \left[\frac{540x^3 - 972x^2 + 232x + 56}{81(x-1)^5} \ln x + \frac{-664x^3 + 54x^2 + 1944x - 902}{243(x-1)^4}\right] y$$

$$h_4^{(1)}(x,y) = \frac{-562x^3 + 1101x^2 - 420x + 101}{54(x-1)^4} \mathrm{Li}_2\left(1 - \frac{1}{x}\right) + \frac{-562x^3 + 1604x^2 - 799x + 429}{54(x-1)^5} \ln x$$
$$+ \frac{17470x^3 - 47217x^2 + 31098x - 13447}{972(x-1)^4} + \left[\frac{89x + 55}{27(x-1)^5} \ln x + \frac{38x^3 - 135x^2 + 54x - 821}{162(x-1)^4}\right] y$$

$$h_5^{(1)}(x,y) = \frac{9x^3 + 46x^2 + 49x}{6(x-1)^4} \mathrm{Li}_2\left(1 - \frac{1}{x}\right) + \frac{81x^3 + 594x^2 + 1270x + 71}{54(x-1)^5} \ln x$$
$$+ \frac{-923x^3 - 3042x^2 - 6921x - 1210}{324(x-1)^4} + \left[\frac{10x^2 + 38x}{3(x-1)^5} \ln x + \frac{-7x^3 + 30x^2 - 141x - 26}{9(x-1)^4}\right] y$$

$$h_6^{(1)}(x,y) = \frac{-32x^2 - 24x}{3(x-1)^3} \mathrm{Li}_2\left(1 - \frac{1}{x}\right) + \frac{-52x^2 - 109x - 7}{3(x-1)^4} \ln x$$
$$+ \frac{95x^2 + 180x + 61}{6(x-1)^3} + \left[\frac{-20x^2 - 52x}{3(x-1)^4} \ln x + \frac{-2x^2 + 60x + 14}{3(x-1)^3}\right] y$$

$$h_7^{(1)}(x,y) = \frac{-20x^3+60x^2-60x-20}{27(x-1)^4}\mathrm{Li}_2\left(1-\frac{1}{x}\right) + \frac{-60x^2+240x+4}{81(x-1)^4}\ln x$$

$$+ \frac{132x^2-382x+186}{81(x-1)^3} + \left[\frac{20}{27(x-1)^4}\ln x + \frac{-20x^2+70x-110}{81(x-1)^3}\right]y \tag{C.17}$$

$$f_3^{(1)}(x,y) = -\frac{28y}{3(x-y)(y-1)} + \frac{2x(11x+3y)}{3(x-1)(x-y)^2}\ln x + \frac{2y[x(25-11y)-y(11+3y)]}{3(x-y)^2(y-1)^2}\ln y$$

$$+ \frac{4(1+y)}{(x-1)(y-1)}\mathrm{Li}_2\left(1-\frac{1}{y}\right) + \frac{4(x+y)}{(x-1)(x-y)}\mathrm{Li}_2\left(1-\frac{x}{y}\right)$$

$$f_4^{(1)}(x,y) = \frac{59x(1-y)-y(59-3y)}{6(y-1)(x-y)} + \frac{4x(7x^2-3xy+3y^2)}{3(x-1)(x-y)^2}\ln x + \frac{4y^2[x(18-11y)-y(11-4y)]}{3(x-y)^2(y-1)^2}\ln y$$

$$+ 2\ln^2 y + \frac{4(1+y^2)}{(x-1)(y-1)}\mathrm{Li}_2\left(1-\frac{1}{y}\right) + \frac{4(x^2+y^2)}{(x-1)(x-y)}\mathrm{Li}_2\left(1-\frac{x}{y}\right)$$

$$f_5^{(1)}(x,y) = -\frac{83+27x(y-1)-27y}{6(x-1)(y-1)} + 4\ln x\left(1+x\frac{\partial}{\partial x}+y\frac{\partial}{\partial y}\right)f_4^{(0)}(x,y)$$

$$- \left\{ \frac{4x[1+x(12+y)-y-6x^2]}{3(x-1)^2(x-y)}\ln x - \frac{2[1+6x^2(y-1)-3x^3(y-1)+x(3y-4)]}{3(x-1)^2(x-y)(y-1)}\ln^2 x \right.$$

$$+ \frac{4y[3x^2(y-1)+xy(3-2y)+y^2(y-2)]}{3(x-1)(x-y)^2(y-1)}\mathrm{Li}_2\left(1-\frac{x}{y}\right)$$

$$\left. + \frac{4[1-3x-x^2(3-6y)-x^3]}{3(x-1)(x-y)(y-1)}\mathrm{Li}_2\left(1-\frac{1}{x}\right) + (x \leftrightarrow y) \right\} \tag{C.18}$$

$$f_8^{(1)}(x,y,z) = -\frac{28y^2}{3(x-y)(y-1)(y-z)} + \left[\frac{4x(7x^2-3xy+3y^2)}{3(x-1)(x-y)^2(x-z)}\ln x + (x \leftrightarrow z)\right]$$

$$- \frac{4y^2x[4y^2+18z-11y(1+z)]+y[3y^2-11z+4y(1+z)]}{3(x-y)^2(y-1)^2(y-z)^2}\ln y$$

$$- \frac{4(1+y^2)}{(x-1)(y-1)(z-1)}\mathrm{Li}_2\left(1-\frac{1}{y}\right) + \left[\frac{4(x^2+y^2)}{(x-1)(x-y)(x-z)}\mathrm{Li}_2\left(1-\frac{x}{y}\right) + (x \leftrightarrow z)\right]$$

$$f_9^{(1)}(x,y,z) = -\frac{28y}{3(x-y)(y-1)(y-z)} + \left[\frac{2x(11x+3y)}{3(x-1)(x-y)^2(x-z)}\ln x + (x \leftrightarrow z)\right]$$

$$+ \frac{2yx[3y^2-25z+11y(1+z)]+y[11z-17y^2+3y(1+z)]}{3(x-y)^2(y-1)^2(y-z)^2}\ln y$$

$$- \frac{4(1+y)}{(x-1)(y-1)(z-1)}\mathrm{Li}_2\left(1-\frac{1}{y}\right) + \left[\frac{4(x+y)}{(x-1)(x-y)(x-z)}\mathrm{Li}_2\left(1-\frac{x}{y}\right) + (x \leftrightarrow z)\right] \tag{C.19}$$

$$\tilde{f}_3^{(1)}(x,y,z) = f_3^{(1)}(x,y) + 4z\left(1+y\frac{\partial}{\partial y}\right)f_3^{(0)}(x,y)$$

$$\tilde{f}_4^{(1)}(x,y,z) = f_4^{(1)}(x,y) + 4z\left(1+y\frac{\partial}{\partial y}\right)f_4^{(0)}(x,y)$$

$$\tilde{f}_5^{(1)}(x,y,z) = f_5^{(1)}(x,y) + 4z\left(1+x\frac{\partial}{\partial x}+y\frac{\partial}{\partial y}\right)f_4^{(0)}(x,y) \tag{C.20}$$

$$\tilde{f}_8^{(1)}(x,y,z,w) = f_8^{(1)}(x,y,z) + 4\,w\left(1 + y\frac{\partial}{\partial y}\right) f_5^{(0)}(x,y,z)$$

$$\tilde{f}_9^{(1)}(x,y,z,w) = f_9^{(1)}(x,y,z) + 4\,w\left(1 + y\frac{\partial}{\partial y}\right) f_6^{(0)}(x,y,z) \tag{C.21}$$

$$q_1^{(1)}(x,y) = \frac{4}{3(x-y)}\left[\frac{x^2\ln x}{(x-1)^4} - \frac{y^2\ln y}{(y-1)^4}\right] + \frac{4x^2y^2+10xy^2-2y^2+10x^2y-44xy+10y-2x^2+10x+4}{9(x-1)^3(y-1)^3}$$

$$q_2^{(1)}(x,y) = \frac{4}{3(x-y)}\left[\frac{x\ln x}{(x-1)^4} - \frac{y\ln y}{(y-1)^4}\right] + \frac{-2x^2y^2+10xy^2+4y^2+10x^2y-20xy-14y+4x^2-14x+22}{9(x-1)^3(y-1)^3}$$

$$q_3^{(1)}(x,y) = \frac{8}{3(x-y)}\left[\frac{-x^2\ln x}{(x-1)^3} + \frac{y^2\ln y}{(y-1)^3}\right] + \frac{-12xy+4y+4x+4}{3(x-1)^2(y-1)^2}$$

$$q_4^{(1)}(x,y) = \frac{8}{3(x-y)}\left[\frac{-x\ln x}{(x-1)^3} + \frac{y\ln y}{(y-1)^3}\right] + \frac{-4xy-4y-4x+12}{3(x-1)^2(y-1)^2}$$

$$q_5^{(1)}(x,y) = \frac{4}{27(x-y)}\left[\frac{(6x^3-9x^2+2)\ln x}{(x-1)^4} - \frac{(6y^3-9y^2+2)\ln y}{(y-1)^4}\right]$$
$$+ \frac{104x^2y^2-202xy^2+86y^2-202x^2y+380xy-154y+86x^2-154x+56}{81(x-1)^3(y-1)^3}$$

$$q_6^{(1)}(x,y) = \frac{4}{9(x-y)}\left[\frac{\ln x}{(x-1)^4} - \frac{\ln y}{(y-1)^4}\right] + \frac{4x^2y^2-14xy^2+22y^2-14x^2y+52xy-62y+22x^2-62x+52}{27(x-1)^3(y-1)^3} \tag{C.22}$$

$$\tilde{q}_1^{(1)}(x,y) = -q_1^{(1)}(x,y) + \frac{2}{3}q_2^{(1)}(x,y)$$

$$\tilde{q}_3^{(1)}(x,y) = -q_3^{(1)}(x,y) + \frac{2}{3}q_4^{(1)}(x,y) \tag{C.23}$$

Bibliography

[1] S. L. Glashow, Nucl. Phys. **22** (1961) 579.

[2] P. W. Higgs, Phys. Lett. **12** (1964) 132.

[3] F. Englert and R. Brout, Phys. Rev. Lett. **13** (1964) 321.

[4] P. W. Higgs, Phys. Rev. Lett. **13** (1964) 508.

[5] P. W. Higgs, Phys. Rev. **145** (1966) 1156.

[6] T. W. B. Kibble, Phys. Rev. **155** (1967) 1554.

[7] S. Weinberg, Phys. Rev. Lett. **19** (1967) 1264.

[8] A. Salam, *Weak and Electromagnetic Interactions*, in N. Svartholm, *Elementary Particle Theory*, Proceedings of the Nobel Symposium held 1968 at Lerum, Stockholm 1968, 367.

[9] G. 't Hooft, Nucl. Phys. **B35** (1971) 167.

[10] G. 't Hooft and M. J. G. Veltman, Nucl. Phys. **B44** (1972) 189.

[11] G. 't Hooft and M. J. G. Veltman, Nucl. Phys. **B50** (1972) 318.

[12] D. J. Gross and F. Wilczek, Phys. Rev. Lett. **30** (1973) 1343.

[13] D. J. Gross and F. Wilczek, Phys. Rev. **D8** (1973) 3633.

[14] D. J. Gross and F. Wilczek, Phys. Rev. **D9** (1974) 980.

[15] H. D. Politzer, Phys. Rev. Lett. **30** (1973) 1346.

[16] S. Weinberg, Phys. Rev. Lett. **31** (1973) 494.

[17] H. Fritzsch, M. Gell-Mann and H. Leutwyler, Phys. Lett. **B47** (1973) 365.

[18] H. Georgi, H. R. Quinn and S. Weinberg, Phys. Rev. Lett. **33** (1974) 451.

[19] H. Georgi and S. L. Glashow, Phys. Rev. Lett. **32** (1974) 438.

[20] H. Fritzsch and P. Minkowski, Ann. Phys. **93** (1975) 193.

[21] H. Georgi, *The state of the Art – Gauge Theories*, in C. E. Carlson, *Particles and Fields*, AIP Conf. Proc. 23, New York 1975, 575.

[22] T. Yanagida, *Horizontal Gauge Symmetry and Masses of Neutrinos*, in O. Sawada and A. Sugamoto, *Proceedings of the Workshop on the Baryon Number of the Universe and Unified Theories*, Tsukuba 1979, 109.

[23] M. Gell-Mann, P. Ramond and R. Slansky, *Complex Spinors and Unified Theories*, Print-80-0576 (CERN). Published in P. van Nieuwenhuizen and D. Z. Freedman, *Supergravity*, Amsterdam 1979, 341.

[24] Y. Fukuda *et al.* [Super-Kamiokande Collaboration], Phys. Rev. Lett. **81** (1998) 1562.

[25] Q. R. Ahmad *et al.* [SNO Collaboration], Phys. Rev. Lett. **89** (2002) 011301.

[26] U. Amaldi, W. de Boer and H. Fürstenau, Phys. Lett. **B260** (1991) 447.

[27] M. B. Einhorn, *The Revival of Technicolor Models*, in G. L. Kane, *Perspectives on Higgs Physics*, Singapore 1993, 421.

[28] I. Antoniadis, Phys. Lett. **B246** (1990) 377.

[29] N. Arkani-Hamed, S. Dimopoulos and G. R. Dvali, Phys. Lett. **B429** (1998) 263.

[30] N. Arkani-Hamed, A. G. Cohen and H. Georgi, Phys. Lett. **B513** (2001) 232.

[31] H. P. Nilles, Phys. Rept. **110** (1984) 1.

[32] H. E. Haber and G. L. Kane, Phys. Rept. **117** (1985) 75.

[33] M. F. Sohnius, Phys. Rept. **128** (1985) 39.

[34] P. Langacker and N. Polonsky, Phys. Rev. **D47** (1993) 4028.

[35] P. Langacker and N. Polonsky, Phys. Rev. **D52** (1995) 3081.

[36] N. Cabibbo, Phys. Rev. Lett. **10** (1963) 531.

[37] M. Kobayashi and T. Maskawa, Prog. Theor. Phys. **49** (1973) 652.

[38] G. Buchalla and A. J. Buras, Nucl. Phys. **B398** (1993) 285.

[39] G. Buchalla and A. J. Buras, Nucl. Phys. **B400** (1993) 225.

[40] G. Buchalla and A. J. Buras, Nucl. Phys. **B412** (1994) 106.

[41] G. Buchalla and A. J. Buras, Nucl. Phys. **B548** (1999) 309.

[42] M. Misiak and J. Urban, Phys. Lett. **B451** (1999) 161.

[43] A. J. Buras, F. Schwab and S. Uhlig, hep-ph/0405132.

[44] A. J. Buras, A. Romanino and L. Silvestrini, Nucl. Phys. **B520** (1998) 3.

[45] G. Isidori, eConf **C0304052**, WG304 (2003), hep-ph/0307014.

[46] G. D'Ambrosio and G. Isidori, Phys. Lett. **B530** (2002) 108.

[47] S. H. Kettell, L. G. Landsberg and H. H. Nguyen, hep-ph/0212321.

[48] A. J. Buras, R. Fleischer, S. Recksiegel and F. Schwab, Phys. Rev. Lett. **92** (2004) 101804.

[49] A. J. Buras, R. Fleischer, S. Recksiegel and F. Schwab, hep-ph/0402112.

[50] S. Adler *et al.* [E787 Collaboration], Phys. Rev. Lett. **79** (1997) 2204.

[51] S. Adler *et al.* [E787 Collaboration], Phys. Rev. Lett. **84** (2000) 3768.

[52] S. Adler *et al.* [E787 Collaboration], Phys. Rev. Lett. **88** (2002) 041803.

[53] S. Adler *et al.* [E787 Collaboration], hep-ex/0403034.

[54] V. V. Anisimovsky *et al.* [E949 Collaboration], Phys. Rev. Lett. **93** (2004) 031801.

[55] http://www.fnal.gov./projects/ckm/documentation/public/proposal/proposal.html.

[56] http://na48.web.cern.ch/NA48/NA48-3/index.html.

[57] http://www-ps.kek.jp/jhf-np/LOIlist/LOIlist.html.

[58] A. Alavi-Harati *et al.* [E799-II/KTeV Collaboration], Phys. Rev. **D61** (2000) 072006.

[59] http://www-ps.kek.jp/e391.

[60] L. Littenberg, hep-ex/0212005.

[61] D. Bryman, hep-ex/0206072.

[62] Y. Grossman and Y. Nir, Phys. Lett. **B398** (1997) 163.

[63] L. J. Hall, V. A. Kostelecky and S. Raby, Nucl. Phys.+**B267** (1986) 415.

[64] G. Colangelo and G. Isidori, JHEP **9809** (1998) 009.

[65] A. J. Buras, G. Colangelo, G. Isidori, A. Romanino and L. Silvestrini, Nucl. Phys. **B566** (2000) 3.

[66] O. Brein, PITHA-04-12, hep-ph/0407340.

[67] G. P. Lepage, J. Comput. Phys. **27** (1978) 192.

[68] G. P. Lepage, CLNS-80/447.

[69] Z. Ligeti and M. B. Wise, Phys. Rev. **D53** (1996) 4937.

[70] J. Kaneko *et al.* [Belle Collaboration], Phys. Rev. Lett. **90** (2003) 021801.

[71] J. Kaneko *et al.* [Belle Collaboration], hep-ex/0408119.

[72] B. Aubert *et al.* [BaBar Collaboration], hep-ex/0308016.

[73] B. Aubert *et al.* [BaBar Collaboration], Phys. Rev. Lett. **93** (2004) 081802.

[74] G. Buchalla, G. Isidori and S. J. Rey, Nucl. Phys. **B511** (1998) 594.

[75] B. Grinstein, M. J. Savage and M. B. Wise, Nucl. Phys. **B319** (1989) 271.

[76] R. Grigjanis, P. J. O'Donnell, M. Sutherland and H. Navelet,
Phys. Lett. **B223** (1989) 239.

[77] G. Cella, G. Ricciardi and A. Vicere, Phys. Lett. **B258** (1991) 212.

[78] M. Misiak, Nucl. Phys. **B393** (1993) 23; Erratum Nucl. Phys. **B439** (1995) 461.

[79] A. J. Buras and M. Münz, Phys. Rev. **D52** (1995) 186.

[80] A. J. Buras, A. Czarnecki, M. Misiak and J. Urban, Nucl. Phys. **B631** (2002) 219.

[81] H. M. Asatrian, H. H. Asatryan and A. Hovhannisyan, hep-ph/0401038.

[82] C. Bobeth, M. Misiak and J. Urban, Nucl. Phys. **B574** (2000) 291.

[83] K. G. Chetyrkin, M. Misiak and M. Münz, Phys. Lett. **B400** (1997) 206;
Erratum-ibid. **B425** (1998) 414.

[84] P. Gambino, M. Gorbahn and U. Haisch, Nucl. Phys. **B673** (2003) 238.

[85] M. Gorbahn and U. Haisch, in preparation.

[86] C. Bobeth, P. Gambino, M. Gorbahn and U. Haisch, JHEP **0404** (2004) 071.

[87] H. H. Asatrian, H. M. Asatrian, C. Greub and M. Walker, Phys. Rev. **D65** (2002) 074004.

[88] H. H. Asatrian, H. M. Asatrian, C. Greub and M. Walker, Phys. Lett. **B507** (2001) 162.

[89] H. H. Asatrian, H. M. Asatrian, C. Greub and M. Walker, Phys. Rev. **D66** (2002) 034009.

[90] H. M. Asatrian, K. Bieri, C. Greub and M. Walker, Phys. Rev. **D69** (2004) 074007.

[91] D. Seidel, hep-ph/0403185.

[92] A. Ghinculov, T. Hurth, G. Isidori and Y. P. Yao, Nucl. Phys. **B685** (2004) 351.

[93] A. Ali, E. Lunghi, C. Greub and G. Hiller, Phys. Rev. **D66** (2002) 034002.

[94] G. Burdman, Phys. Rev. **D52** (1995) 6400.

[95] G. Burdman, Phys. Rev. **D57** (1998) 4254.

[96] A. Ghinculov, T. Hurth, G. Isidori and Y.-P. Yao, Nucl. Phys. **B648** (2003) 254.

[97] H. M. Asatrian, K. Bieri, C. Greub and A. Hovhannisyan,
Phys. Rev. **D66** (2002) 094013.

[98] H. M. Asatrian, H. H. Asatryan, A. Hovhannisyan and V. Poghosyan,
Mod. Phys. Lett. **A19** (2004) 603.

[99] M. Ciuchini, G. Degrassi, P. Gambino and G. F. Giudice, Nucl. Phys. **B534** (1998) 3.

[100] C. Bobeth, M. Misiak and J. Urban, Nucl. Phys. **B567** (2000) 153.

[101] C. Bobeth, A. J. Buras, F. Krüger and J. Urban, Nucl. Phys. **B630** (2002) 87.

[102] T. Muta, *Foundations of Quantum Chromodynamics*,
World Scientific Publishing Co., 1987.

[103] J. Collins, *Renormalization*, Cambridge University Press, 1998.

[104] S. Pokorski, *Gauge Field Theories*, Cambridge University Press, 2000.

[105] M. Böhm, A. Denner and H. Joos, *Gauge Theories of the Strong and Electroweak Interactions*, B. G. Teubner Stuttgart, 2001.

[106] L. D. Faddeev and V. N. Popov, Phys. Lett. **B25** (1967) 29.

[107] R. P. Feynman, Acta Phys. Pol. **24** (1963) 697.

[108] J. C. Ward, Phys. Rev. **78** (1950) 1824.

[109] Y. Takahashi, Nuovo Cimento **6** (1957) 370.

[110] C. Becchi, A. Rouet and R. Stora, Phys. Lett. **B52** (1974) 344.

[111] C. Becchi, A. Rouet and R. Stora, Commun. Math. Phys. **42** (1975) 127.

[112] I. V. Tyutin, LEBEDEV-75-39.

[113] N. Nakanishi, Prog. Theor. Phys. **35** (1966) 1111.

[114] B. Lautrup, Mat. Fys. Medd. Dan. Vid. Selsk. **35** (1967) No. 11.

[115] J. C. Taylor, Nucl. Phys. **B33** (1971) 436.

[116] A. A. Slavnov, Theor. and Math. Phys. **10** (1972) 99.

[117] W. A. Bardeen, A. J. Buras, D. W. Duke and T. Muta, Phys. Rev. **D18** (1978) 3998.

[118] A. J. Buras, hep-ph/9806471 ("Les Houches Lectures 1997").

[119] A. J. Buras, Rev. Mod. Phys. **52** (1980) 199.

[120] G. Buchalla, A. J. Buras and M. E. Lautenbacher, Rev. Mod. Phys. **68** (1996) 1125.

[121] L. F. Abbott, Nucl. Phys. **B185** (1981) 189.

[122] L. F. Abbott, Acta Phys. Pol. **B13** (1982) 33.

[123] L. F. Abbott, M. T. Grisaru and R. K. Schaefer, Nucl. Phys. **B229** (1983) 372.

[124] A. Denner, G. Weiglein and S. Dittmaier, Nucl. Phys. **B440** (1995) 95.

[125] M. Drees, hep-ph/9611409.

[126] S. P. Martin, hep-ph/9709356.

[127] J. Louis, I. Brunner and S. J. Huber, hep-ph/9811341.

[128] A. Salam and J. Strathdee, Nucl. Phys. **B76** (1974) 477.

[129] J. Wess and J. Bagger, *Supersymmetry and Supergravity*, Princeton University Press, Princeton, USA, 1992.

[130] S. Coleman and J. Mandula, Phys. Rev. **159** (1967) 1251.

[131] R. Haag, J. T. Lopuszanski and M. Sohnius, Nucl. Phys. **B88** (1975) 257.

[132] P. Fayet and J. Illiopoulos, Phys. Lett. **B51** (1974) 461.

[133] L. O'Raifeartaigh, Nucl. Phys. **B96** (1975) 331.

[134] S. Ferrara, L. Girardello and F. Palumbo, Phys. Rev. **D20** (1979) 403.

[135] M. T. Grisaru, W. Siegel and M. Rocek, Nucl. Phys. **B159** (1979) 429.

[136] L. Girardello and M. T. Grisaru, Nucl. Phys. **B194** (1982) 65.

[137] M. Misiak, S. Pokorski and J. Rosiek, Adv. Ser. Direct. High Energy Phys. **15** (1998) 795.

[138] J. A. Casas and S. Dimopoulos, Phys. Lett. **B387** (1996) 107.

[139] J. A. Casas, A. Lleyda and C. Munoz, Nucl. Phys. **B471** (1996) 3.

[140] J. A. Casas, hep-ph/9707475.

[141] R. Barbieri and G. Giudice, Nucl. Phys. **B306** (1988) 63.

[142] P. H. Chankowski and S. Pokorski, hep-ph/9702431.

[143] H. E. Haber, hep-ph/9707213.

[144] J. F. Gunion and H. E. Haber, Nucl. Phys. **B278** (1986) 449; Erratum hep-ph/9301205.

[145] C. Bobeth, T. Ewerth, F. Krüger and J. Urban, Phys. Rev. **D66** (2002) 074021.

[146] H. Rzehak, Diploma Thesis, May 2001, University Karlsruhe.

[147] W. Hollik and H. Rzehak, Eur. Phys.+J. **C32** (2003) 127.

[148] G. Buchalla, PhD Thesis, TU Munich, July, 1994.

[149] L. Wolfenstein, Phys. Rev. Lett. **51** (1983) 1945.

[150] R. Fleischer, Phys. Rep. **370** (2002) 537.

[151] S. Eidelman *et al.*, Phys. Lett. **B 592** (2004) 1.

[152] A. J. Buras and L. Silvestrini, Nucl. Phys. **B546** (1999) 299.

[153] B. Grinstein, R. P. Springer and M. B. Wise, Phys. Lett. **B202** (1988) 138.

[154] B. Grinstein, R. P. Springer and M. B. Wise, Nucl. Phys. **B339** (1990) 269.

[155] R. Grigjanis, P. J. O'Donnell, M. Sutherland and H. Navelet, Phys. Rept. **228** (1993) 93.

[156] H. Simma, Z. Phys. **C61** (1994) 67.

[157] G. Cella, G. Curci, G. Ricciardi and A. Vicere, Nucl. Phys. **B431** (1994) 417.

[158] K. G. Chetyrkin, M. Misiak and M. Münz, Nucl. Phys. **B520** (1998) 279.

[159] K. Adel and Y. P. Yao, Phys. Rev. **D49** (1994) 4945.

[160] C. Greub and T. Hurth, Phys. Rev. **D56** (1997) 2934.

[161] M. Ciuchini, G. Degrassi, P. Gambino and G. F. Giudice, Nucl. Phys. **B527** (1998) 21.

[162] A. J. Buras, A. Kwiatkowski and N. Pott, Nucl. Phys. **B517** (1998) 353.

[163] F. Borzumati and C. Greub, Phys. Rev. **D58** (1998) 074004;
Addendum Phys. Rev. **D59** (1999) 057501.

[164] C. Bobeth, PhD Thesis, TU Munich, August, 2003.

[165] S. Schilling, C. Greub, N. Salzmann and B. Toedtli, hep-ph/0407323.

[166] A. J. Buras, C. Bobeth and T. Ewerth, hep-ph/0409293.

[167] K. I. Aoki, Z. Hioki, M. Konuma, R. Kawabe and T. Muta,
Prog. Theor. Phys. Suppl. **73** (1982) 1.

[168] M. Böhm, H. Spiesberger and W. Hollik, Fortsch. Phys. **34** (1986) 687.

[169] A. Denner, Fortsch. Phys. **41** (1993) 307.

[170] See for example Y. Yamada, Phys. Rev. **D64** (2001) 036008, and references therein.

[171] M. Beneke, T. Feldmann and D. Seidel, Nucl. Phys. **B612** (2001) 25.

[172] G. Buchalla and G. Isidori, Nucl. Phys. **B525** (1998) 333.

[173] A. F. Falk, M. E. Luke and M. J. Savage, Phys. Rev. **D49** (1994) 3367.

[174] A. Ali, G. Hiller, L. T. Handoko and T. Morozumi, Phys. Rev. **D55** (1997) 4105.

[175] J. W. Chen, G. Rupak and M. J. Savage, Phys. Lett. **B410** (1997) 285.

[176] C. W. Bauer and C. N. Burrell, Phys. Lett. **B469** (1999) 248.

[177] C. W. Bauer and C. N. Burrell, Phys. Rev. **D62** (2000) 114028.

[178] P. Gambino and M. Misiak, Nucl. Phys. **B611** (2001) 338.

[179] P. H. Chankowski and L. Slawianowska, Eur. Phys. J. **C33** (2004) 123.

[180] S. Eidelman *et al.* [Particle Data Group Collaboration], Phys. Lett. **B592** (2004) 1.

[181] K. Bieri, C. Greub and M. Steinhauser, Phys. Rev. **D67** (2003) 114019.

[182] M. Misiak and M. Steinhauser, Nucl. Phys. **B683** (2004) 277.

[183] C. Jessop, SLAC-PUB-9610, 2002.

[184] P. Koppenburg *et al.* [Belle Collaboration], Phys. Rev. Lett. **93** (2004) 061803.

[185] M. Neubert, hep-ph/0408179.

[186] A. J. Buras, A. Poschenrieder, M. Spranger and A. Weiler, Nucl. Phys. **B678** (2004) 455.

[187] P. Gambino, U. Haisch and M. Misiak, hep-ph/0410155.

[188] G. Hiller and F. Krüger, Phys. Rev. **D69** (2004) 074020.

[189] F. Borzumati, C. Greub, T. Hurth and D. Wyler, Phys. Rev. **D62** (2000) 075005.

[190] A. J. Buras, T. Ewerth, S. Jäger and J. Rosiek, hep-ph/0408142.

[191] P. L. Cho, M. Misiak and D. Wyler, Phys. Rev. **D54** (1996) 3329.

[192] F. Krüger and J. C. Romao, Phys. Rev. **D62** (2000) 034020.

[193] M. Gohrbahn, PhD Thesis, TU Munich, October, 2003.

Acknowledgment

First of all I would like to thank my advisor, Prof. Andrzej Buras, for providing me with the opportunity to work on this and other projects. I appreciate the many helpful advises and the personal support, especially in the time when finishing this thesis.

Next, I would like to thank my collaborator Jörg Urban for the numerous discussions we had and from which I undoubtedly profited a lot. Special thanks also to Christoph Bobeth. I really enjoyed our collaboration and I am looking forward for future projects.

In addition, I would like to thank my other collaborators Frank Krüger, Sebastian Jäger and Janusz Rosiek for many fruitful discussions.

Furthermore, I would like to thank my former roommate Martin Gorbahn and my current roommate Selma Uhlig for the friendly atmosphere in our common office.

Moreover, it is a great pleasure to thank all current and former members of the chairs of Andrzej and Prof. Manuel Drees, and of course Manuel himself, for many stimulating discussions and the very pleasant social environment they provided. My thanks go to Ulrich Haisch, Benedikt Gaißmaier, Michael Spranger, Andreas Weiler, Anton Poschenrieder, Felix Schwab, Athanasios Dedes, Stefan Recksiegel, Dominik Bauer, Elmar Wyszomirski, Rouzbeh Allahverdi, Cyrille Barbot, Chung Lin Shan, Kin-ya Oda, Andreas Weinberger, Monika Blanke and Matthias Jamin.

Last but not least a great thank to my parents and my brother for their support of any kind. I also would like to thank all of my friends here for understanding that I had less time for other things when finishing this work.